TAMPEREEN TEKNILLINEN YLIOPISTO
TAMPERE UNIVERSITY OF TECHNOLOGY

ZHAO FU

A STUDY OF STATIC STRAIN AGING OF SELECTED FERRITIC STEELS

Master's Thesis

Examiners: Associate Professor Pasi Peura and Doctoral Student Henri Järvinen

The examiners and topic of thesis were approved on 31 May 2017

ABSTRACT

TAMPERE UNIVERSITY OF TECHNOLOGY
Master's Degree Program in Materials Engineering
ZHAO FU: A Study of Static Strain Aging of Selected Ferritic Steels
Master of Science Thesis, 85 pages, 11 Appendix pages
May 2017
Major: Materials Science
Examiners: Associate Professor Pasi Peura, Doctoral Student Henri Järvinen

Keywords: Low carbon steel, EN 1.4003 ferritic stainless steel, heat treatment, pre-strain, bake hardening, strain aging, yield strength, elongation

Bake hardening effect is a phenomenon of static strain aging and utilized in the manufacturing of automotive components. Bake hardening occurs at elevated temperature of around 170 °C during the paint-baking cycle of the formed components. It leads to the strength increment by the diffusion of carbon atoms to the dislocations during the drying of paint. Steels with ferritic microstructure are known to be susceptible to aging phenomenon. In addition, low carbon steels and ferritic stainless steels are used to produce certain automotive components. The aim of this work is to study the static strain aging phenomenon of two low carbon steels and a ferritic stainless steel, more importantly, by means of bake hardening tests.

This thesis consists of two parts, namely literature study and research parts. The literature study covers the topics like carbon steel, ferritic stainless steel, strain aging, and bake hardening. Two low carbon steels with small difference of production history and EN 1.4003 ferritic stainless steel were used for the experiments. Bake hardening (BH) tests, consisting of pre-straining to 0%, 2%, 6%, and 10% and following heat-treatments of 170 °C/20min and 230 °C/20min, respectively, were conducted. The purpose of the heat treatments was to simulate the paint baking process after press forming. In addition, to evaluate the aging behavior during storage, a heat treatment of 100 °C/30 min (boiling water) was carried out and was followed by tensile testing, respectively.

The study indicates that two low carbon steels have very similar initial properties and behavior in the experiments. The 170 °C/20min heat treatment increased 41 MPa and 230 °C/20min increased around 130 MPa in yield strength of the low carbon steels, while for EN 1.4003 ferritic stainless steel, these two numbers are 20 and 8 MPa, respectively. The yield strength generally increased and elongation decreased with the increase of heat-treatment temperature and pre-strain. The higher baking temperature led to greater BH index generally. The BH index of low carbon steel increased from 19 MPa to around 54 MPa along with the pre-strain increasing from 0% to 10% when baked at 170°C, while it decreased from 72 MPa to 58 MPa when baked at 230 °C. The 100 °C/30min aging treatment did not produce significant influence on the properties of three investigated ferritic steels. It can be concluded that the bake-hardening is the main mechanism of achieving strength increase, and it heavily depends on the dislocation caused during pre-strain.

PREFACE

This thesis work was carried out at the Department of Materials Science of Tampere University of Technology (Finland) between June 2016 and May 2017.

First of all, I would like to express my utmost gratitude to my thesis supervisor Associate Professor Pasi Peura for offering this research project and giving constructive and helpful advice on the thesis. Special gratitude is also given to M.sc. Henri Järvinen for his help and helpful instruction in the experiments and results analysis throughout this thesis work.

Secondly, I would like to express my thanks to SSAB Europe Oy, Hämeenlinna and Outokumpu Oyj for providing the materials for the experiments. At the meanwhile, I would also thank FinDDRG ry (Finnish Deep Drawing Research Group) for granting the thesis work.

Thirdly, Senior Laboratory Technician Ari Varttila conducted specimen machining work, and few other laboratory technicians and researchers gave some help in the experiment, I would also present my gratitude to them. My thanks is also given to the colleagues of our research group and department for creating a friendly environment.

I would also express my thanks to my parents for their endless support and love, also, my study in Finland would not be available without them. I am here also showing my greatest gratitude to my home country China, which has always been in my mind and soul and given me mental support.

In addition, my sincere gratitute is given to my wife Saara Pitkälä-Fu who has accompanied me and given me lots of help, support and love. Last but not least, I also express my thanks to some important friends in Finland Maarit Sulonen, Steven Kajiti, Amad Ud Din Khattak, Anniina Vainionpää, who gave me lots of help in the life and valuable friendship.

Zhao Fu

Tampere, 15.5.2017

CONTENTS

LIST OF FIGURES

LIST OF SYMBOLS AND ABBREVIATIONS

AISI	American Iron and Steel Institute
AHSS	Advanced high-Strength Steel
BH	Bake Hardening
bcc	Body-centered cubic
BOF	Basic Oxygen Furnace
CO	Carbon Monoxide
CP	Complex Phase
DP	Dual Phase
DSA	Dynamic Strain Aging
DIN	Deutsches Institut für Normung (German Institute for Standardization)
EAF	Electric Arc Furnace
ELC	Extra Low Carbon
EN	European Standard
fcc	Face-centered cubic
HSLA	High Strength Low Alloys
HSS	High-strength Steels
ISO	International Organization for Standardization
MS	Martensitic Steels
IF	Interstitial Free
ppm	Parts per million
rpm	Revolutions per minute
SSA	Static Strain Aging
TS	Tensile Strength
TRIP	Transformation Induced Plasticity
UE	Uniform Elongation
ULC	Ultra-Low Carbon
UTS	Ultimate Tensile Strength
YS	Yield Strength

α-Fe	Ferrite
γ-Fe	Austenite
δ-Fe	Delta Ferrite
ε	Engineering Strain
σ	Engineering Stress
D	Grain Diameter
A_{r3}	Temperature when austenite → ferrite transformation starts during cooling

1 INTRODUCTION

Vehicle shows an increasing significance in the society and our daily life. Low and medium carbon steels (carbon content up to 0.35) are the most widely used materials in the automotive manufacturing. In addition, ferritic stainless steels are also used in some automotive parts. However, they have not reached that much attention with respect to the typical phenomena occurring in the manufacturing routines. Therefore, the pre-straining, bake-hardening (BH) heat treatments, tensile tests, aging treatments were performed to study the static strain aging phenomenon by investigating the bake hardening response.

Static strain aging (SSA) is a general phenomenon in steels typically utilized in bake hardening and multi-phase steels. Bake hardening, in turn, is a phenomenon of SSA, which leads to the strength increment because of the work hardening in the cold working and the strain aging during the subsequent paint baking during manufacturing of automotive components [1]. Low carbon steels are known to be sensitive to SSA behavior, i.e., they show bake hardening when they are subjected to forming and subsequent paint baking during manufacturing of automotive components. For example, Banerjee and Dhal [2] confirmed the strain aging response of low carbon steel. However, the bake hardening behavior of ferritic stainless steels has not reached that much attention even though they are also used in some automotive parts.

But there exists some studies [3-4], which have shown that SSA can also occur in ferritic stainless steels. For example, Palosaari, *et al*. [3] also found that a strength increment of 50 MPa with EN 1.4509 and 1.4521 ferritic stainless steels due to the strain aging. Buono, *et al*. [4] found that the yield strength of AISI 430 stainless steel increased from 465 MPa to 528 MPa with the increase of baking temperature from 180 °C to 245 °C, with a 30 min bake-hardening time. However, the information on the static strain aging of unstabilized ferritic stainless steels is still limited.

Therefore, this research aims at gaining a further understanding of the impact of the static strain aging phenomenon on the mechanical properties, it also studies the behavior of the low carbon steels and EN 1.4003 ferritic stainless steels in the automotive components manufacturing by investigating the response of its mechanical properties. The research is expected to understand how the pre-strain and heat treatment affect the mechanical

properties and how much strength can be increased by the strain aging phenomenon.

Chapter 2 includes some relevant theoretical information, which includes the topics of carbon steel, alloy steel, ferritic stainless steel, strain aging, and bake hardening. Chapter 3 describes the experimental materials and methods, the results are presented and analyzed, some problems and future work in the relevant field are also discussed in Chapter 4. Some significant findings are presented in Chapter 5. Some appendices are also attached in the end of the thesis to provide more detailed information on how the data were produced.

2 LITERATURE STUDIES

2.1 Steel Classification

Steel is a hard and strong iron-based alloy. It is one of the most widely used materials in the current life around the world, especially in the engineering and construction fields. The Carbon content is mostly no more than 2.11%, as shown in Figure 1. It is the most important element for iron and for the properties of steels, the carbon content also affects the hardness, tensile strength, ductility of the steel a lot [5].

The microstructures and properties of the steels are significantly influenced by their composition, therefore, the chemical composition is commonly used as criterion to classify the steels. By chemical composition, the steel can be classified into carbon steels and alloy steels, the difference of which is that in the carbon steel, carbon is the main element, while alloy steels contain more alloying elements for improving some properties.

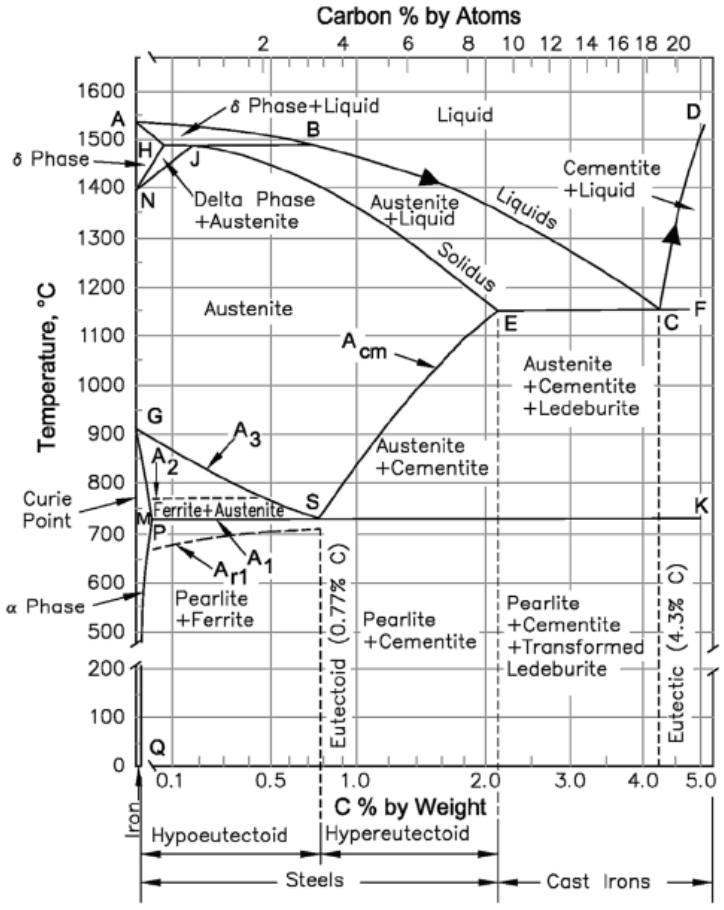

Figure 1. *Iron-carbon phase diagram [6].*

2.1.1 Production of Strip Steel

The development of steel making technologies and the application of vacuum degassing make it easy to control the contents of some elements like carbon, nitrogen, sulphur, etc. Before 1970s, the main parts of the strip steel was casted into ingots with 500 mm thickness, and then be cooled and removed from modules, which is followed by heating to around 1250°C and rolling to slabs with 200-250 mm thickness and cooling [7]. The surface defects were finally removed through scarfing. The different stages of this process were separated [7]. Steel is normally manufactured from two kinds of raw materials: steel scrap and hot metals. Steel scrap is normally produced by using electric arc furnace (EAF), and hot metal is typically produced by blast furnace.

Since the EAF for steelmaking in 1889 by Paul Héroult, EAF has been widely applied in steelmaking and smelting of nonferrous metals, including stainless steel [8]. EAF is also the core process of mini-mills, which produce steel from scrap [9]. An EAF melts minerals or other materials by using electricity. The dry minerals are firstly weighed and mixed, which are then evenly distributed throughout the furnace. Power is supplied through a transformer and graphite electrodes, the electrodes are extended into the furnace and touch the materials, and the electric arc can be formed between the electrodes when power is supplied, as indicated in Figure 2. The electric arc melts the materials and produce a liquid bath [10]. The temperature in EAF is very high depending on the melting point of the metal. There is also a water cooling system to avoid overheating. The melted liquid material is then poured into a mold and sent to the cooling system, the ingot would be solidified and processed to the desired size and shape [10].

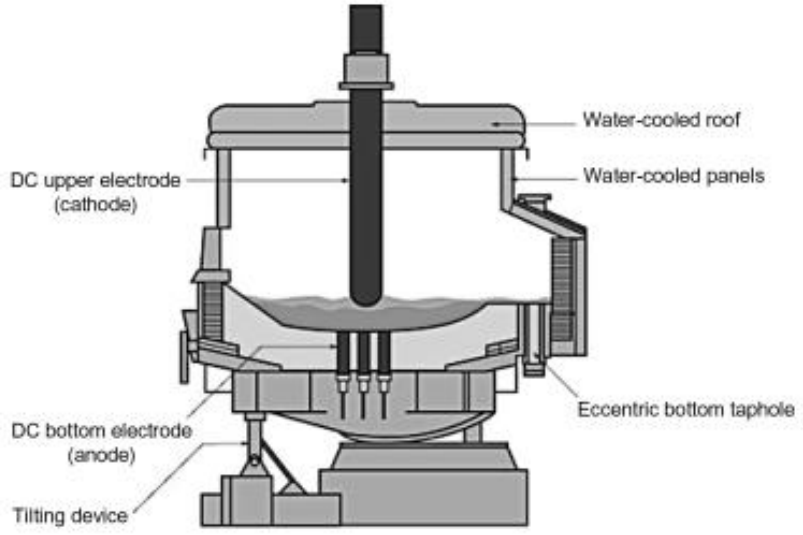

Figure 2. *Diagram of an electric arc furnace with direct current [11].*

Blast furnace is commonly used for manufacturing carbon steels. Figure 3 presents the working process of blast furnace. The coke and sinter, pellets, lump, and flux are charged by using charging conveyor [12]. The charged materials go down because of gravity. The temperature inside furnace increases from throat (200–400 °C), to shaft (400–1800 °C), and to bosh section (up to 2000 °C) [13]. In the lower part of the furnace, hot stove produces hot blast, which is injected into the furnace through tuyere. The hot blast reacts with the coke chemically, and forms carbon monoxide (CO), which reduces the iron oxides in the ferrous ores [12]. At the bottom of the hearth, the molten metal (hot metal) is collected by the torpedo car. The slag is formed at the meanwhile, and it floats on top of the hot metal bath due to its lower density. Liquid hot metal and slag are tapped regularly, and the slag is collected by a slag car [12].

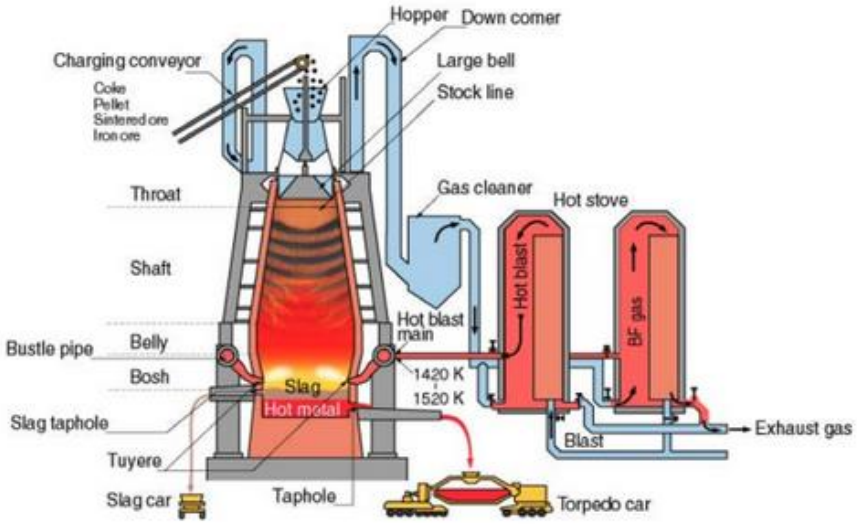

Figure 3. *Illustration of blast furnace process [12].*

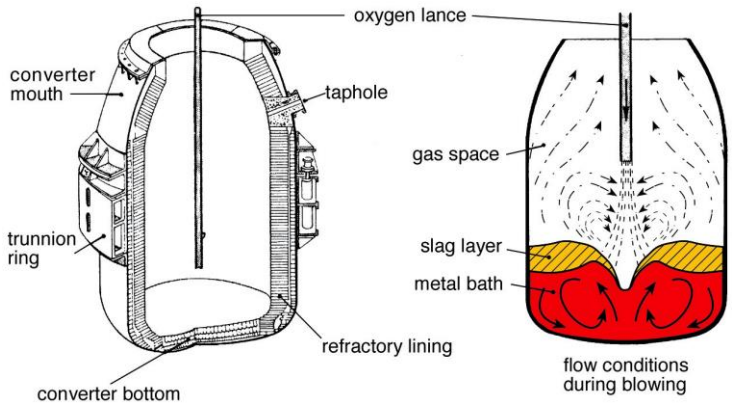

Figure 4. *Schematic of steelmaking process with basic oxygen furnace [14].*

Basic oxygen furnace (BOF) is a steel making furnace to convert the molten pig iron and steel scrap into steel as illustrated in Figure 4. The hot metal is produced from blast furnace and poured into a ladle. High purity of oxygen is then ejected at super high speed

under high pressure to the molten metal through an oxygen lance. The next step is to charge the furnace, the required thermal energy for basic oxygen steelmaking is produced from the oxidation process [14]. A water-cooled copper lance is lowered into the vessel, and the high purity oxygen is injected at supersonic speed. The oxygen ignites the carbon dissolved in the steel to form CO and carbon dioxide, and emits heat, which melts the scrap and removes unwanted elements. Next, the fluxes are fed into the vessel to form slag to balance the basicity and absorb impurities. The steel is finally tapped into a steel ladle, and slag is poured into slag pots.

The continuous casting of steel was developed and widely used in 1960s, in which the strip steel is directly rolled to the slab with ideal thickness [15]. A typical curved continuous casting process is illustrated in Figure 5. The molten liquid steel flows from a ladle to the mold through a tundish. All these operations are protected by slag, which covers vessels, and by ceramic nozzles between vessels. The liquid steel freezes against the cooled copper mold walls and forms a solid shell, as shown in the figure. By running the rolls, which are lower in the machine, the shell is moved out of mold, this movement is supposed to be in a steady rate, which is also the casting speed. The solidifying shell below the mold is to support the remained liquid, the support rolls work to maintain good shape and flat surface of the steel. In the meanwhile, the water spray cools the interfaces between rolls and the strand to maintain surface temperature and avoid regional high temperature due to the rubbing and heat, the cooling works until the molten core is solidified. The strand is cut into slab with the required length.

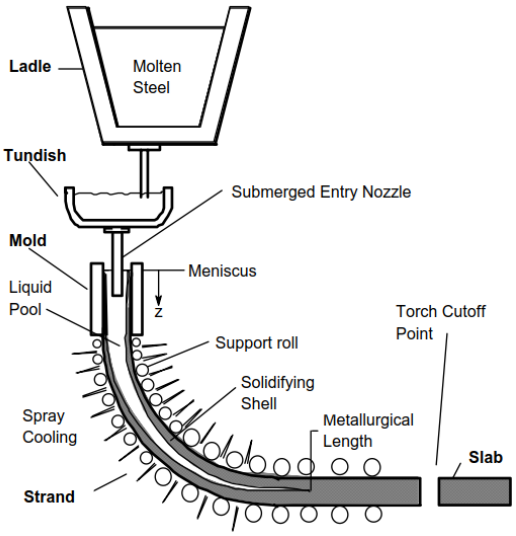

Figure 5. *Schematic of curved continuous casting process [16].*

The first hot-rolling stage included reheating to around 1250 °C and rolling in two linked stages. The two stages are roughing and finishing, which were to reduce the thickness to

30-45 mm, and reduced to 1-12 mm depending on the mill and final hot-rolled gauge requirement [7]. The roughing could be performed with a single reversing stand, through which the steel passes forwards and backwards several times. The finishing is performed with a finishing train which contains normally seven stands. The front end of the strip exists the last stand well before the back end of the strip enters the first stand. The finishing temperature when the steel comes to the last stand is supposed to be over A_{r3} temperature, which is to ensure the constituent transformation happens in the austenite region of the phase diagram, as indicated in Figure. 1. The steel is then cooled before coiling, the temperature of which ranges from 200 °C to 750 °C depending on the metallurgic issues. If needed, the steel is then passed through a pickling line together with hydrochloric acid to remove the oxide on the surface [17].

The cold rolling is carried out by a tandem mill containing typically five stands. Cold rolling makes steel stronger, harder, but more brittle. To reduce the strength and improve the formability, the cold rolled steel usually needs to be annealed. The recrystallization, grain formation and growth, precipitates dissolution happen during the annealing. The interaction of these changes determines the final microstructures and properties of the steel [7]. Batch annealing and continuous annealing are the common methods. Batch annealing is performed in a furnace, the steel is enclosed in it with the protective atmosphere, which has been NHX gas (nitrogen with no more than 5% hydrogen) or pure hydrogen. Pure hydrogen is more preferred for its faster heat transfer, which causes rapid heating and cooling [18]. In continuous annealing, the annealing time is much shorter than in batch annealing, as indicated in Figure 6. The batch annealing temperature can be up to 700 °C for most cases, whereas continuous annealing temperature for strip steels is above 700 °C and often above 800 °C [7, 19].

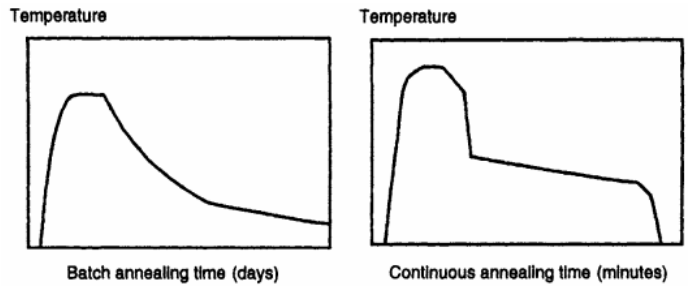

Figure 6. *Schematic of annealing cycles for batch and continuous annealing [7].*

The last stage in steel processing is the temper rolling or skin passing, which is to remove the yield point in the tensile curve to avoid the occurrence of the stretcher-strain markings while the steel is being pressed. The metallic coating with electrolytic process can all be achieved by hot dipping and be applied to the annealed strip surface. [7]

2.1.2 Carbon Steels

By the definition of American Iron and Steel Institute (AISI), carbon steel has no specific content for chromium, nickel, molybdenum, cobalt, tungsten, etc., nor requirements for other elements for obtaining desired properties. Carbon is the main alloying element for steel, the content of carbon can reach 2% in steels. It is usually dissolved in the iron or be present as carbide Fe_3C. The Increase of carbon content can increase the hardness, tensile strength, solid-solution strength, hardenability while reduce the weldability [5, 20]. Carbon steel usually contains up to 1.4% manganese, which prevents the formation of iron sulfide inclusions FeS, which has low melting point and is formed at grain boundaries mostly [20].

Manganese content normally ranges from 0.2% in the steel, in the carbon steel, it is common to reach 1.5% [20]. It also contributes to the increase of solid-solution strength, hardness and hardenability, to be more precise, manganese increases the strength of ferrite. It can also combine with sulphur to form globular manganese sulphides (MnS), which improves machinability. At the same time, it counters the brittleness from sulphur, which is good for the surface finish of the carbon steel [5].

Silicon strengthens the iron by dissolving into it. It also inhibits the grain growth by limiting the prior austenite size. Meanwhile, the addition of silicon increases the ultimate tensile strength and decreases yield stress [21]. It is also a principal deoxidizer in the steel to remove oxygen, and form silicate stringers (silicon dioxide inclusions) [5].

Aluminum contributes to the deoxidization of the steel by extracting gases from the steel, and it also offers the resistance to aging. It increases the hardness and toughness of the steel by combining with nitrogen to form very hard nitride and forming fine grain microstructures. In addition, aluminum does not form carbide either [5].

Chromium increases the hardenability and corrosion resistance of the carbon steel. Sulfur is usually undesirable impurity in the steels, the amount of which is normally strictly limited. When its content is above 0.05%, brittleness may be caused and weldability can be decreased [20]. Similarly, phosphorus is also undesirable impurity, the amount of which is normally strictly limited in the carbon steels, otherwise, it may bring embrittlement in the hardened steels [20]. Molybdenum promotes the carbide formation very well, and increases the hardenability and strength. It is usually in small amount of no more than 0.2% in the carbon steel. Nickel increases the hardenability, toughness and ductility, especially when at low temperature for the carbon steel, and its content is usually

below 0.5% [20]. Vanadium and niobium both increase the hardenability of carbon steel, and they are present in small amount of lower than 0.2% and 0.02%, respectively [20]. The main elements and their functions in the steel are summarized in Table 1.

Table 1. *Main elements in the steels and their functions [5].*

Elements	**Functions**
Carbon	The most fundamental element in the steels. It increases the hardness and strength generally. It can also form cementite Fe_3C with iron.
Manganese	Increases the solid-solution hardness and hardenability. It lowers the hot brittleness, but high content of manganese produces austenitic microstructure and makes the steel brittle.
Silicon	Increases the solid-solution hardness, strength and hardenability. Also removes oxygen in the molten steels. It increases the oxidation resistance, and susceptibility to decarburization.
Aluminum	It contributes to the deoxidization of the steel and it offers resistance to aging. It forms small grains to improve the hardness and toughness.
Nickel	Increases the solid-solution hardness, strength, toughness and hardenability of the steels.
Chromium	Slightly increase the solid-solution hardness, toughness and hardenability of the steels. Increases the corrosion resistance at high temperature. It forms the carbides, which improves the wear resistance.
Molybdenum	Strong carbide former, which improves the creep strength, hardness. It also improves the corrosion resistance in the stainless steels.
Cobalt	Increases hardness at high temperature and the strength of the steels. It is weak carbide former. It decreases the hardenability.
Titanium	It refines the grains to increase the strength and hardness of the steels. It is very strong carbide former, good to combine with nitrogen. It is also strong oxidizer.
Phosphorus	It is impurity in the steel. It improves the machinability and increases the hardness and strength of low-carbon steels.

The mechanical properties of carbon steels are established and affected by the material specifications, the property values can vary within certain range with different material specifications [18]. The properties of the carbon steel cover a wide range, which is affected by the composition a lot. Among all the elements, the content of carbon has a critical impact on the mechanical properties, which is demonstrated in Figure 7. It can be seen that the hardness, tensile strength, yield strength (YS), reduction, and elongation are all affected significantly by the variation of carbon content.

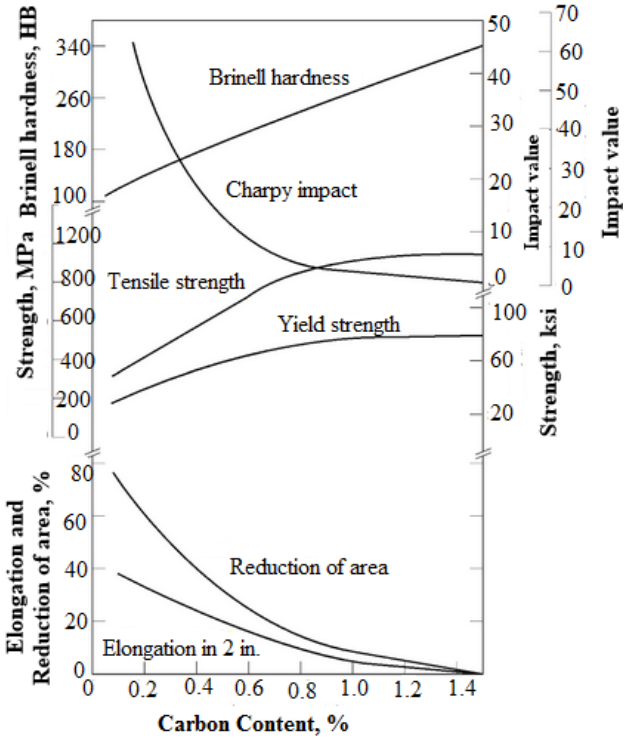

Figure 7. *Variations of mechanical properties of as-rolled 25 mm daim bars of plain carbon steels as a function of carbon content [22].*

By the carbon content, carbon steel can be classified into low-carbon steels, medium-carbon steels, high-carbon steels, ultrahigh-carbon steels, the carbon contents of which range between 0-0.30%, 0.30%-0.60%, 0.60%-1.00%, and 1.25%-2.00%, respectively [7]. With the increase of carbon content, the hardness and tensile strength, and toughness are increased, while brittleness is decreased.

Low carbon steels contain no more than 0.3% carbon. They are mostly applied to manufacture the flat-rolled products, e.g. strip or sheet, under cold-rolled and annealed condition. When the carbon content is below 0.1%, the carbon steel has good formability, which makes it ideal material for the automobile body panels and wire products. When the content is up to 0.3% with manganese content up to 0.4%, it is good for rolled steel structural plates. While when the manganese content reaches 1.5%, the carbon steel is ideal material for forgings, seamless tubes, and boiler plates [22].

Medium-carbon steels contain 0.30% to 0.60% carbon and 0.60% to 1.65% manganese [22]. They have good thermal processing property and poor weldability. Due to the higher carbon content, their hardness and strength are higher, brittleness and toughness are lower than in low-carbon steels. Medium-carbon steels are mostly applied for gears, crankshafts, axles, forgings, and etc. They can be applied under the quenched and tempered condition when the carbon content reaches 0.5% [22].

High-carbon steels contain 0.60% to 1.00% carbon and 0.30% to 0.90% manganese [22]. They have fully pearlitic microstructure, which is very fine structure and makes the steel very hard, while less ductile than medium-carbon steels [23]. The strength and hardness are further higher, brittleness and toughness are lower than the medium-carbon steels due to the increase of the carbon content. They are often applied for springs and high-strength steel wires [22-23]. They are also called tool steels since they are well used as the material for some tools like saw blades, knives, chains, shear blades, etc. [23-24].

Ultrahigh-carbon steels contain 1.25% to 2.00% carbon [25]. As indicated in Figure 1, its microstructure is cementite and pearlite at low temperature (below 1000 K), with the increase of temperature, austenite would occur and the portion of cementite would be decreased. The further increase of temperature would increase the portion of austenite and ferrite is also possible to occur. Therefore, they usually have very high hardness and strength, which makes them ideal materials for some knives, molds and other tools.

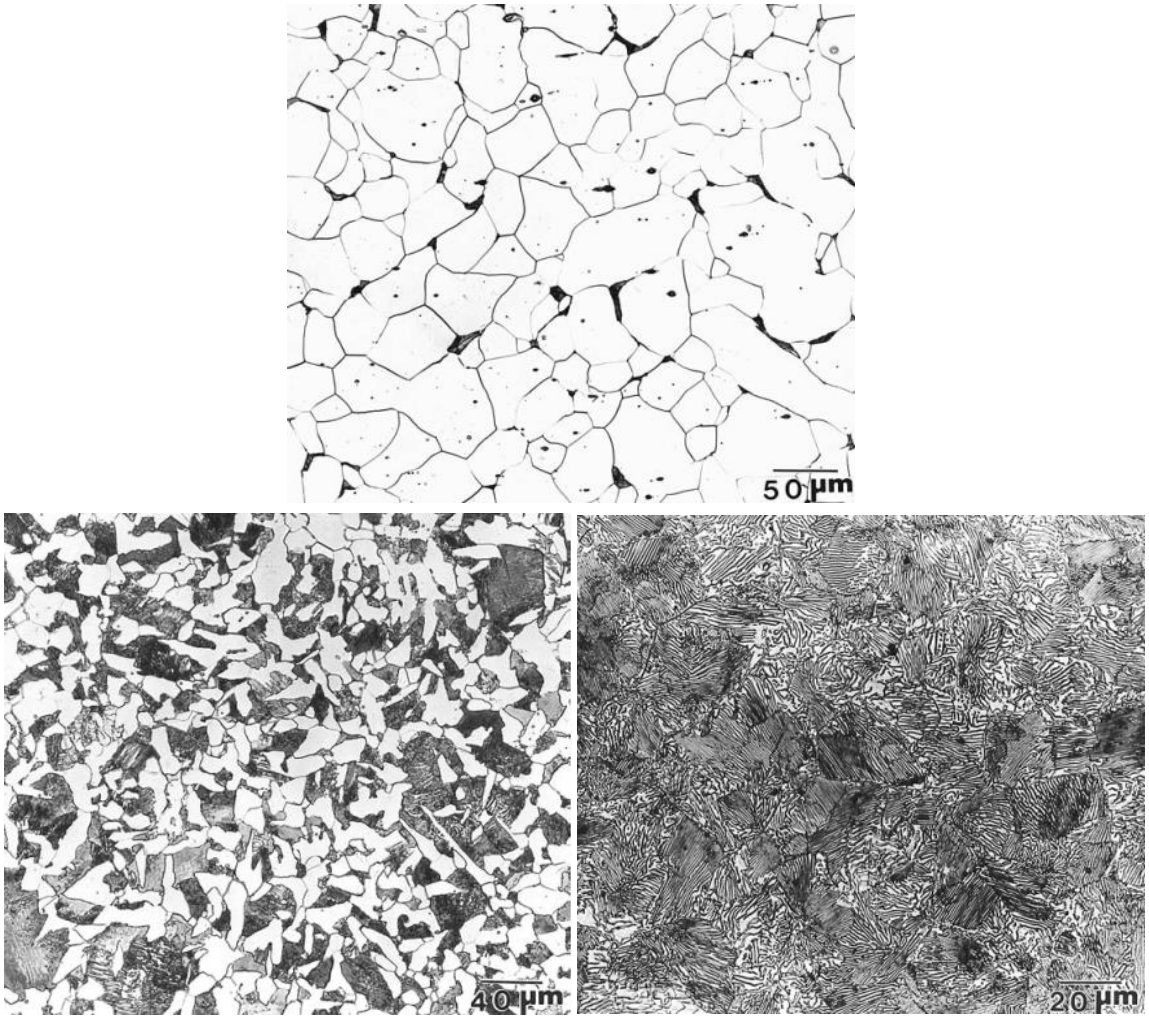

Figure 8. *Micrographs of (a) low carbon AISI/SAE 1010 steel; (b) medium carbon AISI/SAE 1040 steel; (c) high carbon AISI/SAE 1095 steel [5].*

The difference of compositions also influences the microstructures of the steels. Low-carbon steel consists mainly ferrite grains, which is the white etching part in Figure 8(a), and pearlite, which is the dark etching part shown in Figure 8(a). The ferrite grains and pearlite in the medium-carbon steels is shown in Figure 8(b) with white etching and dark etching parts, respectively. In high-carbon steels, there are mainly pearlite matrix and grain-boundary cementite, which is shown in Figure 8(c).

Low-carbon steel consists of mainly ferrite, as indicated in Figure 1, for example, a steel with 0.4% C consists of single phase austenite (γ-Fe), with cooling slowly, some austenite transform to ferrite (α-Fe) when the temperature is above 727 °C. When it is cooled to below 727 °C, the remained austenite transform to pearlite which contains ferrite and cementite (Fe_3C), in this region, the solubility of carbon in ferrite decreases rapidly with the temperature going down. With the increase of the carbon content, $\gamma \rightarrow \gamma + \alpha$ transformation temperature decreases, the ratio of pearlite to ferrite increases remarkably, and the full pearlite microstructure can be achieved with 0.8% carbon.

The grain size of ferrite has very important effect on the properties of low carbon strip steel. The yield strength increases with the increase of ferrite grain size, while it is also influenced by solid solution and precipitation. The solid solution effect is related to the atomic concentration of the solute atoms and difference of atomic size between the iron and the solute element. The precipitation strengthening can be achieved by adding titanium, niobium and vanadium, which are strong in forming carbides and nitrides. The precipitation strengthening effect depends on the volume fraction and size of the precipitates [7]. However, some precipitates can diffuse into each other. Thus, the composition would depend on the austenite matrix in equilibrium state and temperature. Apart from the precipitation reactions, some carbide forming elements like titanium and niobium also influences the recrystallization kinetics during hot rolling. These elements in solid solution may be involved in solute drag, which retards the recrystallization process. Meanwhile, the strain-induced precipitation also retards the recrystallization. In general, the combined effects of initial austenite grain size, rolling temperature, amount of deformation affect the recrystallization [26].

During the cooling of the recrystallized austenite structure, ferrite grains prefer to nucleate at the austenite grain boundaries. Meanwhile, due to the grain elongation in the rolling, the grain boundary area in increased in the non-recrystallized austenite, which increases the number of nucleation sites. Generally, the ferrite grains from the deformed non-recrystallized austenite are finer than those from the recrystallized austenite [7]. Ouchi [27] found that the ferrite grain size decreases with the increase of the cooling rate. For

the combined strengthening effects of the grain refinement, solid solution, and precipitation, there is a limit, thus, transformation strengthening is applied to gain the tensile strength over 500 MPa [7].

When a steel is cooled from the austenite state to around 450 °C rapidly, the ferrite region is surpassed and the austenite would transform to bainite. Bainite consists of lath-shape ferrite grains with misorientation between the grains and high-angle boundaries of the packets [26]. The microstructure of bainite consists of non-lamellar mixture of ferrite and carbides, which can be classified into upper and lower bainites. Upper and lower bainites are both formed as aggregates of some small plates or laths of ferrites, the essential difference lies in the nature of the carbide precipitates, the ferrite in the upper bainite does not contain precipitate. Besides, upper bainite is formed at higher temperature and has coarser structure than the lower bainite [28]. Figure 9 illustrates their microstructures. It can be seen that the ferrite in lower bainite makes the needlelike structure. The refined microstructure in the lower bainite is also the reason for its higher strength.

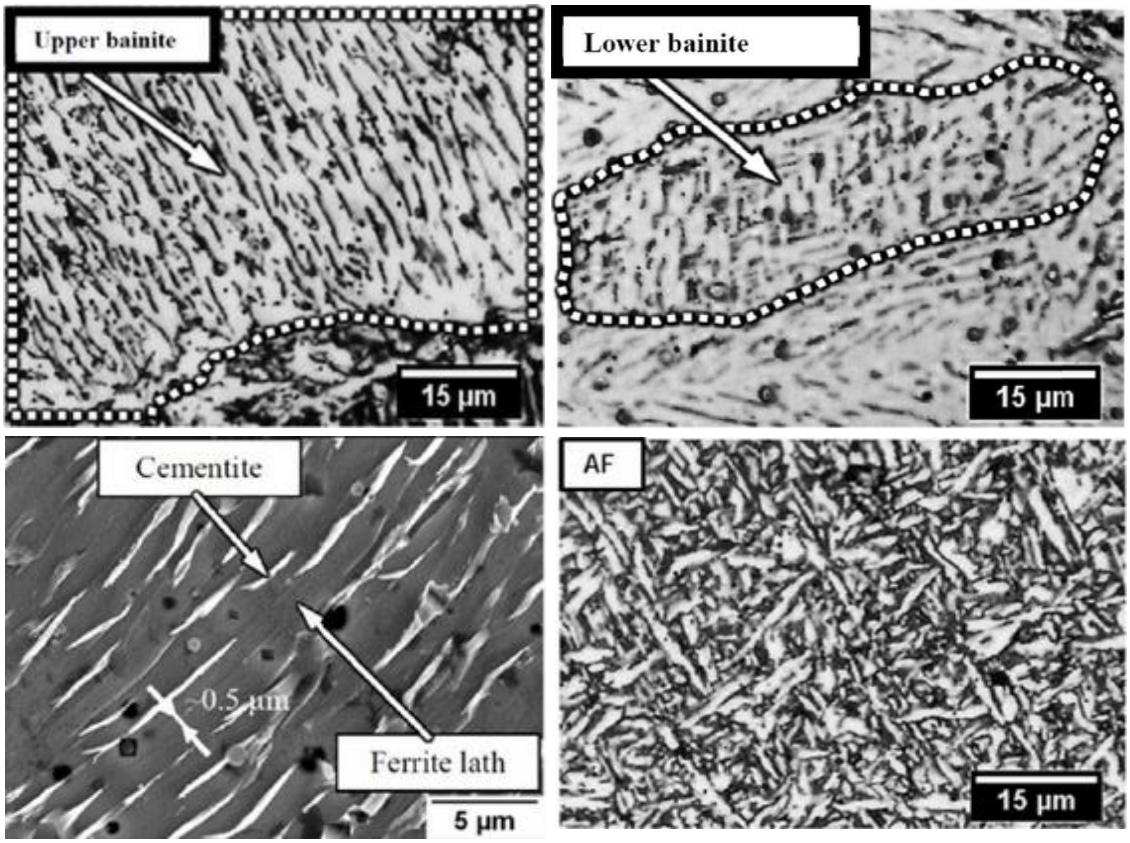

Figure 9. *Micrographs of (a) upper bainite and (b) lower bainite with intra-lath carbide segregation; (c) SEM image of upper bainite; (d) Acicular ferrite [29].*

Acicular ferrite has similar transformation temperature and mechanism as bainite, and it is often described as intragranularly nucleated bainite [30]. Madariage *et al*. [31] claimed

that acicular ferrite plates can grow in morphological packets, which are similar to the bainite morphology. Bhadeshia [32], Rees and Bhadeshia [33], Sugden and Bhadeshia [34] all suggested that bainite can be changed to acicular ferrite just by controlling the nucleation sites. However, acicular ferrite shows distinctive difference from bainite in the structure, which is shown in Figure 9(d). Acicular ferrite has higher strength and toughness than bainite [30].

Apart from those phase transformation and occurrence, the effect of the deformation structure development is also significant during the rolling process. During the deformation, more dislocations are created, and they tend to cluster together. Thus, a sub-grain structure with high dislocation density would be formed. The deformation process also brings some stored energy, which depends on the mean dislocation density, sub-grain size, similarities and differences from adjacent sub-grains, etc. In addition, the deformation is also affected by the crystal structure. Iron can have face-centered cubic (fcc) or body-centered cubic (bcc) structure, the deformation happens usually only along certain slip plane with certain slip direction by the movement of the dislocations. This would lead to the phenomenon that grains with certain orientations would store more deformation energy than the grains with other orientations. This stored deformation energy would lead to selective nucleation of the new grains during recrystallization when the steel is heated, Decker and Harker [35] concluded that the initial recrystallized grains would occur in the high energy regions and they would consume the energy of the region, making the nucleation harder.

The cold reduction also affects the grain size, greater cold reduction generally leads to finer grain size, but the cold reduction itself is also influenced by the alloying elements in the solution and precipitates. Meanwhile, hot band grain size affects the size and texture of the recrystallized grains, it also affects the cold rolling and annealing textures [36].

Low-carbon steel is primarily applied to the manufacture sheet steel and strip steels with outstanding formability. It is most widely applied in the automotive manufacturing field, which is attributed to its good formability, weldability, elasticity and low price. [7]

2.1.3 Low Alloy Steels

Alloy steel is formed by adding small amount elements to the steel. For low-alloy steels, the alloying elements are often added for increasing hardenability, improving mechanical properties and toughness, decreasing the environmental effect when in certain service conditions [17]. Manganese, chromium, silicon, nickel are the common alloying elements.

High Strength Low Alloys (HSLA) is an important category of low-alloy steels. It is designed to offer better general mechanical properties. The chemical composition of HSAL steels depends on the thickness and property requirements, for example, the HSLA sheet or plate steels have carbon content of 0.05% - 0.25% [37]. It can also contain small amounts of nickel, chromium, copper, titanium, nitrogen, and etc. It uses small amount elements to reach very high strength, which is 345-620 MPa in the rolled, annealed, quenched, and normalized conditions [5, 37]. Many HSLA steels have very low carbon content like 0.06%, yet its yield strength can reach 485 MPa, which is attributed to refinement of the grain size and precipitation strengthening with the presence of titanium, niobium, and vanadium [37]. Figure 10 shows the microstructure of a HSLA, the light etching constituent shows the ferrite, the dark etching constituent shows the pearlite.

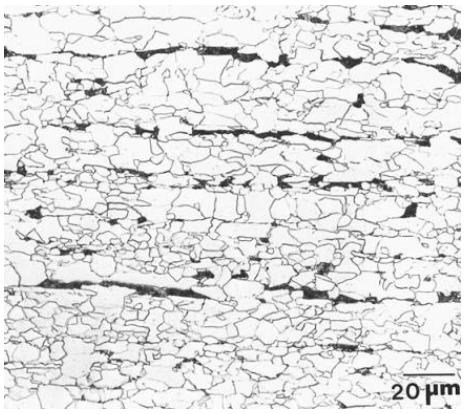

Figure 10. *Micrograph of a high strength low alloyed linepipe steel [5].*

High alloy steels generally has very good corrosion resistance, this group of steels also include the stainless steels, heat resistant steels, and tool steels [5]. Alloy steels are often used in structural, cutting, and electrical aspects, for example the structural applications include the bridges, machine tools, vehicles, cutting applications include cutting edge, electrical applications include core steel, electrical-resistance devices, and etc [38].

2.2 Stainless Steels

Stainless steel is part of high alloy steel group. As it known that many metals undergo corrosion in the real applications. Among the applied metals and alloys, apart from the most common iron-based alloys and steels, there are also iron-chromium alloys, which own excellent corrosion resistance and are known as stainless steels. Stainless steel is roughly defined as the iron alloys which contain at least 10.5% of chromium and have good corrosion resistance [39].

2.2.1 Categories of Stainless Steels

The stainless steel family consists of several categories, which can be classified by different ways. By metallurgical phases in the microstructures at room temperature, stainless steel can be classified into ferritic, austenitic, martensitic, duplex, and precipitation hardened stainless steels. The composition range and properties of which are shown in Table 2. The relationship between these categories is shown in Figure 11, which illustrates the contents of the main elements chromium and nickel of different categories of stainless steels, it can be seen that ferritic stainless steels consist of very high chromium content and relatively low nickel content.

Table 2. *Composition ranges of different stainless steels [40].*

Steel category	**Composition (wt%)**					**Hardenable**	**Ferro-magnetism**
	C	Cr	Ni	Mo	Others		
Martensitic	›0.10	11-14	0-1	-	V	Hardenable	Magnetic
	›0.17	16-18	0-2	0-2			
Martensitic-austenitic	‹0.10	12-18	4-6	1-2		Hardenable	Magnetic
Precipitation hardening		15-17	7-8	0-2	Al,	Hardenable	Magnetic
		12-17	4-8	0-2	Al,Cu,Ti,Nb		
Ferritic	‹0.08	12-19	0-5	‹5	Ti	Not hardenable	Magnetic
	‹0.25	24-28	-	-			
Ferritic-austenitic (duplex)	‹0.05	18-27	4-7	1-4	N, W	Not hardenable	Magnetic
Austenitic	‹0.08	16-30	8-35	0-7	N,Cu,Ti,Nb	Not hardenable	Non-magnetic

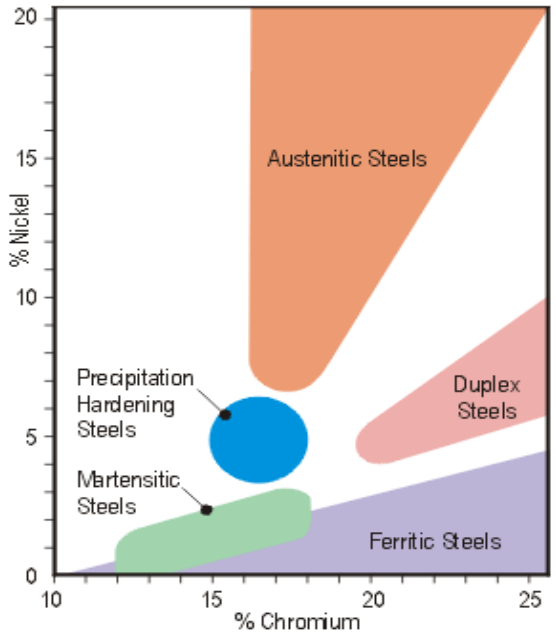

Figure 11. *Chromium contents of different categories of stainless steels [41].*

The toughness of the above types of stainless steels vary a lot depending on the chemical composition. Besides, the toughness generally increases with the increase of temperature [40]. Impact toughness is a frequently used measurement. Figure 12 presents the impact toughness of different types of stainless steels from -200 to 100 °C. It indicates that impact strength of different stainless steels increase differently with the increase of temperature.

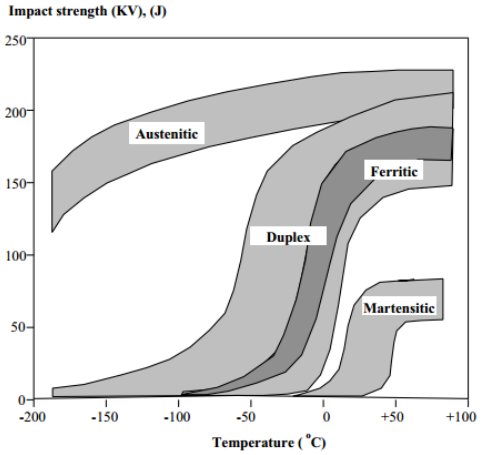

Figure 12. *Impact toughness of different types of stainless steels [40].*

It can be seen that all types of stainless steels, except austenitic stainless steels, exhibit a toughness transition. Austenitic stainless steel owns obviously higher impact toughness over the temperature range than other types of stainless steels. Martensitic stainless steels have much lower impact toughness than other steels since martensite has very high hardness while very low toughness. Its transition temperature is around room temperature, while for ferritic and duplex stainless steels, the transition temperatures range from -50 °C to 0 °C. More mechanical properties of different stainless steels are in Table 3.

Table 3. *Mechanical properties of selected stainless steels [42].*

			Average tensile properties					
			Yield strength, 0.2% offset		Ultimate tensile strength		Elongation in 50.8 mm	
UNS or AISI type	Condition	Rockwell hardness	MPa	ksi	MPa	ksi	(2.0 in.), %	Reduction of area, %
Austenitic stainless								
Type 304	Annealed	81 HRB	241	35	586	85	60.0	70.0
N08020	Annealed	84 HRB	276	40	621	90	50.0	65.0
S20161	Annealed	93 HRB	365	53	970	140	59.0	64.0
S21800	Annealed	95 HRB	414	60	710	103	64.0	74.0
Ferritic								
Type 405	Annealed	81 HRB	276	40	483	70	30.0	60.0
Type 430	Annealed	82 HRB	310	45	517	75	30.0	65.0
Duplex								
S32950	Annealed	100 HRB	570	82	760	110	38.0	78.0
Martensitic								
Type 410	Annealed	82 HRB	276	40	517	75	35.0	70.0
	Oil quenched from 1010 °C (1850 °F) and tempered:							
	at 250 °C (500 °F)	43 HRC	1089	158	1337	193	17.0	62.0
	at 593 °C (1100 °F)	26 HRC	724	105	827	120	20.0	63.0
Type 420	Annealed	92 HRB	345	50	655	95	25.0	55.0
	Oil quenched from 1038 °C (1900 °F) and tempered at 316 °C (600 °F)	52 HRC	1482	215	1724	250	8.0	25.0
Type 440C	Annealed	97 HRB	448	65	758	110	14.0	30.0
	Oil quenched from 1038 °C (1900 °F) and tempered at 316 °C (600 °F)	57 HRC	1896	275	1975	285	2.0	10.0

2.2.2 Structure and Composition of Ferritic Stainless Steels

Ferritic stainless steels have a bcc crystal structure, which is the same as pure iron at room temperature. Ferritic stainless steels have ferritic single phase structure and it is stable at all temperatures. Chromium (11-17% content) is the principal element which keeps the excellent corrosion resistance. Nickel and manganese are supposed to be little in content, and carbon and nitrogen traces should be decreased to the minimum amount. However, when the temperature reaches 1394°C, the delta ferrite (δ-Fe) would be formed, as indicated in Figure 1. The typical microstructure of the ferritic stainless steels are shown in Figure 13. The ferrite structure of AISI 409 is smaller than that in AISI 439.

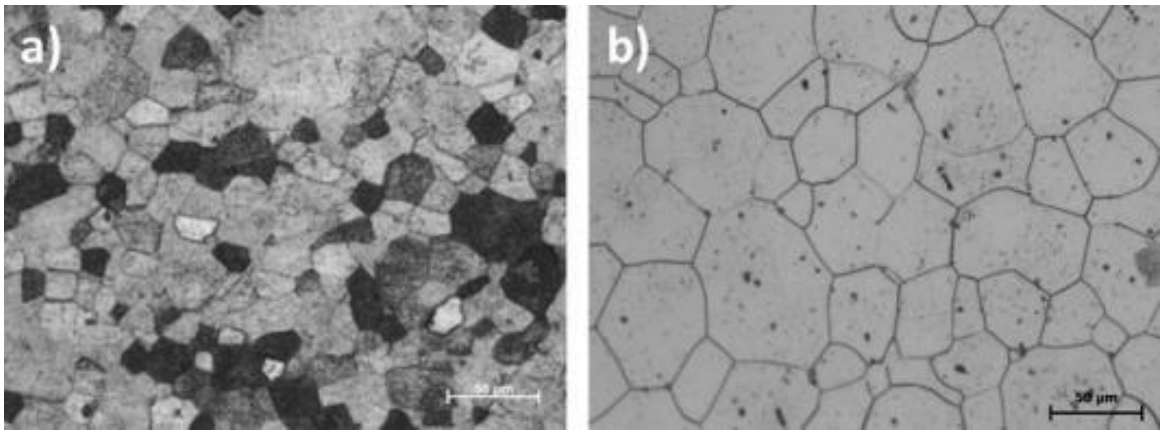

Figure 13. *Micrographs of ferritic stainless steel: (a) AISI 409; (b) AISI 439 [43].*

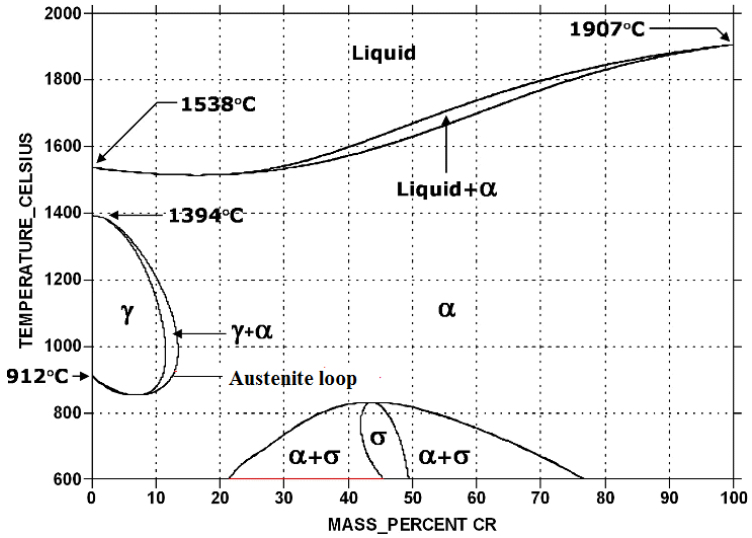

Figure 14. *Phase diagram of Fe-Cr alloy system [44].*

The specific microstructure constituents are influenced by the chromium content and the temperature, which is shown in Figure 14. It can be seen that when the chromium content is more than 12.7%, the alloy is fully ferritic with temperature up to its melting point. However, the common commercial ferritic stainless steels contain some amount of

austenite-forming elements, such as carbon and nitrogen. They make the actual chromium content range from 11% to 19% at elevated temperature when some austenites are formed [44-45]. The formed austenite lowers the rapid growth rate of ferritic grains at the elevated temperatures. The alloy can become fully ferritic at the normal solution annealed state, and become super ferritic grades when the chromium content is over 20% [45]. Super ferritic grades have very high content of ferrite and excellent corrosion resistance.

Schaffer diagram, which is initially used for determining the welded structures, is also a useful tool to study the phases and structures of the stainless steels, as shown in Figure 15. It explains the structures of the steel as a function of the contents of nickel and chromium. Compared with other stainless steels, ferritic grades have lower nickel and higher chromium contents.

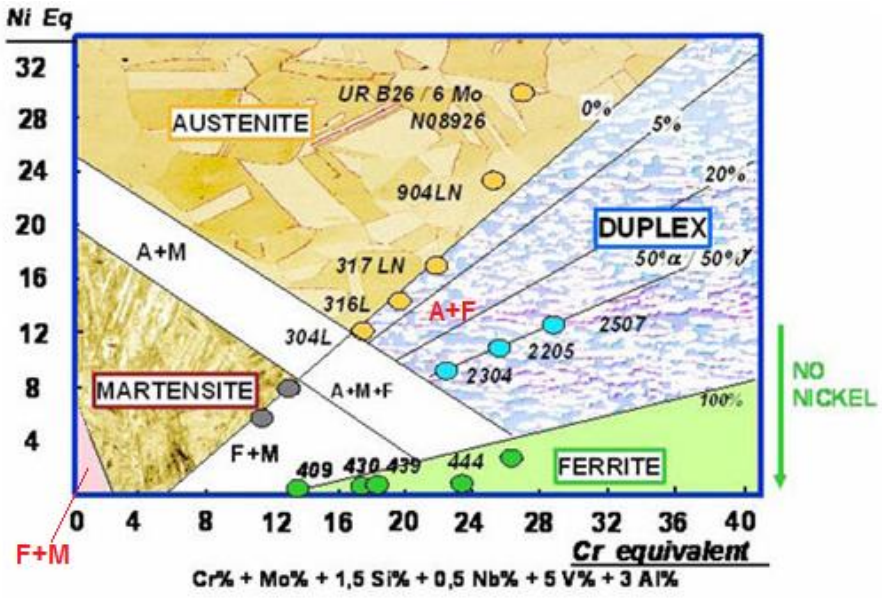

Figure 15. *Schaffer diagram of stainless steels [46].*

Intermetallic phases can also be formed in the ferritic steels. The most common one is the σ, which is formed at temperature 500-800 °C when chromium content is at around 22-76% [44]. σ is hard, brittle tetragonal phase with equal parts iron and chromium, the formation of which causes Cr depletion of the adjacent ferrites. σ phase is mostly formed along the grain boundaries and interface area, since the formation relies on the diffusion of chromium [47]. Figure 16 shows the morphology of σ with a phase transformation image. It was also found that the precipitation mechanism of the σ phase accompanies the χ phase in the δ-ferrite matrixes, and the precipitation of the σ phase causes degradation of the stainless steels [48].

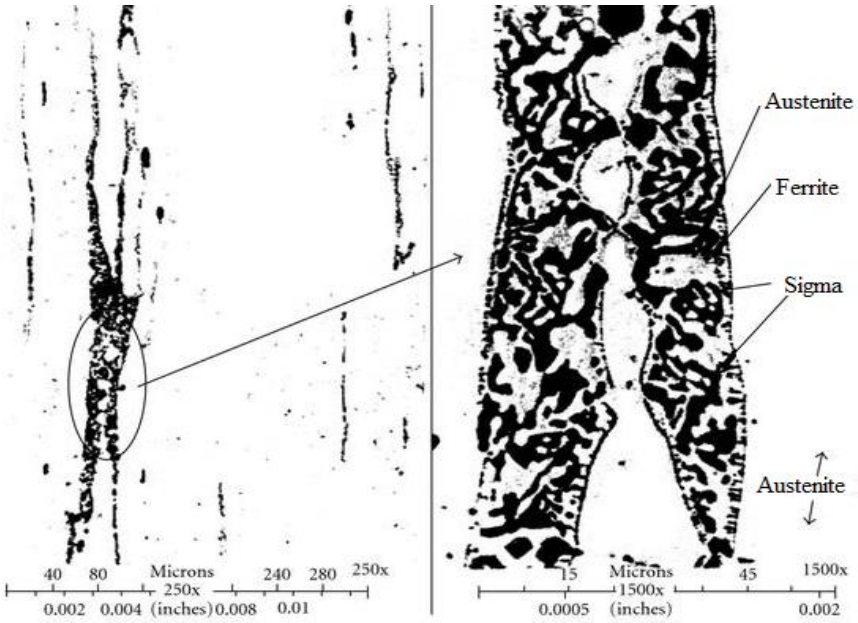

Figure 16. *Micrographs of the $\delta \rightarrow \sigma + \gamma 2$ transformation in AISI 304 stainless steel (650°C, 31000 h) [49].*

Another phase may occur in the stainless steel is the α' phase, which is formed through temper embrittlement at 475 °C [47]. Temper embrittlement is the segregation of phosphorus to prior austenitic grain boundaries and it does not occur in fully ferritic alloys. It has the same composition as σ phase, but exist at lower temperature. It has the same structure as ferrite, but there is chromium and iron atoms in an ordered bcc matrix. These atoms occupy the sites equivalent to two interlocking simple cubic matrices. Since its lattice matches the ferrite lattice well, the precipitate is coherent and cause hardening, as illustrated in Figure 17. The three stainless steels all show that the formation of α' phase takes over 70 h in these stainless steels, and the hardness increases steadily with its formation.

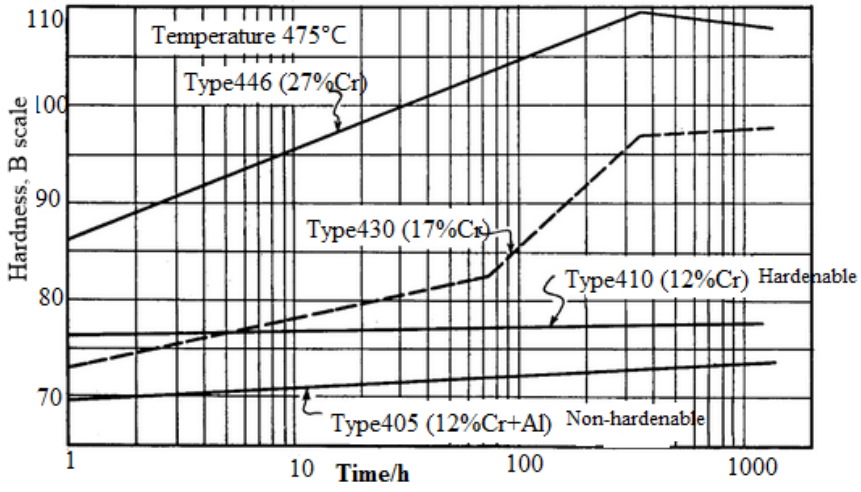

Figure 17. *Diagram of hardness as a function of time of few ferritic stainless steels during the formation of α' phase [47].*

Ferritic stainless steel is essentially Fe-Cr alloy with 11-30% Cr, other alloying elements like molybdenum, nickel, aluminum, titanium, etc. are also contained [42]. The specific composition greatly influences the constituents and the properties of the steel. Different grades of ferritic stainless steels based on the composition have been classified and regulated by standardization associations, like International Organization for Standardization (ISO), Deutsches Institut für Normung (DIN, in English, the German Institute for Standardization), EN, and etc.

Ferritic stainless steels are classified into different groups according to the chromium and molybdenum contents. The ferritic grades can also be categorized into standard grades and specific grades based on the composition specification, in the industry, the application of standard grades took up 91% in 2006, while specific grades took up 9% [46].

2.2.3 Categories of Ferritic Stainless Steels

Ferritic stainless steel grades are usually classified into five groups which consists of three families of standard grades and two of 'special' grades. The three standard ferritic grades are classified by the chromium content, with 10% - 14%, 14% - 18%, and 14% - 18% (with stabilization elements), respectively. The standard grades take up around 90% in application, whereas special grades take up to 10% [46]. In this section, AISI designation is used, which is different from EN designation.

In group 1, the stable austenite domain is at 1100-1200 °C, and a minimum of 13% Cr, no Ni and other low interstitial elements like carbon or nitrogen, may lead to a fully ferritic microstructure [46]. Figure 1 indicates that a ferrite → austenite transformation can happen when heated. Meanwhile, the grain refinement can be achieved, for example by applying mechanical vibration or electromagnetic force, and the martensitic transformation would happen in the steels with stable austenite loop (as indicated in Figure 14) when quenched to the room temperature.

In ferritic stainless steels, the amount of carbon is very small, which makes it not good heat treatable and have good corrosion resistance and oxidation resistance, but the hardness generally increases with carbon content. Besides, increasing the temperature can increase the carbides dissolution, which increases carbon content and hardness as well. However, when the temperature reaches 1150 °C, the δ-Fe would be formed, as indicated in Figure 18, δ-Fe is very brittle and lowers the steel's hardness [46].

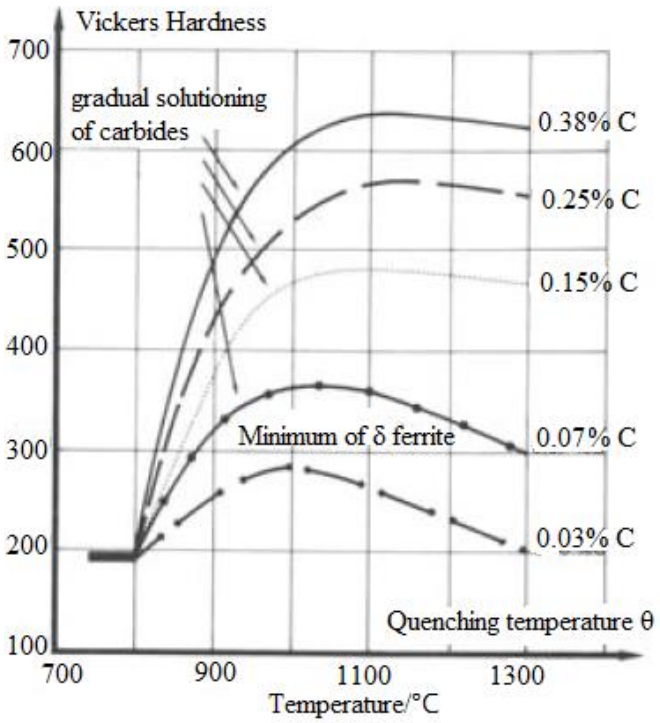

Figure 18. *Effects of carbon content on mechanical properties of 13% Cr stainless after quenching and after relieving with 200°C heat treatment [46].*

AISI 409 and 410L are typical ferritic stainless steels. AISI 409 was applied for automotive exhaust system silencer, and AISI 410L is ideal material for containers, LCD monitors framers [46]. Generally, group 1 ferritic stainless steels are suitable for the slightly corrosive environment.

Group 2 ferritic stainless steels contain 16-18% Cr, and the carbon content usually ranges within 0.02-0.05%, nitrogen content is generally at around 0.03%, and the carbon and nitrogen contents influence the microstructure a lot [46]. At high temperature, the structure consists of austenite and ferrite, while the fast cooling to room temperature would make the austenite/ferrite mixed region transfer to ferrite/martensite mixed microstructure. The final heat treatment is usually needed, and it depends on the composition of the steel. The microstructure after final heat treatment is a mixture of ferrite and carbides, the carbides is closely related to the carbon content and the former austenite enriched in carbon. Group 2 ferritic grades are quite brittle when welded, this is due to the grain coursing at high temperature in the heat affected zone of the welded part and the intergranular carbide precipitation [46]. They have higher corrosion resistance than Group 1 grades due to the higher Cr content. AISI 430 is the most common stainless steel of Group 2, which is widely used in household utensils like dishwashers, water pot, and etc.

Group 3 ferritic stainless steels contain 16-18% Cr and small amount stabilizing elements like Ti, Nb and Zr. These stabilizing elements tie up carbon or nitrogen in the stable compounds. They have strong affinities with other residential elements like sulphur and oxygen besides, which forms microstructures, and this also makes the fully ferritic microstructure at all temperature, and Cr-carbide precipitations are inhibited [46]. The stabilization property can be optimized by adding proper alloying elements regarding the service environment and property demands. Typically, the stability increases from NbC to TiC and to ZrC, especially ZrC is very stable at high temperature. These steels have better formability and weldability than Group 1 and 2 grades due to high portion of ferritic structure. They are applied to exhaust systems and welded parts of washing machines.

Group 4 ferritic grades are molybdenum alloyed with over 0.5% molybdenum and 17-18% chromium. The increased molybdenum promotes the ferrite formation and makes the steel a fully ferritic microstructure, and most of them are also fully stabilized by Ti or Nb elements [46]. They are more sensitive to the intermetallic phase precipitation when heated at high temperature, the corrosion resistance is relatively lower than other grades due to the lower Cr content. They are ideally used for solar water heaters, parts of exhaust systems, electric kettle, for example. AISI 444 is a typical grade in this group.

The group 5 ferritic grades have chromium and molybdenum contents of 25-29% and 3%, respectively [46]. The high Cr and Mo contents also make the ferritic microstructure. The intermetallic phase precipitations make them very sensitive to the embrittlement, for this, the carbon and nitrogen contents should be controlled at extremely low level for the structure stability. Nickel can lower the brittle-ductile transition temperature, but can also increase the phase precipitation, thus, its overall effect is uncertain. Grades AISI 445, 446, and 447 are in group 5, they can be applied to very severe corrosive environment.

2.2.4 Properties of Ferritic Stainless Steels

(1) Corrosion Resistance

Structural Applications of Ferritic Stainless Steels project [50] studied the behavior and durability of the ferritic stainless steels in different atmospheric environments. They exposed the flat sheets with different surface finish months in different places for up to 18 months. Besides, the laboratory tests were also performed to. It was found that only grade EN 1.4003 developed obvious corrosion. The study revealed the ferritic stainless steels' good resistance to different environments and corrosion in general. But they exhibited less resistance to crevice corrosion due to the lack of nickel [51].

(2) Physical Properties

European standards for stainless steel gives physical properties of stainless steels, the physical properties of the relevant ferritic grades are presented in Table 4, in which a carbon steel and austenitic grade 1.4301 are listed for comparison. It shows that ferritic grades have much higher thermal conductivity that the austenitic grades, which ensures high efficiency in the heat transfer. Meanwhile, they exhibit lower thermal expansion property, which makes them stable and less distortion when being heated.

Table 4. *Physical properties of some ferritic stainless steels [52-53].*

Grades (EN designation)	1.4003	1.4016	1.4509	1.4521	Carbon Steel
Density (g/cm^3)	7.7	7.7	7.7	7.7	7.7
Electric Resistivity (Ω*mm^2/m)	0.60	0.60	0.60	0.80	0.22
Specific Thermal Capacity (J/kg°C)	460	460	460	460	440
Thermal Conductivity (W/m°C)	28	26	26	26	53
Coefficient of Thermal expansion 0-100°C (10-6/°C)	10.4	10.0	10.0	10.4	12
Elastic Modulus ×10^3 (N/mm^2)	220	220	220	220	210

(3) Mechanical Properties

Plenty of mechanical properties can be presented and explained with engineering stress-strain curve. The difference of stress-strain behavior of ferritic stainless steel from other steels is presented in Figure 19. It exhibits higher strength and ductility than carbon steel. Table 5 presents some mechanical properties of some ferritic grades.

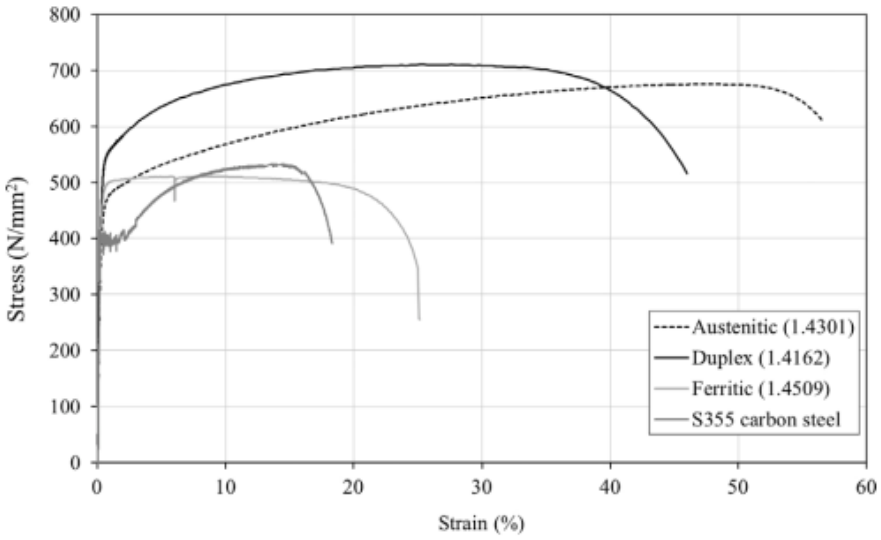

Figure 19. *Comparison of stress-strain behavior of austenitic, duplex, ferritic stainless steels and carbon steel [53].*

Table 5. *Mechanical properties of some ferritic stainless steels [54].*

Grades (EN designation)	1.4003	1.4016	1.4509	1.4521	1.4621	1.4301
Elastic Modulus, E (GPa)	194	183	198	194	184	-
0.2% Proof Strength, $f_{0.2}$ (N/mm^2)	330	311	331	375	359	-
1% Proof Strength, $f_{1.0}$ (N/mm^2)	357	333	353	396	373	-
Ultimate Tensile Strength, f_u (N/mm^2)	359	458	479	542	469	-
Fracture Elongation, A (%)	51	38	43	44	56	-
Nonlinearity factor, n	15.4	15.4	18	20.2	20.4	8
$f_{0.2(EN)}$ (N/mm^2)	280	260	230	300	-	230
$f_{u(EN)}$ (N/mm^2)	450-650	450-650	430-630	420-640	-	540

The high rupture elongation also indicates good formability. The relatively low rupture strain compared with duplex and austenitic stainless steels also corresponds to this. The 1% proof strength is just a little higher than the 0.2% proof strength, which indicates a rapid and short period of elastic deformation before plastic deformation.

According to Cortie and Toit [55], when the temperature is below 500 °C, there is very low solubility of carbon and nitrogen in the ferritic stainless steels. The excess of carbon and nitrogen will combine with the alloying elements which help form the carbide, as carbides or carbonitrides, in the matrix and precipitate, while the precipitation of the matrix of chromium carbides can be very harmful, especially to the corrosion resistance. The super-ferritic stainless steels are susceptible to the intermetallic compounds, which are precipitated when exposed at temperatures of 600 °C to 900 °C. The alloying elements normally increases these phase formation processes. In addition, the stainless steels with chromium content over 14% are susceptible to the decomposition, which results in the hardening and embrittlement of the alloy [55].

Ferritic stainless steel has higher YS value, and a lower work hardening rate than austenitic stainless steels. In addition, its ductility is reasonable and ultimate tensile stress is moderate, and toughness is relatively poor. The lower work hardening rate also makes it difficult to be strengthened through heat treatment, and it makes relatively low strength at high temperature compared with austenitic stainless steel. These properties of some ferritic stainless steels are compared in Table 6, in which the materials are designated with ASTM designation system, type 409 is equivalent to EN 1.4512, type 430 is equivalent to EN 1.4016, and type 304 is equivalent to EN 1.4301 [45]. The relatively high fracture elongation, together with Table 5 indicates good plasticity and formability.

Table 6. *Mechanical properties of ferritic stainless steels in annealed condition [55].*

Material	0.2% proof stress (MPA)	Ultimate tensile strength (MPA)	Elongation to fracture (%)	Strain-hardening coefficient, *n*
0.15% C carbon steel	285	385	37	0.20
Type 409	275	470	30	0.18
Type 430	345	515	25	0.18–0.22
Fe–29% Cr–4% Mo–2% Ni	400	550	20	~ 0.20
Type 304	255	620	70	0.30–0.50

In the production and treatment, ferritic stainless steels are annealed at temperature 750–950 °C, for avoiding austenite formation, which would transform to martensite while cooling and cause embrittlement [52]. Due to the high (C + N) / Cr ratio, which is easy to cause martensite formation and embrittlement in the heat-affected zone, ferritic stainless steels have poor weldability [56]. However, the modern ferritic steels are fully ferritic at all temperature, which improves the weldability. However, the grain growth in the heat affected zone reduces the ductility, which should be avoided. Meanwhile, ferritic stainless steels are also sensitive to the hydrogen embrittlement [52].

2.3 Strain Aging

Aging is a metallurgic phenomenon which refers to the increase of strength and hardness, together with the decrease of ductility and toughness at a given temperature. It especially occurs in low carbon steels. The aging is essentially attributed to the changes of state or location of solute elements. When the steel is firstly strained by plastic deformation and then it is to age, it has been strain aged. Technically, strain aging can be defined as the variation of the properties of an alloy due to the interaction among the interstitial atoms and dislocations [57].

Aging consists of quench aging and strain aging. Quench aging involves the precipitation from a supersaturated solid solution. Strain aging involves the redistribution of solute elements to the dislocation strain fields. Strain aging can be categorized into static and dynamic modes, when the strain aging occurs without plastic deformation, it is static; whereas when it occurs during the plastic deformation, it is dynamic. [58]

2.3.1 Static Strain Aging in Steel

Strain aging in the steel involves positioning carbon and nitrogen interstitial atoms which are in the solution in ferrite. This process causes some compression on the surrounding

crystal structure. Meanwhile, the dislocation stress fields contain tension regions due to the stress concentration, thus, migrating the carbon and nitrogen interstitial atoms into the tension region associated with dislocation would lower the energy and reach more stable status, thus, the migration happen naturally [58]. However, when the dislocations are moved away from the preferable carbon and nitrogen atoms, the strengthening effect is produced and the energy is improved. Therefore, this dislocation movement process demands some extra force, which leads to the increase of yield strength, as illustrated in Figure 20. This yield strength increment is manifested in the upper yield point.

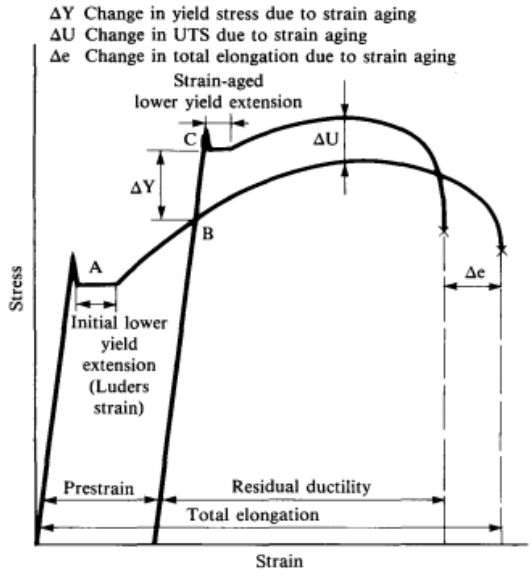

Figure 20. *Schematic representation of the influence of strain aging on the stress-strain curve for low carbon steel [59].*

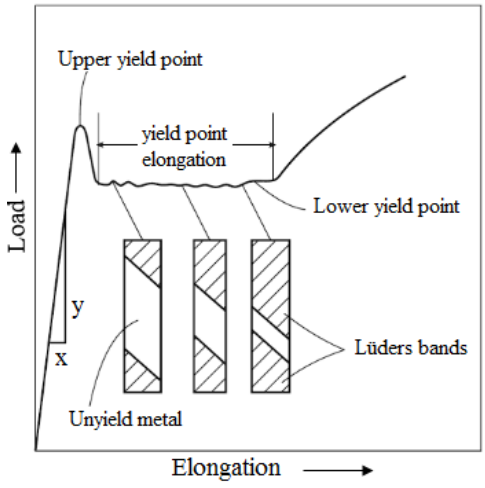

Figure 21. *Load-elongation curve of a low-carbon steel with Lüders bands [60].*

When the yield stress reaches the upper yield point, the dislocations move away from their carbon or nitrogen “atmosphere”, and lots of them would allow deformation to occur rapidly, and this process would lead to the decrease of yield stress to the lower yield point.

This yield stress decrease happens in stages, it is essentially related to the changes in Lüders bands, as illustrated in Figure 21. After the yield point elongation is achieved, the strain hardening would occur.

Figure 1 also shows that increasing pre-strain increased the ultimate tensile strength (UTS) increment of both dual phase carbon steel and micro-alloyed steel, which indicated that the value of ΔY (variation in yield stress due to strain aging). Yield strength is sensitive to the dislocation density and it depends on the solute segregation.

2.3.2 Dynamic Strain Aging in Steel

The aging process occurs slowly at room temperature and more rapidly at higher temperature, because the elements diffusion is aided by raising temperature. When the aging process occurs in the alloys which contain solute atoms and can rapidly and strongly segregate into dislocation sites and lock them during the strain aging, it is dynamic strain aging [61]. Therefore, the occurrence of dynamic strain aging (DSA) can be attributed to the interaction of diffusing solute atoms and mobile dislocations during the plastic flow. DSA is also a hardening mechanism for many materials, and it manifests itself by "jerky" or serrated plastic flow and inhomogeneous yielding [62].

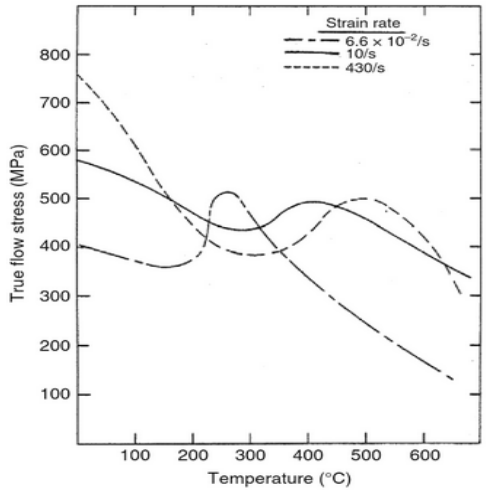

Figure 22. *True flow stress – temperature relations of low carbon steel showing anomalous strain rate effect due to dynamic strain aging [63].*

Figure 22 is an example showing DSA behavior. It can be seen that the true flow stress peak occurs at higher temperature with the increase of strain rate. When the carbon and nitrogen interstitial atoms are so mobile that the moving dislocations cannot pull away, the strain aging effect is produced and the dislocation movement is inhibited, the flow stress reaches the maximum and the peak occurs [58]. In this example, the anomalous strain rate effect creates a region at around 250°C. In most cases, raising strain rate

increases strength, whereas it is opposite in this region. In such regions, increasing strain rate increases average dislocation velocities and the amount of dislocation, and the strain aging effect cannot keep up, which leads to the strength decrease at higher strain rate.

2.3.3 Mechanisms and Metallurgical Causes

Strain aging is essentially due to the diffusion of carbon and nitrogen atoms to the dislocation sites in the solution. To start with, an atmosphere of carbon and nitrogen atoms is formed along the dislocation to stabilize it. But extended aging drives sufficient carbon and nitrogen atoms to form precipitates along the dislocations. These precipitates prevent the motion of subsequent dislocations, and causes hardening and the reduction of ductility. The aging at high temperature also leads to a saturation value above which the further aging does not affect [59]. Aging temperature and time are the predominant factors which influence strain aging.

Figure 21 presents the typical stress-strain curve of the low carbon steels. The aging process can be divided into two stages. The first stage is the diffusion of interstitials atoms (mainly carbon and nitrogen atoms) to the dislocation sites to form Cottrell atmosphere around the dislocations. The second stage is the carbides formation and precipitation on the dislocation. The Cottrell-Bilby theory [64] points out that the solutes are drawn to the dislocation core, and diffuse along the core to feed the precipitates particles at the intervals along the dislocations. The precipitated particles increase the UTS and the work hardening process and reduce the overall elongation, which is labelled as Δe in Figure 20. In some cases, when the concentration of solute is low, only the first stage works [1].

Cottrell's theory states that the carbon and nitrogen atoms in the solution diffuse to the positions of minimum energy to reduce the total distortional energy. The elastic interaction is strong enough to saturate the carbon or nitrogen atoms completely, which leads to the formation of a row of atoms along the core of the dislocations [1]. This segregation is the Cottrell atmosphere. Extra stress is required for the movement of the dislocations, which tear some dislocations away from their restraining impurity atoms, and causes an increase of stress. This corresponds to the upper yield stress, marked as point A in Figure 20. At the upper yield stress, some dislocations are moving, and when the dislocation line is taken out of the influence of interstitial atoms, it can slip and move at a lower stress, which is termed lower yield stress, marked as B in the figure. This theory also indicates that only a low concentration of carbon and nitrogen atoms is needed for pinning along the whole dislocation lines in the annealed low carbon steel [64]. This is a pioneering theory in strain ageing behavior, however, there is still doubt if the upper yield

point is related to tearing the dislocations away from their atmosphere. Besides, the theory could not explain the sharp yield point, which is related to very low density of dislocations [1]. New dislocations can be generated at stress concentrations points like the grain corners, boundaries, interfaces, edges, etc.

The presence of interstitial elements is the most predominant factor for strain ageing. The atoms are spread in the constituents of the microstructure like iron carbides. Nitrogen atoms and some carbon atoms which are not absorbed in the iron carbides, and they exist in the phases which are rich in iron. After the cooling of the steel, these atoms migrate through the crystal structure to the dislocation sites due to the lattice distortion in the crystal. The migration process of these atoms also stabilize the crystal, making the slip of the dislocation line more difficult. [1]

The diffusion process is directly affected by the temperature due to the thermal energy. The complicated microstructure and higher carbon content make the strain ageing not happen at room temperature since the massive diffusion of atoms such microstructures take higher energy [65]. Generally, bake hardening at temperatures of 150–370 °C for 1–5 h is necessary for developing aging effects [66].

There is also a second strengthening mechanism, which occurs when the plastic deformation is performed to the steel [66]. When the dislocations are broken, they would move and interact with each other, which causes pinning of each other and make movement and diffusion more difficult, thus decreasing mobility and increasing strength, ductility and toughness are also lowered at the same time. In addition, when heat treatment is applied, the steel is further hardened and strengthened, and the ductility and toughness are reduced at the meanwhile. The effects of these two processes cause great damage to the toughness of low carbon structural steel. These are also the main causes and effects of strain ageing.

2.3.4 Control of Strain Aging

As discussed above, the presence of interstitial atoms (mainly carbon and nitrogen atoms) is the predominant factor causing strain ageing, and very small amount of them can cause strain ageing. Therefore, one goal and approach for controlling strain ageing is to eliminate the interstitial elements, especially carbon and nitrogen atoms. The measures can be taken from steel making procedure. Rajendrem, *et al*. [67] found that the gap and processing time in the continuous casting process are the major causes for nitrogen pickup, thus, and suggested controlling these factors at primary and secondary steelmaking

processes, as well as at continuous caster, can eliminate the pickup of nitrogen. Huo [68] suggested basic oxygen steelmaking route is more effective than conventional electric arc furnace steelmaking route. Huo [68] also suggested to introduce iron carbide powder into the molten bath at the relatively late part of the melting to get ideal nitrogen content. However, the expense is always of concern and it is difficult to find an approach which can remove nitrogen completely.

Another idea to eliminate nitrogen is to form nitride with aluminum, which is also important for controlling grain size during the heat treatment and cooling period. This can remove the free nitrogen from the steel and reduce the strain ageing [66]. But it is not always effective since some aluminum-deoxidized steels are susceptible to strain aging. Deoxidation is an important measurement of eliminating nitrogen. Some deoxidizers are very effective, for example, coarse-grained steels can be treated with small amount of aluminum, titanium, or zirconium [69].

Reducing the loss of toughness in the strain aging is another approach. To achieve this, it is necessary to apply heat treatment after straining to cause over-aging, which causes a loss in hardness and an increase of ductility [59]. This approach is effective for some products like pressure vessels, but not for bridges or other large-scale structures. The limitations of the approach are the high cost and shape change, which is due to the possible distortion and creeping when applied for large structures [64].

Generally, the control of strain ageing is closely related to the causes of strain ageing, i.e. carbon and nitrogen atoms and concentration, heat treatment temperature and time, etc. are what need to be controlled, especially eliminating the entry of nitrogen. However, even the approaches mentioned above can help to control the effects of strain ageing, there is no single approach that can avoid or reduce it completely. When the strain aging is difficult to be eliminated, especially in the large and complex structures, high performance steels are designed with toughness that can meet the requirements. [70-71].

2.4 Bake Hardening

2.4.1 Background of Bake Hardening

Bake hardening (BH) is a phenomenon of the strain aging, and it is also the mechanism of the strength increment in the strain aging. It utilizes the phenomenon of strain aging to provide an increase in the yield strength of the formed components. In the application of auto-body panels, this strength increment is developed during the low temperature (150-

200 °C) paint baking [72]. It was developed in 1980s for improving the strength of the parts manufactured for demanding stretch forming applications and utilized in the painting [73]. It is especially ideal for the cold formed sheet metallic parts which requires good formability, and it does not affect the production cost much [74].

The increase of yield strength occurs in the thermal treatment during the paint baking of the steel is the bake hardening effect. These steels are generally soft, but they have excellent plasticity and formability, while they achieve high strength during the paint baking. From the metallurgical viewpoint, bake hardening is essentially an elevated temperature strain aging process caused by the migration of the interstitial solute atoms (mainly carbon and nitrogen atoms) to the dislocation sites. The diffusion process is affected by temperature, the amount of free carbon and nitrogen atoms, grain size, the density and amount of dislocation [73-74]. Meanwhile, the nitrogen atoms also diffuse to the dislocation sites fast even at room temperature. Besides, their movement makes strain aging, the increase of the yield strength is thus very difficult to be controlled [75]. The nitrogen is precipitated in the form of AlN and removed from the solid solution. Consequently, the final properties of the bake hardening steels is mainly determined by the dissolved carbon [76].

The increase of the yield strength can also be achieved by alloy design, which involves the chemical composition of the steel. Carbon is the most important element in such steels, the content of which used to be over 0.05%, however, the vacuum degassing technique enables 0.01–0.03% carbon bake hardening steels, which are called extra low carbon (ELC) steel. What's more, the ELC grade steels with less than 0.003% carbon with excellent formability can be produced nowadays, and 0.0015–0.0025% carbon creates the optimum bake hardening effect and avoid room temperature aging [73, 77].

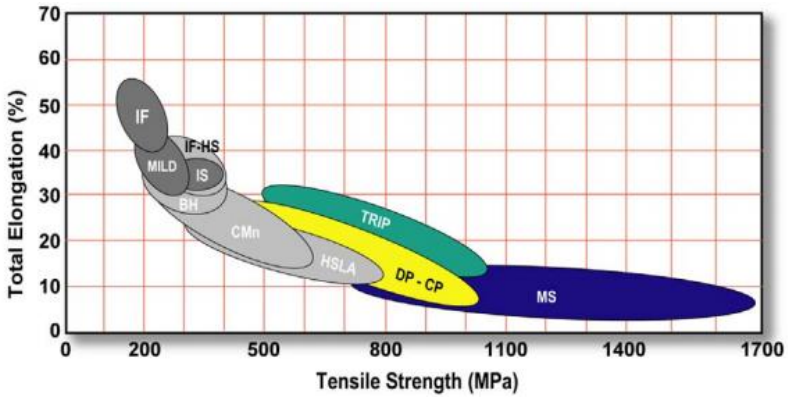

Figure 23. *Schematic representation of strength-elongation combination of different types of steels used in the parts of cars [78].*

The tensile properties of bake hardening steels are compared with other grades of steels in Figure 23. The lower strength steels are in dark grey, and the high-strength steels (HSS) are in light grey, the advanced high-strength steels (AHSS), which include Dual Phase steel (DP steel), Complex Phase (CP) steel, Transformation Induced Plasticity (TRIP) steel, Martensitic Steels (MS) are in colors. Bake hardening (BH) steels have low YS value and good formability, which makes it ideal material for forming complex parts.

In the process of shape forming and paint baking, the occurrence of aging leads to discontinuous yielding which increases yield strength. The yield strength increase of the bake hardening steel is compared with the tensile behavior of mild interstitial free (IF) steel and high strength rephosphorised steel in Figure 24. It shows that the bake hardening steel can achieve both good shape and good dent resistance.

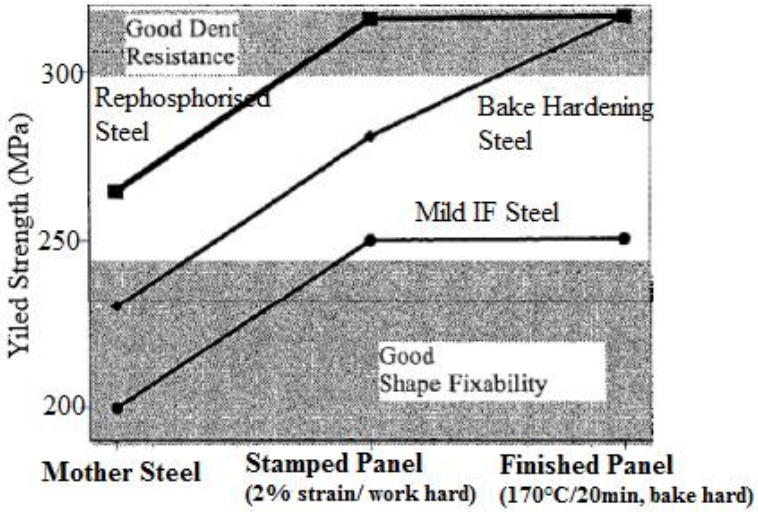

Figure 24. *Schematic illustration of the behavior of bake hardening steel compared with mild IF steel and rephosphorised steel [79].*

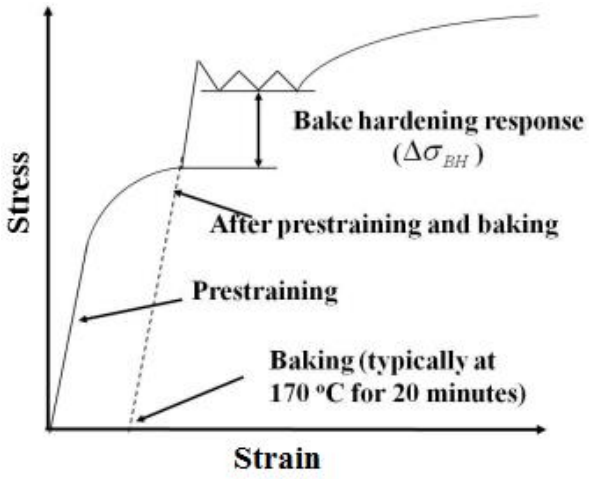

Figure 25. *Schematic representation of bake hardening response in tensile test [80].*

Bake hardening steels exhibit an increase in yield strength after pre-straining. Figure 25 illustrates a typical bake hardening response of in the tension test after pre-straining. The sharp yield strength, yield point elongation and modified work hardening behavior are important features and properties [81]. The bake hardening behavior is measured in the following process: the specimen is firstly pre-strained to 2% with tension at room temperature, then be unloaded, aged at 170 °C for 20 min and then tensile tested again at room temperature [82]. The bake hardening response is defined as the difference between the lower yield stress after baking and the final flow stress after pre-straining, as shown $\Delta\sigma_{BH}$ in Figure 25. De [83] found that the yield strength can be increased 30-40 MPa for ultra-low carbon steels.

2.4.2 Mechanisms

The yield strength increase from the bake hardening is mainly attributed to the static strain aging, which is essentially a diffusion process. The interstitial atoms (mainly carbon and nitrogen atoms) migrate to the dislocation sites and lock the mobile dislocations, which causes the increase of the yield strength via discontinuous yielding since the new mobile dislocations are created to keep the plastic flow going on [84].

Conttrel and Bilby [64] firstly studied the theory and kinetics of dislocation pinning in the strain aging, found that carbon atoms segregate to form the atmosphere around the dislocations, which is called Conttrel atmosphere. Wilson and Russell [85-87] continued the study on the strain aging, explored the theories and mechanisms of the strain aging, and proposed the following stages of aging in the mild steels: (a) stress induced ordering of interstitial atoms; (b) interstitial atoms segregation and dislocation locking by Cottrell atmospheres; (c) formation and precipitation of solute cluster. The whole mechanism is explained as below.

Snoek [88] studied the effect of small amount of carbon and nitrogen atoms on the iron's properties. He found that when the external force is applied on the material, the crystal expands along the direction of the force, the interstitial atoms would migrate to occupy the dislocation sites in the strain direction. While when the force is removed, the interstitial atoms are distributed again randomly, which is the stress induced ordering, and it's also named "Snoek effect". When the applied force exceeds the elastic limit of the specimen, the new dislocations are produced. If such pre-strained material is then thermally treated with aging at short time and higher temperature, the interstitial atoms will migrate to these new dislocation sites and lock them by forming an atmosphere around the dislocations, which is named Cottrell atmosphere [86-87].

With more and more solute atoms are attracted to the dislocation strain area, a solute cluster can be formed, and in some extreme cases, when the solute cluster is strong enough, it would make these interstitial atoms along the cores of dislocations [89]. Wilson and Russell [87] also supported the above point. They found that the precipitates (carbide particles for instance) would be coherent once they are formed. The process of bake hardening is illustrated in Figure 26.

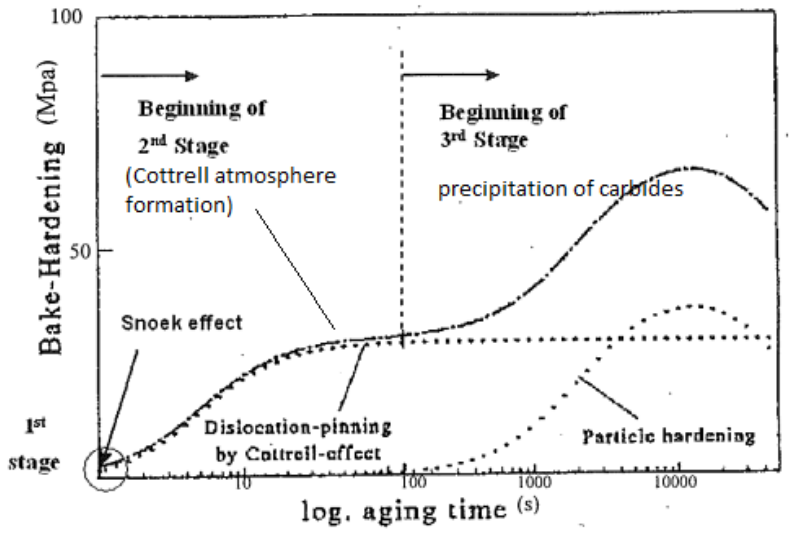

Figure 26. *Schematic illustration of three stages in bake hardening [90].*

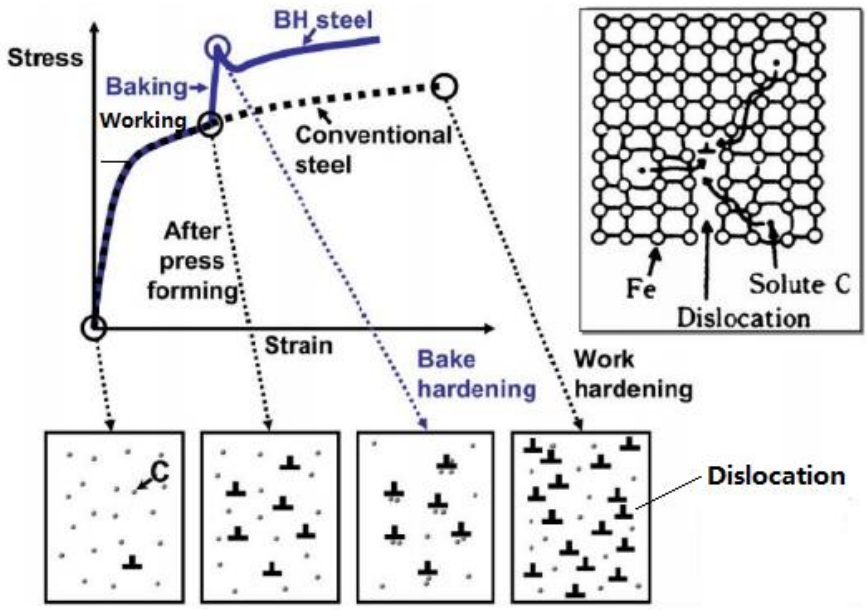

Figure 27. *Diagram of engineering stress-strain curve of low carbon steel demonstrating the variation of dislocation and carbon atoms [91].*

To gain a further understanding of how the bake hardening affects the properties of the material, Kurosawa *et al*. [91] studied motion of solute carbon atoms and variation of dislocations at different phases. It was found that, very few dislocations exist before the

external force is applied. With the increase of the force and pre-strain, more dislocations are created, which produce work hardening effect. Afterwards, the bake-hardening heat treatment enables more solute carbon atoms to move to the dislocation sites, while the amount of dislocations is not significantly increased, the mobility of the dislocation is reduced, which produce a bake hardening effect. These two hardening effects contributes to the final yield strength increase of the material. Figure 27 illustrates the dislocation situation of the specimen at different period of bake hardening treatment.

2.4.3 Kinetics of Bake Hardening

The bake hardening process, which consists of three stages of Snoek effect, Cottrell atmosphere formation, and particle hardening (carbide precipitation), is essentially a diffusion process. The carbide precipitation only occurs after the formation of Contrell atmosphere, however, it is not accurate to simply understand the process by adding the three periods, since the different influence of each stage on the bake hardening behavior should be considered. Cottrell-effect is the most dominant stage among three stages, which is restricted by the long time and high temperature, as shown in Figure 28.

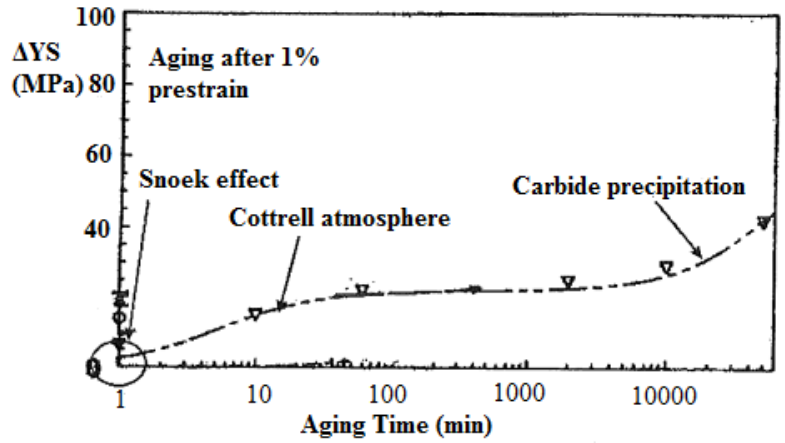

Figure 28. *Schematic presentation of the yield strength as a function of ageing time during bake hardening process [80].*

In theory, the increase of yield strength during bake hardening can be expressed as:

$$\Delta\sigma_{BH} = \Delta\sigma_{Snoek} + \Delta\sigma_{Cottrell} + \Delta\sigma_{Precipitation} \quad \text{(Eq 2)}$$

Where $\Delta\sigma_{Snoek}$, $\Delta\sigma_{Cottrell}$, and $\Delta\sigma_{Precipitation}$ are the strength increments due to the Snoek effect, Cottrell atmosphere, and carbides precipitation, respectively. However, Elsen and Hougardy [74] considered that the final BH response is basically affected by two effects, namely Cottrell atmosphere formation and the particle precipitation during bake hardening. The curve above also shows that the Snoek effect has very slight effect on the

yield strength increment. Thus, the expression of the yield strength increment is:

$$\Delta\sigma_{BH} = \Delta\sigma_{Cottrell} + \Delta\sigma_{Precipitation} \quad \text{(Eq 3)}$$

However, this expression is just for a general understanding of the BH response, Elsen and Hougardy did not consider the influence of solute atoms and other elements on the yield strength increments. The influence of several factors on the bake hardening responses are discussed in the next section.

2.4.4 Influence of Interstitial Atoms

As mentioned above, the bake hardening is essentially a diffusion process which relies on the migration of the interstitial atoms. Thus, the content of the interstitial carbon and nitrogen atoms has significant influence on the bake hardening. For BH steels, sufficient "shelf life" is always necessary to ensure that the material would not undergo aging and deteriorate in the transportation and storage before actual application. BH steels are expected to have at least 3 months "shelf life", and Bhagat's study [92] about calculating the "shelf life" of BH steel also exhibits a close relationship of the nitrogen and carbon content with the "shelf life". Nitrogen is especially deleterious since it diffuses rapidly even at room temperature and makes aging and lead to the formation of Lüders bands (stretcher strain), which should be avoided [75].

The BH response increases with the increase of solute carbon in the steel, since more interstitial atoms are available and more solute can pin the dislocations, which forms solute cluster more rapidly. Snick supported this [79], claiming that when the carbon content increases from 0 to 40 ppm, the bake hardening responds a yield strength of 50-80 MPa. However, it was noticed that the further increase of carbon content does not increase the yield strength, and it would be stable at certain amount. Hainai *et al*. [93] studied the effect of solid solution strengthening elements on the bake hardenability with Al-killed steel which contained only 0.04% carbon content. They found that the increase of yield strength reaches maximum when the sum of the content of carbon and nitrogen is 20 ppm. However, that study did not reveal if the BH response can increase more when the content of the solute atoms is over 20 ppm. Nevertheless, with the further increase of carbon content, they would segregate and lock the dislocations even in the pre-straining and reduce the BH response. This is demonstrated in Figure 29, in which ppm is short for parts per million.

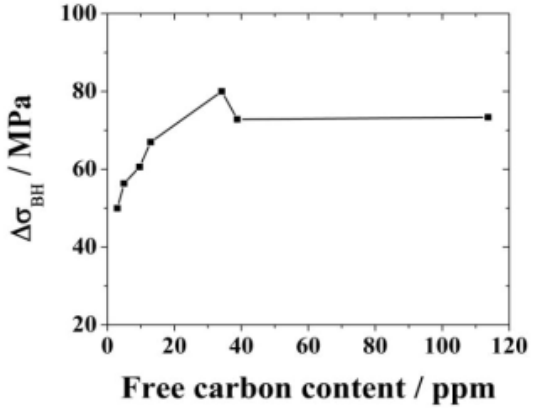

Figure 29. *Yield strength increment as a function of free carbon content during bake hardening response [79].*

The effect of the increase of the carbon content on the room temperature aging and BH response can also be understood by different levels of carbon content. Rubianes and Zimmer [94] found that when the carbon content is no more than 3 ppm, steels are very stable at room temperature and bake hardening is not shown, which is the region Ⅰ in the Figure 30. When the carbon content is above 3 ppm while lower than 7 ppm, the steels have good BH response from 20 to 60 MPa yield strength increase, and have resistance to the room temperature aging. When the carbon content is over 7 ppm, the yield strength increase is excellent, but it does not increase much with the further increase of carbon content, whereas the room temperature aging is very likely to happen. Thus, BH grade steels are supposed to be designed in region Ⅲ.

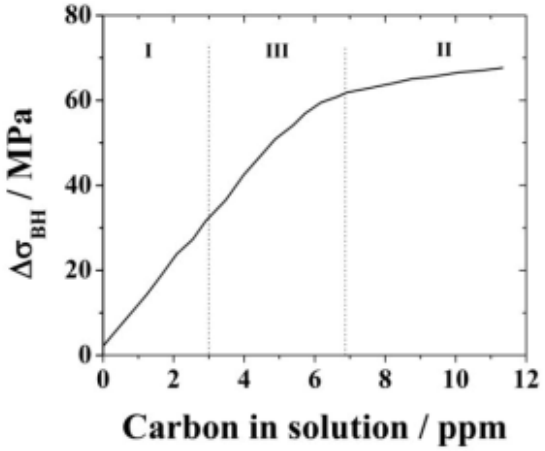

Figure 30. *Yield strength increment as a function of carbon content in solution during bake hardening response [94].*

2.4.5 Influence of Pre-strain

Generally, many parts or components undergo small amount of straining during the forming process or other processes before bake hardening. Thus, it is necessary to subject the specimens to a small amount of pre-strain at room temperature, for the simulation of

the real situation. De *et al*. [95] studied the BH behavior of ultra-low carbon (ULC) steel, they found that the maximum increase of yield strength at the end of Cottrell atmosphere was the same for all the experimented pre-strain levels (1%, 2%, 5%, 10%), as shown in Figure 31, the amount of pre-strain did not influence the Cottrell atmosphere formation. The mechanism is the saturation of the dislocation sites, that the required Cottrell atmosphere for saturation is the same for all dislocations and does not change with the increase of dislocation density within strain range.

Elsen and Hougardy [80] studied the mechanism of bake hardening, and found the increase of yield stress in the bake hardening contains two successive steps. The first step is the Cottrell atmosphere formation, as discussed above. The second step is the carbides precipitation. They also found the decrease of yield strength increment with the increase of pre-strain level during the second step, which indicates that most carbon atoms segregate to the dislocations at the first step.

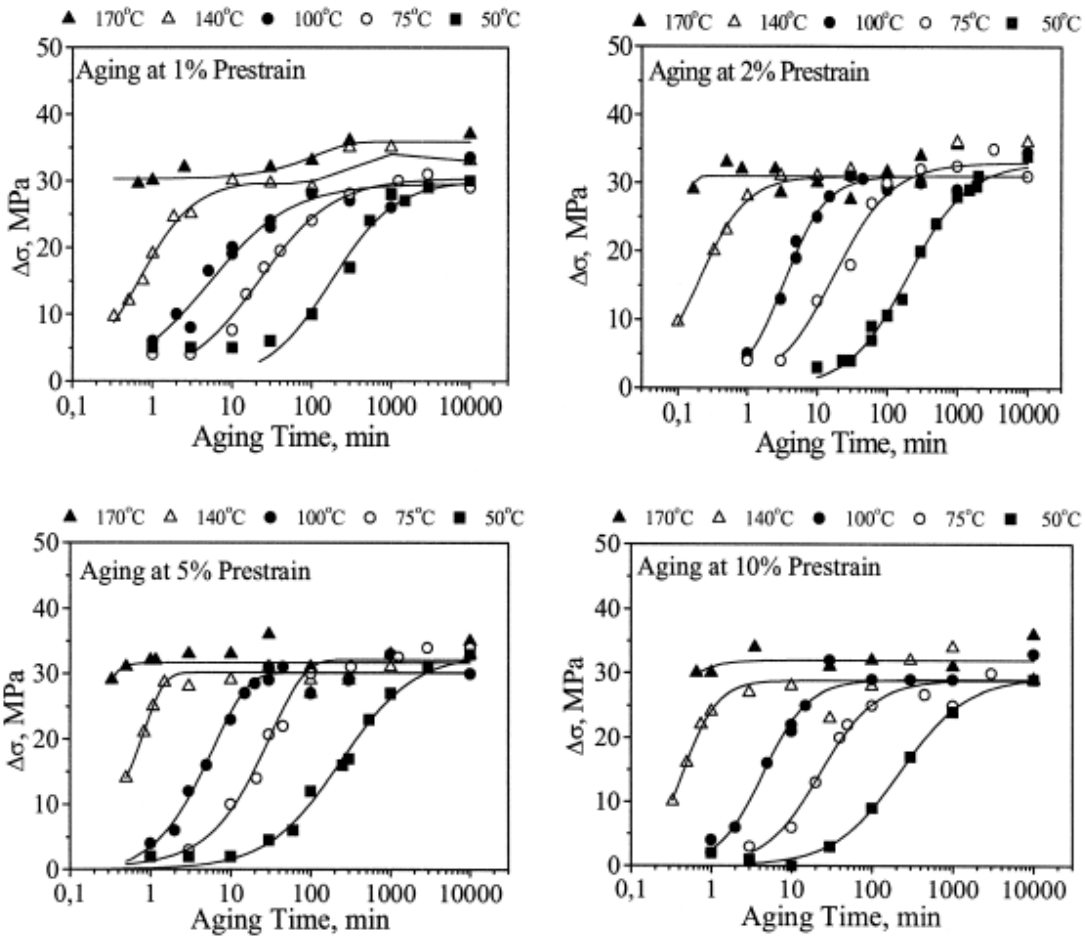

Figure 31. *Increase of yield strength of ultralow carbon steel with different pre-strains of 1%, 2%, 5%, and 10%, respectively [83].*

De *et al*. [83] studied the dislocation density with ULC steel, and found the increase of

yield strength is mainly from the first step and not much from the precipitation step. However, this is not applied to ELC steel, in which, the BH response is mainly from the precipitation step. Tang *et al*. [96] studied the effect of pre-strain on the properties of TRIP steel, finding that the yield strength increases markedly with the increase of pre-strain within the range of 0 – 4%, while it increases slightly when the pre-strain ranges from 4% to 16%. Kuang *et al*. [97] studied similarly with dual-phase steel, finding that the yield strength increases obviously with increase of the pre-strain from 0% to 1%, while when pre-strain ranges from 1% to 8%, the yield strength even decreases. Many similar studies reveal that the effect of pre-strain level on the BH response is related to the material itself, but a common result is that the BH response increases with the increase of pre-strain within a very small range.

2.4.6 Influence of Baking Temperature and Time

Since the strain aging depends on the diffusion of interstitial atoms, temperature and time are the dominant factors affecting the diffusion. Therefore, it is necessary to discuss the effect of baking temperature and time on the strain aging.

De, *et al*. [83] studied the BH behavior of ULC steel with different aging time and temperature, they found that the yield stress firstly increases with the baking time (or aging time) until the yield strength increment reaches certain limit of 30-40 MPa, then remains almost stable even the baking time continues increasing, the maximum increase of yield stress is independent of aging temperature, which was shown in Figure 31. Meanwhile, Figure 31 also illustrates that with the increase of baking temperature from 50 °C to 170 °C, the yield strength increases faster and reaches the stable yield strength in shorter time, and this applies to different pre-strain levels.

Dehghani and Jonas [98] investigated dynamic-static bake hardening and dynamic bake hardening, they found that both hardening achieve higher yield strength than the conventional bake hardening. The scientists pre-strained the specimens at elevated temperatures before bake hardening. Their results showed that the BH response is remarkable when the baking temperature is higher than the pre-straining temperature, while the BH response gets very slight when the baking temperature is lower than pre-straining temperature. The mechanism for the latter case is that the relatively higher pre-straining temperature causes massive interstitial atoms migration, Cottrell effect, and carbide precipitation. However, the large amount of carbides limits the response in the relatively low temperature bake hardening.

3 MATERIALS AND EXPERIMENTS

In this chapter, the experimental materials and procedures are introduced, the procedure of micrographic observation is described and initial micrographs are presented. In addition, the basis of tensile test data analysis is discussed and the principles for determining bake hardening and aging indexes are presented.

3.1 Materials

The investigated materials consisted of three commercial steels: two low carbon steels and a ferritic stainless steel (EN 1.4003). The samples of the carbon steels were provided as tensile specimens by SSAB Europe Oy (Hämeenlinna). The samples of the EN 1.4003 ferritic stainless steels were provided by Outokumpu Oyj.

In this thesis, two low carbon steels are named steel A and steel B, EN 1.4003 ferritic stainless steel is named steel C. The chemical analysis of the three experimental steels are presented in Table 7. As indicated in the chemical composition, two low carbon steels have quite similar chemical composition. The ferritic stainless steel (steel C) is unstabilized, i.e., it is not alloyed with stabilizing elements Nb, Zr or Ti.

The steels A and B had been produced in the continuous production lines combining continuous annealing and subsequent hot-dip galvanizing. Steel A had been annealed at 740 °C and steel B at 780 °C. The difference of the annealing temperature can cause the difference of free carbon contents in the solution, which is vitally important to the bake hardening behavior. The coiling temperature was the same, 720 °C, in both cases.

Table 7. *Chemical compositions (% by weight) of three experimental materials.*

Materials	C	Si	Mn	P	S	Al	Cu	Cr	Ni	N	B
A	0.072	0.01	0.211	0.005	0.0092	0.024	0.021	0.249	0.035	0.0038	0.0016
B	0.073	0.015	0.223	0.009	0.01	0.036	0.017	0.301	0.041	0.0037	0.0021
C	0.013	0.34	1.36	-	-	-	-	11.24	0.36	0.0057	-

3.2 Metallographic Observation

The initial microstructures of the test materials were investigated by using the optical microscope. The cross-sectional samples of each material were prepared. The samples were cut to both transverse and longitudinal directions with respect to the original rolling direction. The metallographic observation of the specimens consists of two parts, namely sample preparation and microstructure observation.

The sample preparation followed a standard procedure. The cross-sectional samples were cut by using a cutting machine Struers Discotom-10. The sample pieces were then mounted in epoxy in vacuum with machine Struers CitoVac. The samples were ground with a number of grinding steps with sandpapers of different levels of smoothness (P320 – P600 – P800 – P1200 – P2000). In the operation, the sandpaper was fixed on the spinning pan of the Buehler Phoenik 4000 sample preparation system, and the spinning speed was set at 300 revolutions per minute (rpm) and force was set at 20 N, the specimens were grinded with each sandpaper for 1 minute.

After grinding, polishing was performed with the same machine of grinding, the spinning speed of the pan was 150 rpm, the force was 20 N, the polishing paper was changed every 30 seconds. The samples were polished with 3 µm and 1 µm diamond solutions, which was applied every minute. The polishing was supposed to make the specimen surface very smooth and bright.

Finally, for two low carbon steels, the specimen surface was etched with 4% nital for 6-7 seconds; for ferritic stainless steel, the specimen surface was etched with etchant V2A (100 ml water, 100 ml hydrochloric acid, 10 ml nitric acid), which was heated up to around 80 °C. However, there were some problems when etching ferritic stainless steel. Thus, only one image (transverse to the rolling direction) of the ferritic stainless steel is presented in Figure 32. The etched sample surface was then examined with optical microscope, and the microstructure pictures were taken.

Optical micrographs of the investigated steels in as-received condition are presented in Figure 32. As can be seen, low carbon steels A and B consist primarily of ferrite and randomly distributed cementite (the dark micro-constituent mostly at the grain boundaries and intersection are of the grains in the pictures). Steel A and B also show very similar microstructure. The grains of steel C are generally flatter and less evenly distributed than the grains in steels A and B. In comparison, the microstructure of steel C shows smaller amount of cementite due to lower carbon content.

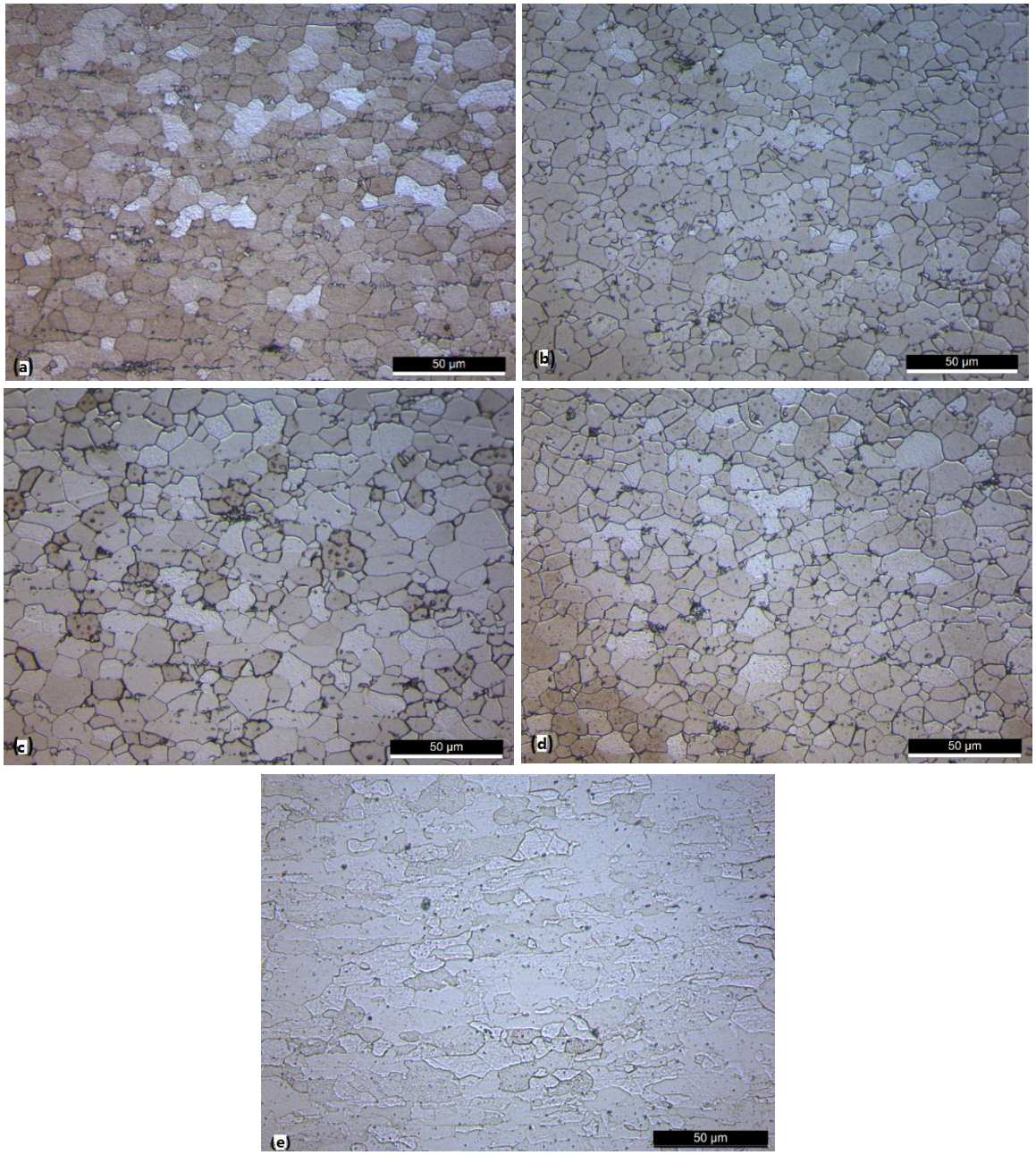

Figure 32. *Optical micrographs of the investigated steels: (a) A material of longitudinal direction, (b) A material of transverse direction, (c) B material of longitudinal direction, (d) B material of transverse direction, (e) C material (EN 1.4003 ferritic stainless steel) of transverse direction.*

The mean linear intercept method was used to measure the grain size of the initial materials. Two optical images with 50× objective lens magnification of each material were used, and eleven straight lines were made in each image, as shown in Figure 33. The numbers of intercepts were counted, and the length of the lines were shown. Thus, an average value of the grain size can be determined from each line. Therefore, there were 22 lines and 22 average values of grain size were available for each material. To eliminate the error, the maximum and minimum values were deleted, and the remained 20 average

values were used to calculate the final average grain size (diameter) *D* by using the following formula. The grain sizes of three as-received steels are presented in Table 8.

$$D = \frac{1}{20} * [\frac{L1}{n1} + \frac{L2}{n2} + \ldots + \frac{L20}{n20}] \quad \text{(Eq 1)}$$

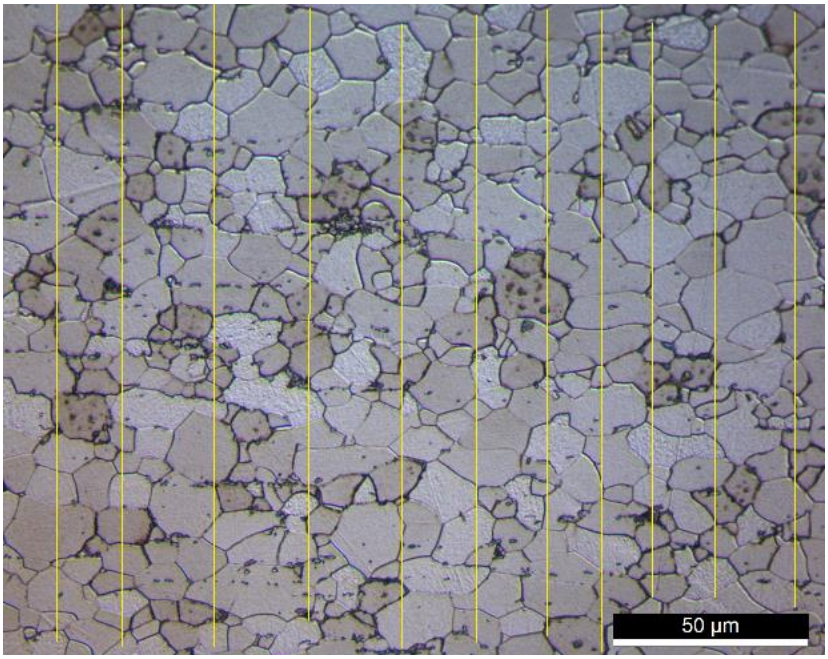

Figure 33. *Illustration of the method of measuring grain sizes of initial materials.*

Table 8. *Grain diameters of as-received materials*

Materials	A	B	C
Grain Diameters (µm)	7.0	7.7	7.9

3.3 Bake Hardening Test

The as-received materials were subjected to bake hardening tests. The specimens were first pre-strained to 0, 2, 6, or 10 %. After that, the pre-strained samples were subjected to baking treatments of 170 °C/20 min and 230 °C/20 min. Finally, the mechanical properties of the bake hardened specimens were determined with quasi-static tensile tests.

Each specimen was given a series number from 1 to 18, like A1 to A18, B1 to B18, and C1 to C18. Then the specimens were classified according to the experimental plan, as shown in Table 9. To eliminate the error from experiments and specimens, two specimens were used for repeated experiments to determine the properties, the values of the properties are the average values of the two results.

Table 9. *Experimental plan for the bake hardening tests.*

	Steel A	**Steel B**	**Steel C**
No Bake Hardening	A1, A2	B5, B6	C1, C2
170℃/20min	A3, A4	B1, B2	C3, C4
230℃/20min	A5, A6	B3, B4	C5, C6
2% pre-strain	A7, A8, A9, A10	B7, B8, B9, B10	C7, C8, C9, C10
6% pre-strain	A11, A12, A13, A14	B11, B12, B13, B14	C11, C12, C13, C14
10% pre-strain	A15, A16, A17, A18	B15, B16, B17, B18	C15, C16, C17, C18
2% + 170℃/20min	A7, A8	B7, B8	C7, C8
2% + 230℃/20min	A9, A10	B9, B10	C9, C10
6% + 170℃/20min	A11, A12	B11, B12	C11, C12
6% + 230℃/20min	A13, A14	B13, B14	C13, C14
10% + 170℃/20min	A15, A16	B15, B16	C15, C16
10% + 230℃/20min	A17, A18	B17, B18	C17, C18

3.3.1 Tensile Testing

The tensile test specimens of the material A and B had been machined according to international standard ISO 6892: 1998 (gauge width 20 mm). The testing direction was perpendicular to the original rolling direction. The dimensions of the specimens are described in Table 10. The dimensions of each individual tensile test specimen were measured by a using a micrometer.

Table 10. *Dimensions of the tensile specimens.*

	Carbon Steel Specimens	**Stainless Steel Specimens**
Thickness t	0.55mm	1.97mm
Width of gage section W	1-6: 19.3mm Others: 16mm Exceptions: B15-B18	16mm
Gage length G	120mm	120mm
Overall length L	25mm	23.5mm
Length of grip section B	30mm	30mm
Width of grip section c	50mm	43mm

However, after pre-straining and baking treatments the specimens were re-machined to reduce the width of the gauge length to around 16mm, and the radius of the curvature was reduced to 10mm. It was to avoid the localization of the necking occurring at the softer area where the work hardening during pre-straining had not occurred. While there were also exceptions like specimens B15 to B18, the machining was not successful with these specimens in the first step. Thus, the gauge width was exceptionally small. The dimensions before and after re-machining are presented in Appendix A.

Figure 34 shows an example of the tested specimen without re-machining. In this case, the necking has localized to the softer non-pre-strained areas and resulted in the formation of "banana-shaped" specimen, i.e., the necking has actually initiated on both sides of the specimen. The observed phenomenon needs to the taken into account in the standard bake hardening experiments.

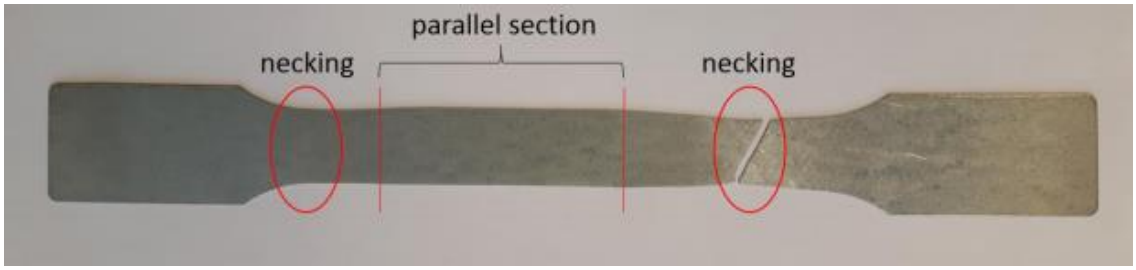

Figure 34. *Example specimen showing the necking at softer areas in pre-strained and baked condition. The specimen was re-machined after pre-straining in order to avoid the observed phenomenon.*

Figure 35. *Instron 8801 hydraulic testing machine [99].*

Both pre-straining and final property testing were carried out with an Instron 8801 servo-hydraulic testing machine, as illustrated in Figure 35. An extensometer (Instron 2630-100 Series) with a gauge length of 50 mm was used to measure elongation. The mechanical properties in all conditions were determined using a quasi-static strain rate of 1 x 10^{-3} 1/s. The same deformation rate was used in pre-straining. In all cases, two repetited tests were carried out for reducing the influence of scatter and gaining more reliable results.

The extensometer was mounted on the surface of one side of the flat specimen, as illustrated in Figure 36. The mechanical part transfers extension from the specimen to the internal transducer via knife edges [100]. Since there is no relative movement between the specimen and the extensometer when the extensometer is tightly fixed on the specimen with the rubber band, the movement of the extensometer corresponds to the movements of the specimen. To prevent the sharp edge cutting the rubber band, the edges of hard and thick specimens are better to be wrapped with tape.

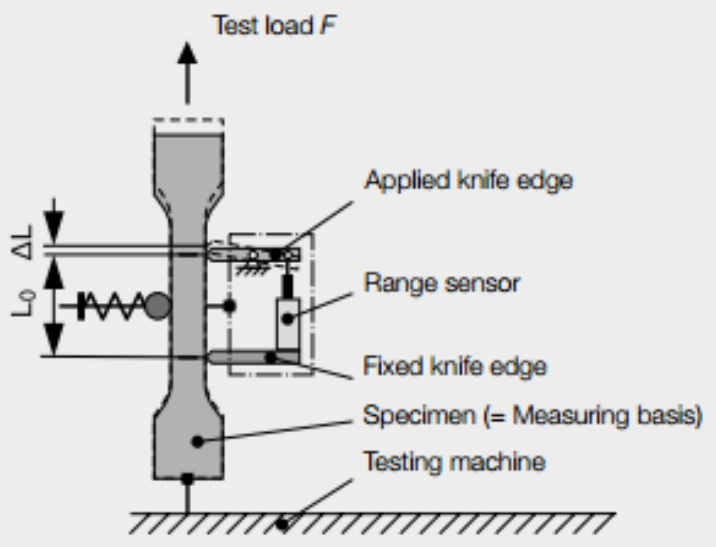

Figure 36. *Schematic of strain measurement with clip-on extensometer [100].*

The pre-straining and tensile testing were performed according to the specifications of the EN-10002 tensile testing standard. During the pre-straining of the test pieces, the testing rate was kept constant, and all tensile tests were performed by using the same actual speed of the piston. In the case of carbon steels, the specimens were very thin by thickness and were susceptible for small bending during closing the grips of the testing machine. In the case of materials A and B, small tension was manually applied to avoid bending of the specimens during closing the grips, which easily occurred for specimens with a thickness of only 0.55 mm. After that, the testing was carried out in the same manner as described above.

The data of piston position, load and strain were recorded during the tensile test. The value of extensometer was balanced to zero before the test was started. However, the extensometer was very sensitive with small external vibrations and thus, the value differed slightly from zero. Consequently, the engineering strain was calculated as the ratio of elongation to the original length, and it was given by:

$$\varepsilon = (\varepsilon_r - \varepsilon_0) / (50 - \varepsilon_0) \quad \text{(Eq 4)}$$

Where ε_r is the recorded extensometer strain, ε_0 is the initial strain of the extensometer before testing, and 50mm is the gague length of the used extensometer.

The tensile stress is the ratio of normal stress to the cross section area. Thus, the engineering stress can be calculated as follows:

$$\sigma = F_n / (t * w) \quad \text{(Eq 5)}$$

Where F_n is the load (in N) at corresponding time, t is the thickness (in mm) of the cross section, w is the width (in mm) of the cross section, thus, $t*w$ gives the original cross section size of the test piece. σ is the engineering stress in N/mm^2, which corresponds to MPa.

After that, the engineering stress-strain curves were calculated which allowed the determination of mechanical properties. An example curve is shown in Figure 37. Tensile strength is the highest point of engineering stress-strain curve. Uniform elongation is the elongation corresponding to the ultimate tensile strength. The total elongation is the elongation when the specimen is ruptured. The yield strength (YS), tensile strength (TS), uniform elongation (UE), and total elongation A50 (the measuring gage length is 50 mm) are the main properties of concern.

In some cases, a sharp yield point was appeared after bake hardening treatments. However, in some cases, no sharp yield point was observed from stress-strain data. In such cases, the 0.2% proof stress was used to determine the yield stress, i.e., 0.2% offset method was applied, as illustrated in Figure 37. In these materials, the stress at which the material switches from elastic deformation to plastic deformation is not easy to detect, thus, the offset yield strength is determined. A straight line is constructed parallel to the initial portion of the stress strain curve but offset by 0.2% from the origin point 0, as shown in Figure 37. The 0.2% offset yield strength is the stress at the crossing point of the constructed straight line and the actual stress-strain curve.

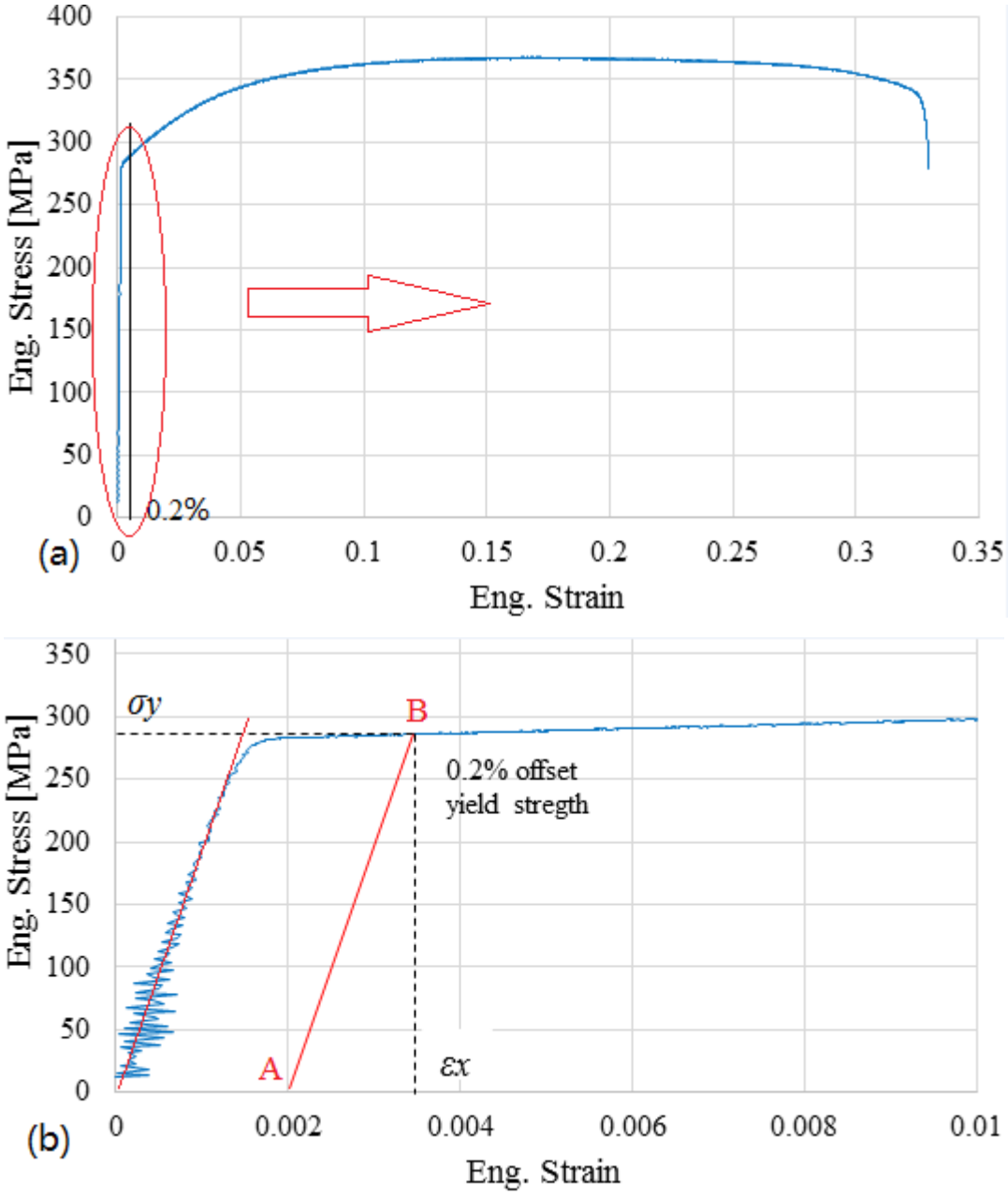

Figure 37. *Diagram of 0.2% offset yield strength determination with engineering strain-stress curve without sharp yield point.*

Due to the low sheet thickness of carbon steel and vibrations of the testing machine, the stress-strain data showed some noise. In these cases, a straight line can be constructed in the central position of the scattered area, as shown in Figure 37 (b). The slope of the constructed line *AB* is equal to Young's modulus.

In some tests, the stretching and fracture happened at the edge area or outside the gauge section, as shown in Figure 38, which can cause backward straining and discontinuous yielding, and produce the stress-strain curve like the one shown in Figure 39. The negative strain after upper yield depends on the way metals yield within a parallel area of material.

There is also stress concentration at the jaw faces in parallel specimens, and it would also propagate through the steel in certain direction. The yielding takes place outside of gauge section and lead to the stress drop, and makes tensile strength and corresponding uniform elongation not available or not important any more.

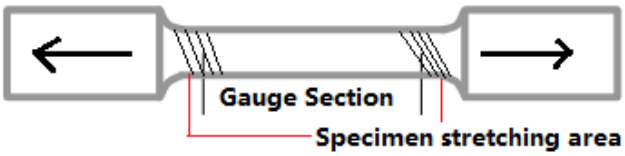

Figure 38. *Schematic diagram of tensile test piece in which the fractures are not in the ideal gauge section.*

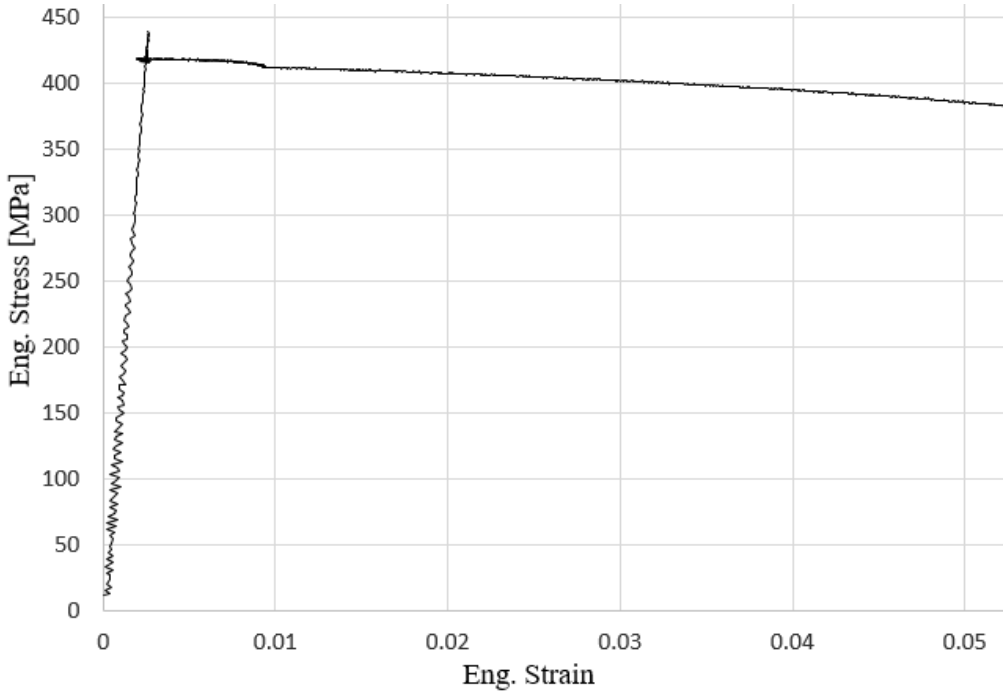

Figure 39. *Example of engineering stress-strain curve of the discontinuous yielding specimens in the tests.*

3.3.2 Bake Hardening Heat-treatments

The heat-treatment procedure of baking was carried out according to the standard EN 10325-2006 by using a fan-assisted furnace Thermo Scientific Heraeus. The specimen temperature was measured with K-type thermocouples and a Fluke 52 thermometer, and the thermocouple was attached to one reference specimen which was contacted with the actual specimens. In the operation of heat treatment, the specimen was heated up to 170 °C or 230 °C in in the furnace. By the standard, the specimens are supposed to be heated up to 168 °C (when aiming for 170 °C) within 5 min and heated up to 228 °C (when aiming for 230 °C) within 7 min, respectively. All the specimens had been heated

up to the targeted temperature within the required time in the operation. Then, the specimen was kept in the furnace isothermally for 20 minutes and be cooled to the room temperature in the air. The heat treatments are illustrated in Figure 40.

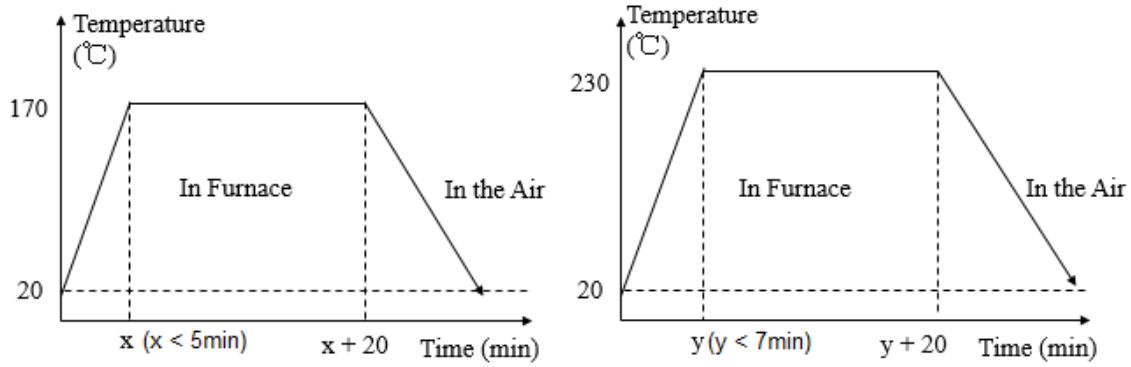

Figure 40. *Schematic presentation of heat treatment procedures in the experiments.*

However, some problems also occurred in the operation. Due to the leakage of little heat, the actual temperature of the specimen was slightly lower than the furnace temperature. Thus, the furnace temperature was normally set at around 174 °C and 234 °C to ensure the specimen temperature is around 170 °C and 230 °C. But in few cases, the time record did not start simultaneously when the specimen was being heated. Thus, there can be some errors in the time control. While, the standard EN 10325-2006 also permits a limited range of time of (20 ± 0.5) min. Another difficulty was to control the specimen temperature, which also depends on the furnace properties and thermocouple accuracy. The temperature was not so stable at the ideal temperature in some cases, and thus, opening the furnace door a little bit for a while can lower the temperature when it was too high. The heat treatments went generally smoothly, the small errors did not cause significant problems.

3.3.3 Determination of Bake Hardening Index

The bake hardening effect can be evaluated using a standardized concept of a bake hardening index described more in detail in EN 10325-2006. A principle for the determination procedure of the BH index is presented in Figure 41 and Figure 42. The value of BH index is given by formula $BH_2 = R_{eL,t}$ (or $R_{p0.2,t}$) $- R_{p0.2,r}$. $R_{eL,t}$ is the yield strength of lower point when the engineering stress-strain shows a sharp yielding point, as illustrated as point A in Figure 41. $R_{p0.2,t}$ is the yield strength of the crossing point of 0.2% offset line with the tensile test curve when the engineering stress-strain does not show a sharp yielding point, as illustrated as point A in Figure 39. $R_{p0.2,r}$ is the yield strength of point B illustrated in Figure 38 and Figure 39.

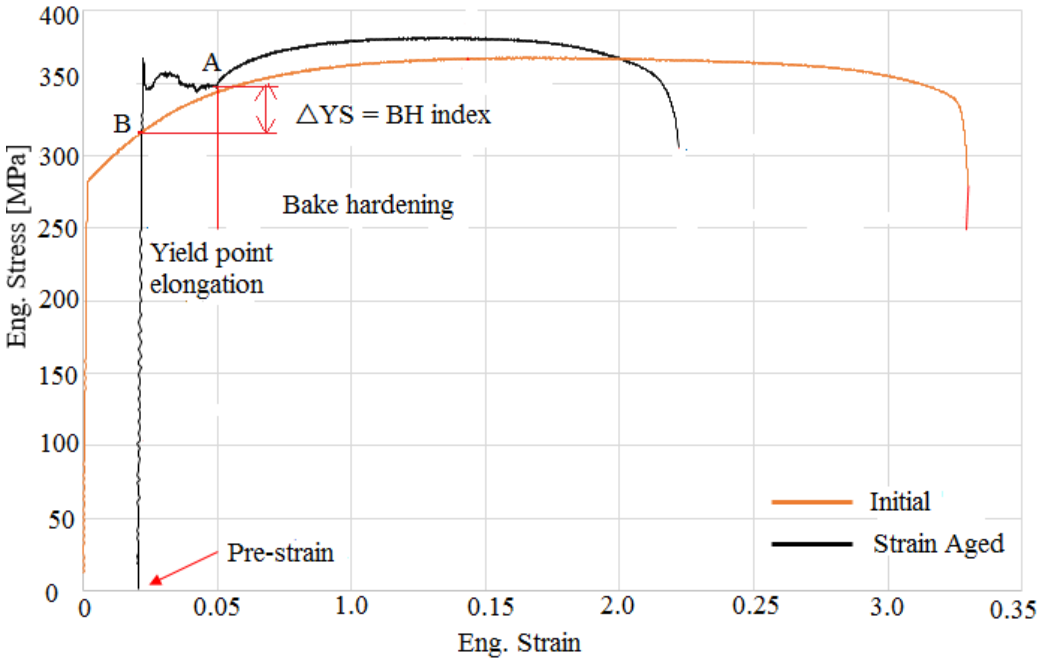

Figure 41. *Schematic illustration of bake-hardening index BH2 determination method applied for low carbon steels.*

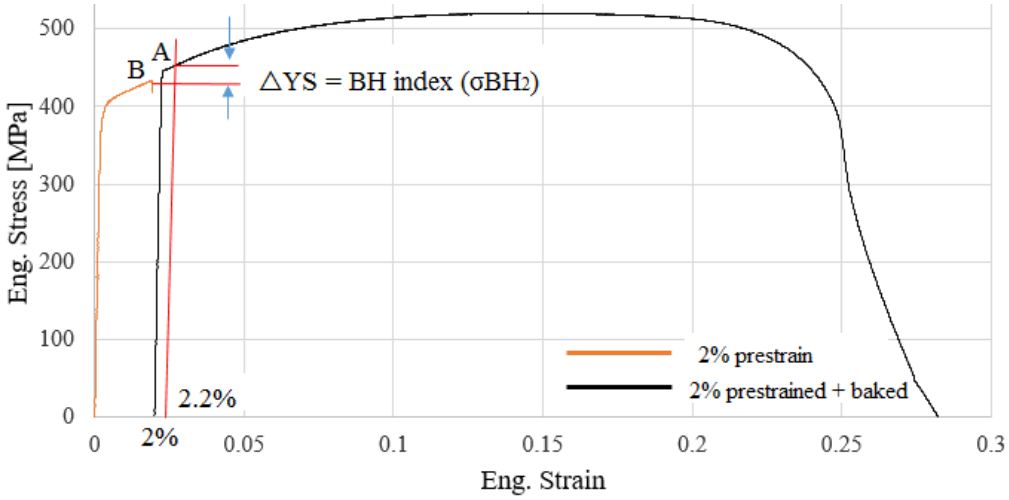

Figure 42. *Schematic illustration of bake-hardening index BH2 determination method applied for ferritic stainless steels.*

For the low carbon steel, a sharp yield point normally appeared after bake hardening in the engineering stress-strain curve. Therefore, the BH index is determined with the yield point and the stress when the pre-straining ends, as presented in Figure 41. For stainless steel, there was no sharp yield point in the engineering stress-strain curve. Therefore, the BH index was the determined by the difference of 0.2% offset yield strength after heat treatment and 0.2% offset yield strength of the pre-strained material, which is the same sample as tested after heat-treatment, as shown in Figure 42. The bake hardening index is presented by plotting the engineering stress-strain curves with the data of the specimen after heat treatment and the data of initial material.

3.4 Aging Index Test

In addition to bake hardening tests, an additional aging treatment was carried out in order to evaluate the aging behavior during storage. In this procedure, two unstrained specimens were hold in boiling water (100 °C) for 30 min and cooled in air to room temperature. Quasistatic tensile tests were followed after the heat treatment. The aging indexes of this type were determined by calculating the difference of the yield strength aroused by the aging treatment. The treatment is illustrated in Figure 43. The aging indexes are determined by calculating the difference of the yield strength aroused by the aging treatment. The method of determining the index is the same as described in the Chapter 3.3.3.

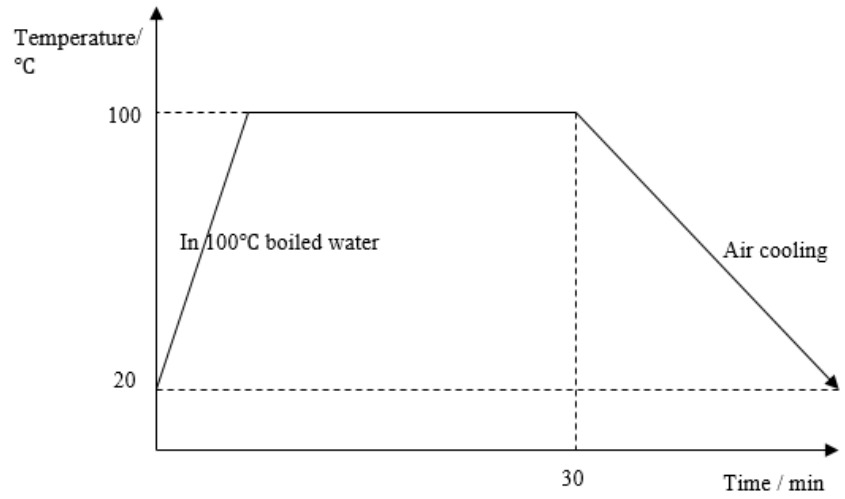

Figure 43. *Schematic diagram of aging treatment technology in the experiments.*

4 RESULTS AND DISCUSSION

In this chapter, the initial properties of the three experimental materials are presented. In addition, the results of the bake hardening tests and aging tests, which also include the bake-hardening (BH) index determination result, are presented. In addition, the obtained material behavior are discussed, and some findings are concluded.

4.1 Initial Properties

To study the initial mechanical properties of the experimental materials, two tensile tests of each material were carried out. Engineering stress-strain curves were plotted and the yield strength tensile strength, uniform elongation, and total elongation were determined.

Materials tested in as-received condition did not show sharp yield point, i.e., the point where material behavior changes from elastic to plastic is relatively difficult to observe. Thus, 0.2% offset method was used to describe yield strength of the materials in as-received condition. TS is the ultimate tensile strength, uniform elongation is the elongation corresponding to the ultimate tensile strength, and the total elongation is the elongation when the specimen is ruptured. The initial properties of the experimental steels are presented in Table 11.

Table 11. *Initial mechanical properties of experimental materials.*

	YS 0.2% (MPa)	**UTS (MPa)**	**Uniform Elongation**	**Total Elongation**
Material A	285	370	17.5%	30.4%
Material B	277	367	18.6%	36.8%
Material C	409	519	15.6%	27.9%

As can be seen, the steel C (ferritic stainless steel) has higher initial strength than steel A and B, while the initial yield strength and initial tensile strength of steels A and B are very similar. However, the measures of elongation, especially the total elongation, of steel C is slightly smaller than that of steels A and B. The mechanical properties are determined by the combination of chemical composition and processing history of steels, both of which has effect on the grain-size and phases present, for example. The stainless steel contains higher carbon content, which enhances the hardness and strength of the material,

meanwhile, the high contents of chromium, nickel, silicon, and manganese also contribute to the high strength. Das [73] reported that the higher annealing temperature improves the bake-hardening response.

4.2 Bake Hardening Test Results

The experimental plan of each specimen was shown in the previous chapter in Table 9. The principal idea followed in this thesis is to compare the tensile properties of as-received condition with the ones after bake hardening treatments. Consequently, the effect of pre-strain and baking temperature can be determined.

4.2.1 Effects of Bake Hardening

The effects of bake-hardening heat treatment without pre-straining can be determined by comparing the mechanical properties of the initial status with those after the heat-treatment. Appendix B presents the representative engineering stress-strain curves for materials tested in initial condition and after bake hardening heat treatments without pre-strain.

The effects of static strain aging, i.e., the bake hardening effect with pre-straining, can be correspondingly determined by comparing the initial properties with the ones measured after pre-straining and bake-hardening heat treatments. Appendix C presents the representative engineering stress-strain curves showing the effect of bake hardening. In this thesis, two different heat treatment procedures, namely 170 °C/20min and 230 °C/20min, and different pre-strain from 0% to 2%, to 6%, and to 10% were performed. Two repeated tests were used to determine the values presented in Figures 45, 46, 48, and 49.

The YS values were determined in different methods depending on the characteristic of the engineering stress-strain curve. When the yielding period was shown in the engineering stress-strain curve, the YS value was determined based on the higher yield point, as indicated with yield strength 1 in Figure 44(a). In case where sharp yield point was not present, the 0.2% offset yield strength method was used to determine YS value, as illustrated in Figure 44(b). There were also curves like Figure 44(c), in which the sharp yield point was followed by a rapid reduction in strength and after that the strength level was stabilized to a certain level. In such cases, the YS value was also determined with the 0.2% offset yield strength method, as indicated in Figure 44(c).

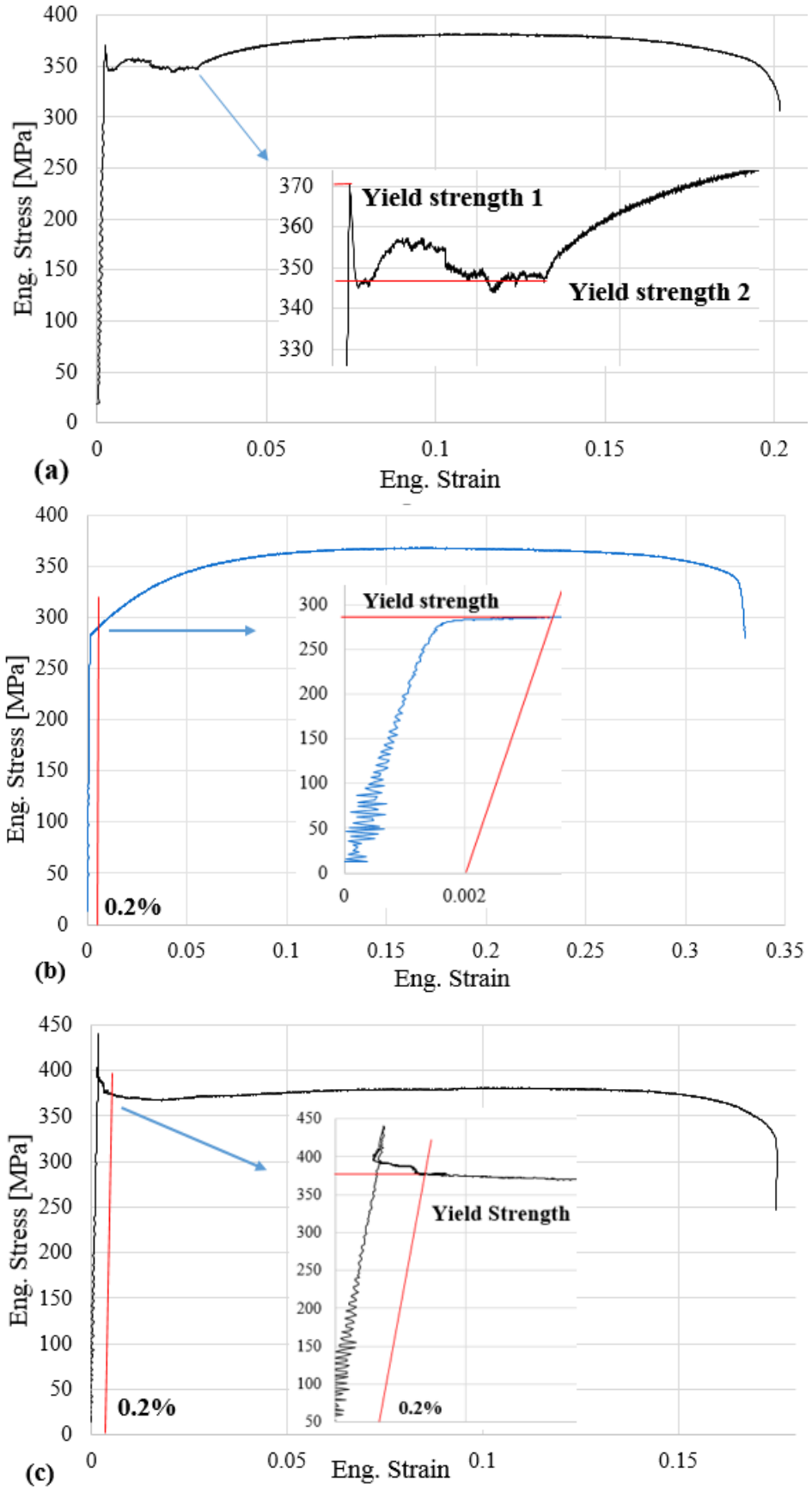

Figure 44. *Illustration of yield strength value determination methods with different engineering stress-strain curves.*

Figure 45 presents the yield strength of the materials A and B at different status. The yield strength values were determined by using higher yield point values, as indicated with yield strength 1 in Figure 44(a).

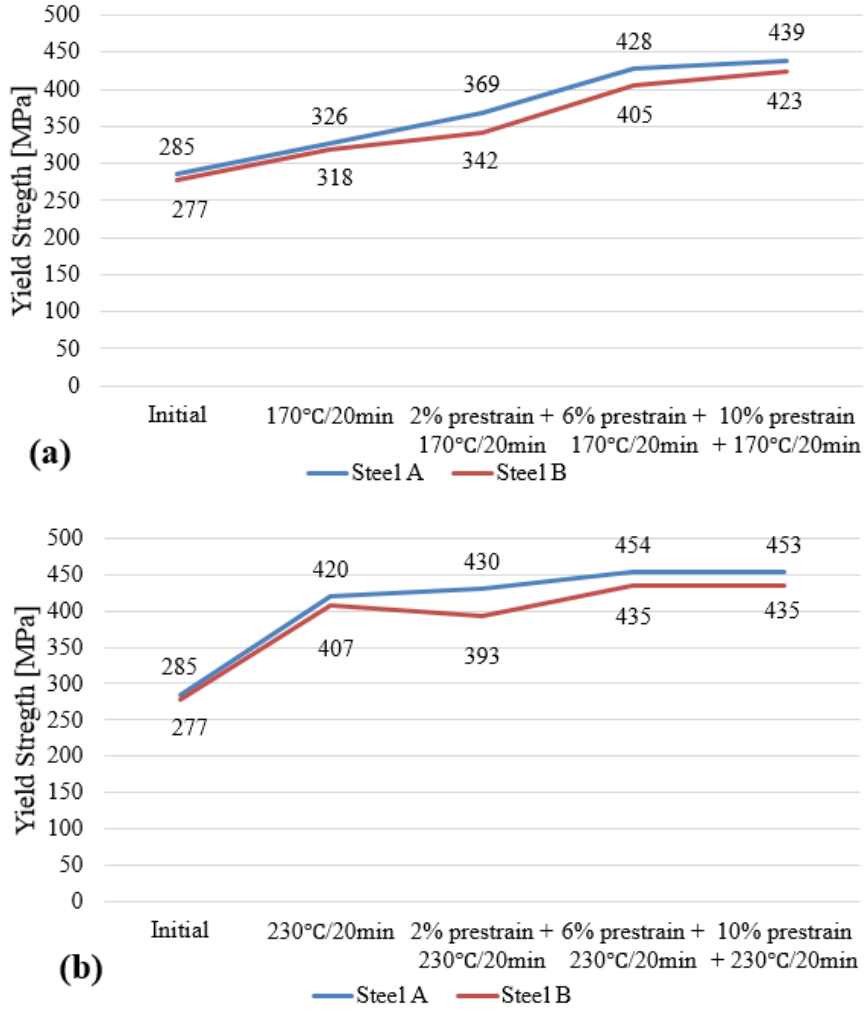

Figure 45. *Yield strength (determined with higher yield point) of steels A and B at initial status and after different pre-straining and bake hardening treatments.*

As can be seen in Figure 45(a), the 170 °C/20min heat treatment without pre-strain resulted in an increase of 41 MPa in yield strength for both steels A and B. Figure 45(b) indicates that 230 °C/20min heat treatment without pre-strain led to an increase of 135 and 130 MPa to steels A and B, respectively. At the meanwhile, with the 170 °C/20min heat treatment, the increase of pre-strain level from 0% to 10% led to a ΔYS of 113 MPa and 105 MPa to steels A and B, respectively. However, the ΔYS were 33 MPa and 28 MPa to steels A and B, respectively when baking temperature was 230 °C. Two low carbon steels showed very similar yield strength with the increase of pre-strain under both baking temperatures. The small difference of ΔYS at 230 °C is because the fact that higher temperature without pre-strain is already enough to generate sharp yield point.

Figure 46 presents the lower yield strength values of the steels A and B, as indicated with yield strength 2 in Figure 44(a).

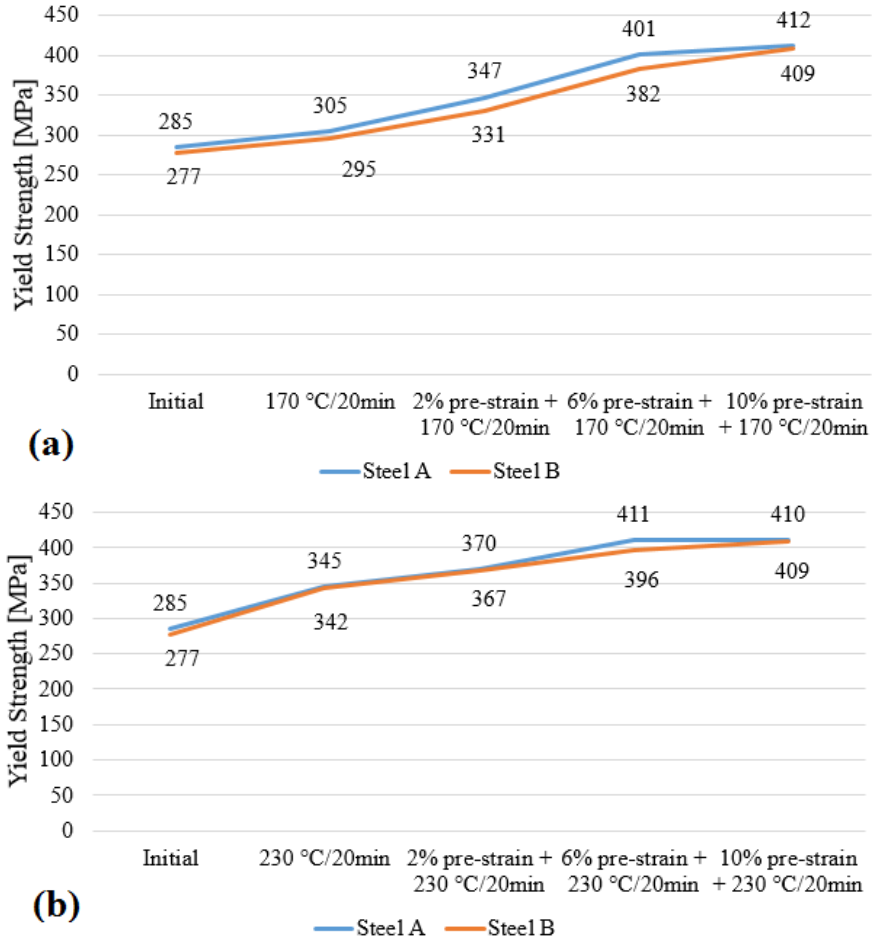

Figure 46. *Yield strength (determined with lower yield point) of steels A and B at initial status and after different pre-straining and bake hardening treatments.*

As indicated in Figures 45 and 46, the lower yield point values were increased similarly with the increase of pre-strain. The values of yield strength determined with lower yield point are generally lower than those determined with higher yield point, otherwise, no significant difference in material behavior is shown between Figures 44 and 45.

The above-discussed results can be explained with the theories of SSA. According to Pelleg [101], the interstitial atoms settle down under the dislocation line to form the Cottrell atmosphere, and these atoms cause lattice distortion by forming a stress field around themselves. However, the preferential location of the interstitial C and N atoms below the dislocation is controlled by diffusion, which depends on the diffusion time and temperature. When the atoms diffuse into the dislocation core, they stay there and pin the dislocation, thus, a higher force is needed to tear such a dislocation away from its atmosphere. This extra force corresponds to the upper yield point. After removing the

dislocation, it is free to move to a lower stress, which produce lower yield point. Thus, the difference exhibited between the YS values in Figures 45 and 46 reveals the extra stress needed for getting the dislocation away from the Cottrell atmosphere.

In metals, the deviation from linearity can be considered as yield point if the elastic-plastic transition is a gradual process. In this case, there is a sudden drop of lower point, as illustrated as Figure 44(a). According to Cottrell and Bilby's theory [64], yielding phenomenon involves the movement of interstitial solutes, mainly C and N atoms. The inhomogeneous deformation initiates at the points of stress concentration, especially at the grips which hold the specimen during the tensile test. It propagates through the specimen as Lüders bands, which occurs when the sharp yield drops, as illustrated in Figure 47. The propagation of Lüders bands continues with the deformation going on, until the Lüders bands cover the entire specimen. Therefore, the propagation of Lüders bands causes yield point elongation.

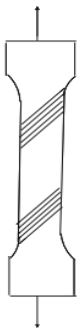

Figure 47. *Lüders bands at 45° from the tensile axis [101].*

The occurrence of Lüders bands is attributed to the pinned dislocations and the high stress [101]. The dislocation pinning heavily depends on the returned interstitial C or N atoms, which form Cottrell atmosphere to lock the dislocations and achieve the strength increase. Higher temperature baking increases the diffusion rates of the interstitial C and N atoms, which promotes the process of interstitial atoms return and yield point return. The similar theory was also reported by Cottrell and Bilby [64]. This is the reason for the much higher yield point when baked at 230 °C than at 170 °C, as presented in Figure 46 and Figures 1 and 2 of Appendix B.

It is important to note that the sharp yield point is seen even without pre-straining, as indicated in Figures 1 and 2 of Appendix B. This maybe because the heat treatment provides the energy to the C and N interstitial atoms, which can move to occupy the octahedral interstitial and create crystal distortion and dislocations [101]. The dislocations can be locked by the Cottrell atmosphere and achieved strength increase, as explained above. This result indicates that there must exist a significant amount of mobile

dislocations in initial condition. Otherwise, the heat-treament without pre-straining should not result in the formation of sharp yield point.

It can be concluded that the baking temperature has a strong effect in the material behavior: the strength was clearly increased more by 230 °C baking, as indicated in Appendix B. The heat treatment did not affect the elongation much, while the increase of pre-strain decreases ductility steadily and significantly.

Hanai, *et al*. [102] concluded that yield strength increment is attributed to the grain size and amount of interstitial carbon and nitrogen atoms. They also pointed out that when the content of carbon and nitrogen reaches 10 ppm, the yield strength increment heavily depends on the grain size. However, the grain sizes of A and B materials are 7.0 μm and 7.7 μm, respectively, which shows very slight difference. This corresponds to the similar △YS values of steels A and B with both heat treatments.

Figure 48 shows the effect of bake hardening heat-treatments in the total elongation of steels A and B without and with pre-straining.

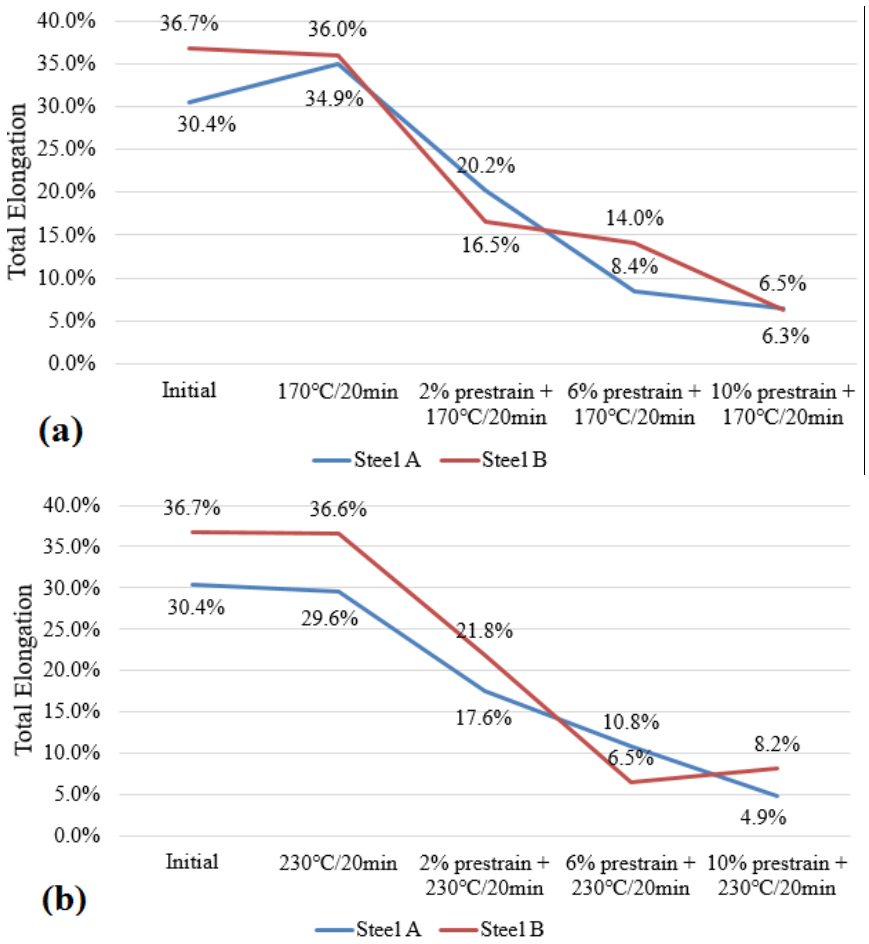

Figure 48. *Total elongation of steels A and B at initial status and after different pre-straining and bake hardening treatments.*

Figures 47 and 48 indicate that the two steels exhibit very similar behavior when it comes to the elongation behavior in general. The total elongation decreased steadily with the increase of pre-strain as a result of both heat treatments, which indicates that the ductility was decreased and strength was increased steadily with the increase of pre-strain. However, the bake hardening treatment without pre-strain produced a small variation in the total elongation of both steels A and B. Nevertheless, the variation was more significant when the pre-strain was applied. This reveals that the pre-strain contributes significantly to the work hardening phenomenon, which is related to the plastic deformation, even work hardening also produces effect on the total elongation. In addition, based on Figures 45, 46, and 48, it can be concluded that for the two low carbon steels, the strength increased, the total elongation and ductility decreased with the increase of pre-strain level. Seth had the similar finding with low carbon BH220 steel [74].

Figures 49 and 50 present the mechanical properties of steel C (EN 1.4003 ferritic stainless steel) after different treatments. The YS values were determined with 0.2% proof stress, since no sharp yield point was observed after bake hardening tests. This is the reason why UTS and UE values were taken for steels C, but not for steels A and B.

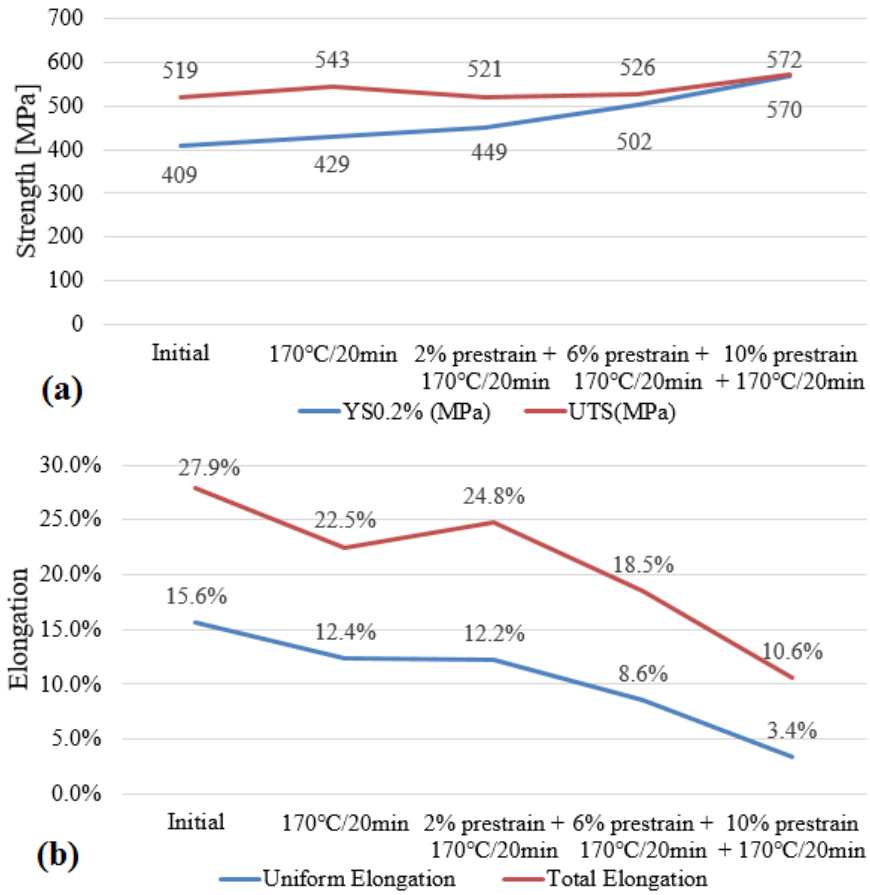

Figure 49. *Mechanical properties of steel C at initial status and after different pre-straining and 170 °C/20min bake hardening treatment.*

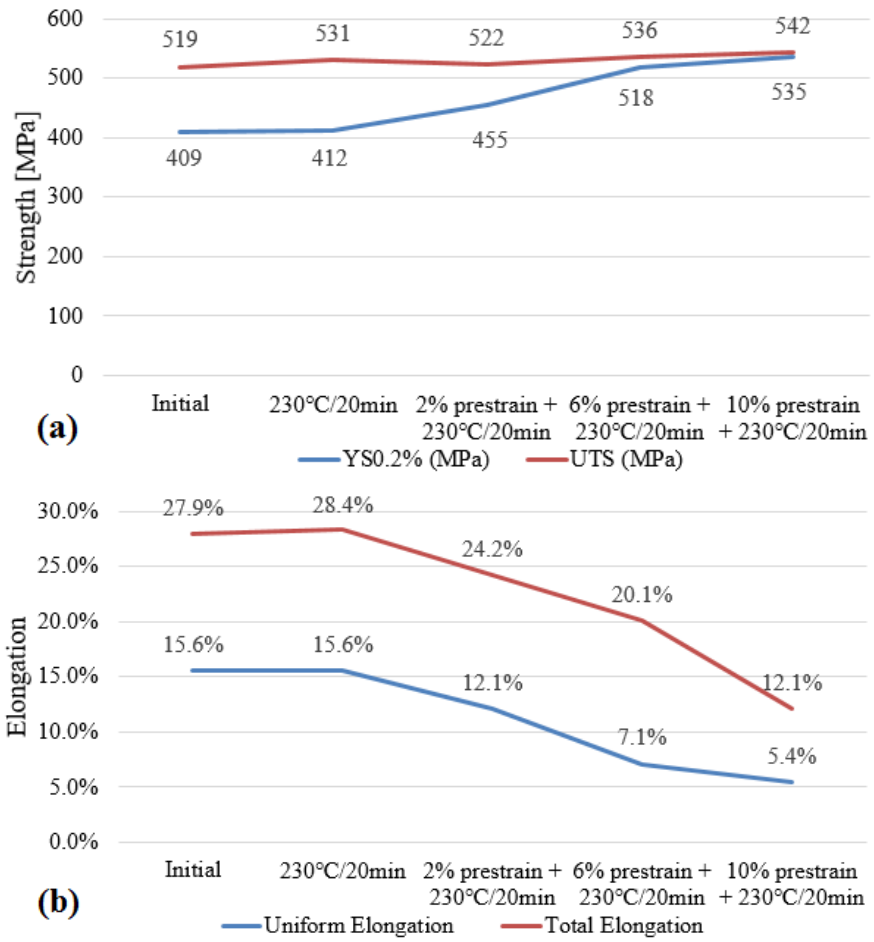

Figure 50. *Mechanical properties of steel C at initial status and after different pre-straining and 230 °C/20min bake hardening treatment.*

Figure 49(a) indicates that in the case of steel C, 170 °C/20min heat treatment increased a yield strength of 20 MPa and tensile strength 24 MPa of steel C. The impact of heat treatments on the elongation of steel C is not as significant as that of steels A and B. Besides, Figures 48 and 49(b) show that 170 °C/20min heat treatment without pre-strain did not produce significant influence on the elongation of two low carbon steels, while it produced a reduction effect on the uniform elongation and fracture elongation of steel C. However, 230 °C/20min heat treatment had no significant influence on the elongation of all three materials, as indicated in Figure Figures 48(b) and 50(b).

In comparison, Figure 50(a) shows that the △YS value of steel C is much smaller than that of low carbon steels. Since the values for steel C are only 20 MPa and 3 MPa with 170 °C/20min and 230 °C/20min, respectively. The bake hardening effect is heavily dependent on the diffusion of the interstitial atoms into the locations sites and Cottrell atmosphere formation process [64]. However, the diffusion depends on the diffusion time and temperature, which is essentially related to the energy provided [101]. In addition, the amount of mobile dislocations in initial condition can have an effect. The small

increase in the yield strength of steel C reveals that the diffusion of interstitial atoms in the stainless steel requires higher energy than the two low carbon steels. Similar result was also reported by Palosaari, *et al* [103], who found that activation energies for EN 1.4509 and EN 1.4521 ferritic stainless steels are 150.7 KJ/mol and 146.3 KJ/mol, respectively, which are greater than that of ultra-low carbon bake hardenable steels, 80 KJ/mol.

To study the effect of different level of pre-straining, pre-strains of 2 %, 6% and 10 % were applied and followed with the baking at 170 °C and 230 °C for 20 min. The engineering stress-strain curves for the specimens with different pre-strain and same bake hardening are presented in Appendix C. Figures 49 and 50 suggest that for EN 1.4003 ferritic stainless steel, with the same bake-hardening treatment, the tensile strength increased, while the elongation and ductility decreased with the increase of the level of pre-strain. This result is also applied to the two low carbon steels.

Figure 45, 46, 49, and 50 show that for the three experimental materials, the △YS values were reduced when the pre-strain increased from 6% to 10%, in comparison with the increase between 2% and 6%. Lower level of pre-strain naturally leads to the smaller amount of mobile dislocations. However, the amount of free C and N is always limited. It is possible that with higher pre-strain values, there was not sufficient free interstitial atoms to lock dislocations. Besides, the increased work hardening response in greater when the pre-strain increased from 2% to 6%, in comparison with the response between 6% to 10% pre-strain, as illustrated in Figure 51. Work hardening also contributes to the △YS value. However, with higher level of pre-strain, higher dislocation density makes the solute atoms insufficient to provide pinning for all dislocations [104].

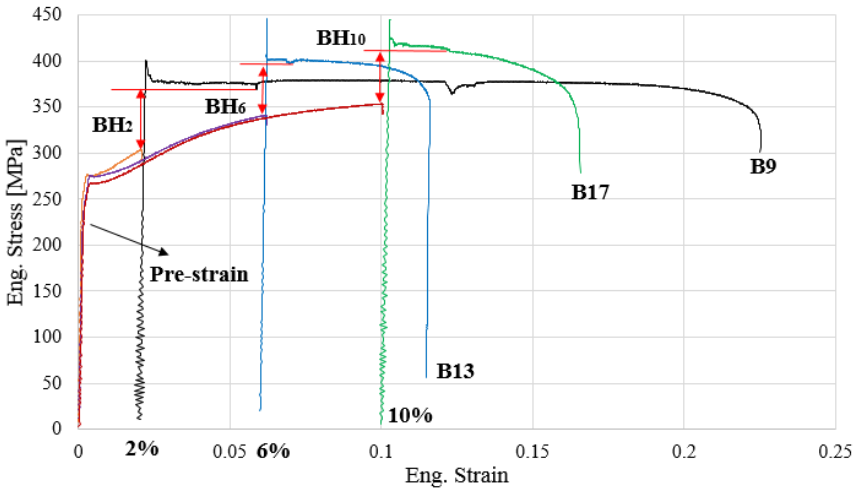

Figure 51. *Illustration of the bake-hardening indexes determination. Tensile test specimens: B9 (2% pre-strain and 230 °C/20min), B13 (6% pre-strain and 230 °C/20min), B17 (10% pre-strain and 230 °C/20min).*

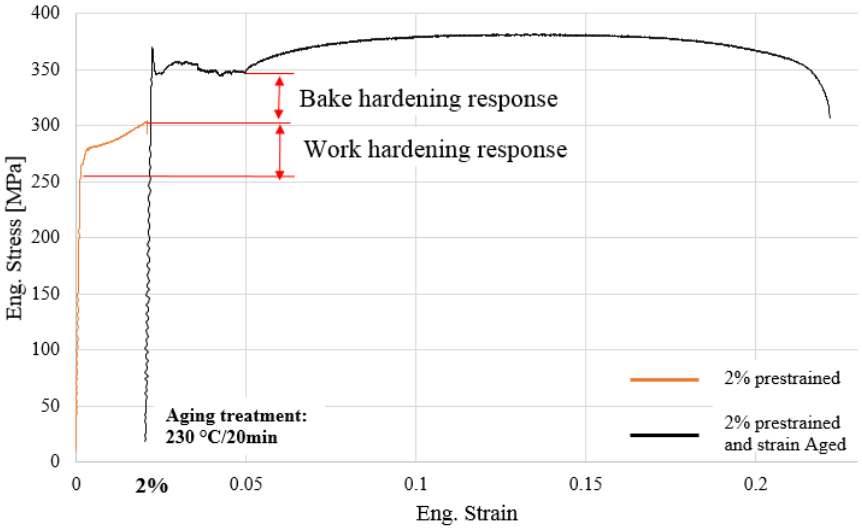

Figure 52. *Illustration of bake-hardening response and work-hardening response in the engineering stress-strain curve.*

With the increase of pre-strain, work hardening effect is increased, the dislocation density is increased and the Cottrell atmosphere formation is enhanced. The combination of work hardening and Cottrell atmosphere formation leads to the increase in strength. This is why with the same heat treatment, the yield strengths increased with the increase of the level of pre-strain within 0-10%, as presented in Figure 45, 49 and 50.

Bake hardening typically results in the increase in yield strength, but also influences other mechanical properties. Static strain aging takes place in two steps, and the final effect depends on the combined effects of them. When the external force is applied on the material, the crystal would expand, the interstitial C and N atoms would migrate to occupy the dislocation sites in the strain direction. When the force is removed, the interstitial atoms are distributed again randomly, which is named “Snoek effect”. This process increases the ductility while lowers the strength of the material. However, this process produces very small impact and lasts very short time, as illustrated in Figure 26. When the force exceeds the elastic limit of the specimen, new dislocations are produced. When such pre-strained material is then thermally treated, the interstitial atoms will migrate to these new dislocation sites and lock them by forming the Cottrell atmosphere around the dislocations [86-87]. The process of Cottrell atmosphere formation increases the yield and tensile strengths while lowers the ductility of the material. That is why the yield strength was greater when baked at 230 °C than that with 170 °C baking for all three experimental materials. The effect of the Cottrell atmosphere formation is much more significant than the “Snoek effect”. Therefore, the overall effect shows much of the Cottrell atmosphere formation stage. That is why the results show that the strength generally increases with the increase of pre-strain and baking temperature.

When more and more interstitial atoms are attracted to the dislocation strain area, a solute cluster can be formed, and in some extreme cases, when the solute cluster is strong enough, these interstitial atoms would be along the cores of dislocations [89]. As indicated in Figure 26, no particle hardening phase is present during the Cottrell atmosphere formation period. However, the particle hardening effect is increased rapidly when the aging continues after Cottrell atmosphere formation. Nevertheless, this particle hardening effect would reach a saturation point, after which further aging would reduce the particle hardening phases.

4.2.2 Bake-Hardening Index Determination

The method for determining BH index was introduced in Chapter 3.3.3. As discussed earlier, several kinds of yielding behavior and engineering stress-strain curves appeared during tensile tests. In the case of low carbon steels (steels A and B), the bake hardening treatments resulted in the formation of sharp yield point, whereas the stress-strain curves measured for ferritic stainless steel (steel C) did not show this phenomenon. For these two categories, the BH indexes were determined by the illustrated methods, which is also approved by the standard EN 10325: 2006. In some cases, the stretching and fracture happened at the edge area or outside the gauge section, and caused backward straining and discontinuous yielding, their stress-strain curves are like the one shown in Figure 39. For these curves, the 0.2% offset yield strength method was applied to determine the yield strength.

The BH indexes of ferritic carbon steels (steel A and B) are presented in Figure 53 and 54. Appendix D presents the detailed data of BH indexes of three materials. The determined BH indexes of two ferritic carbon steels are quite similar. With the 170 °C/20min heat treatment, the BH indexes of two low carbon steels increased from around 19 MPa to around 54 MPa steadily with the increase of pre-strain from 0% to 10%. However, with the 230 °C/20min heat treatment, the BH indexes of two low carbon steels decreased from around 70 MPa to around 58 MPa steadily along with the increase of pre-strain from 0% to 10%. The two low carbon steels exhibited very similar behavior in terms of BH indexes.

Figures 53 and 54 also reveal that the values of BH index are greater with higher baking temperature, especially when the pre-strain level is low. It is because the higher baking temperature provided greater thermal energy, which increased the diffusion rate of the carbon atoms in the material. As a result, the interaction of dislocations and interstitial carbon atoms was increased and greater yield strength increment was achieved.

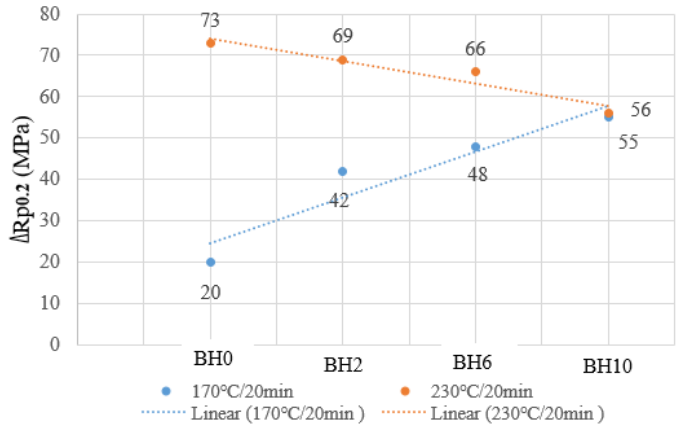

Figure 53. *Bake-hardening indexes for steel A with two bake-hardening heat treatments.*

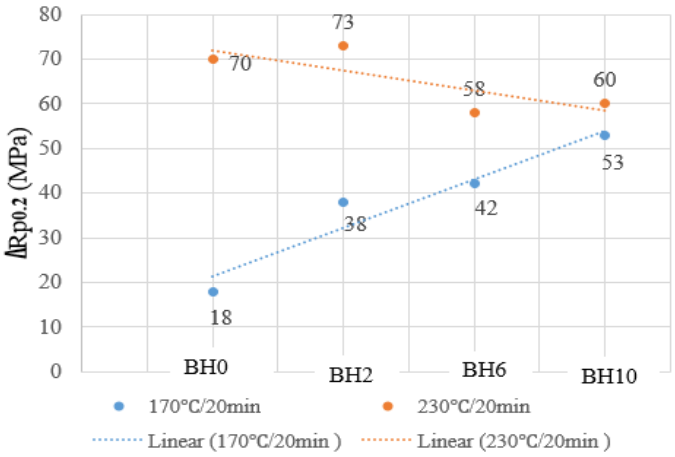

Figure 54. *Bake-hardening indexes for steel B with two bake-hardening heat treatments.*

Figures 53 and 54 illustrate that when baking temperature was 230 °C, BH indexes follow a general decreasing trend with the increase of pre-strain. This is because the high temperature provided sufficient thermal energy, which increased the diffusion rate of interstitial C atoms into the dislocation cores. However, with the increase of pre-strain, larger amount of dislocations were produced, but the work hardening effect is less increased with the further increase of pre-strain, as indicated in Figure 51. Thus, there was not very significant increase of the amount and density of dislocations even the pre-strain was increased further to 10%. The maximum point of the Cottrell atmosphere formation had been reached or was very close, the further increase of pre-strain led to lower ΔYS value.

However, when baking temperature was 170 °C, BH indexes followed the trend of $BH_2 < BH_6 < BH_{10}$, which is opposite to the case when baking temperature was 230 °C. Since at lower temperature of 170 °C, the interstitial atoms diffused slowly due to the lack of thermal energy. The dislocation density with the same level of pre-strain are supposed to be the same. However, the Cottrell atmosphere formation saturation point had not been

reached when baked at 170 °C due to the low diffusion process. Thus, when the pre-strain was increased, larger amount of dislocations were available for the mobile C atoms to diffuse into. Thus, higher ΔYS value was achieved.

Das, *et al*. [105] reported the same phenomenon that the ΔYS decreases with the increase of pre-strain level. This is because the aging condition did not give sufficient time to ensure the dislocation pinning to be completed. This is consistent with the earlier findings of Cottrell and Bilby [64]. De, *et al*. [83] found that maximum increase in yield strength corresponding to the completion of Cottrell atmosphere formation on the dislocations depends on the level of pre-strain, while increasing baking temperature can only improve the maximum ΔYS value slightly. Therefore, there is certain "saturation" point when the Cottrell atmosphere has been at or around the dislocations and the further increase of pre-strain level can hardly produce strength increase effect. The phenomenon of $BH_2 > BH_6 > BH_{10}$ when baking temperature was 230 °C is attributed to this.

The BH indexes for EN 1.4003 ferritic stainless steel (steel C) are presented in Figure 55. With 170 °C/20min heat treatment, ΔYS was decreased when pre-strain increased from 0% to 2%, which is probably due to the specimen scattering. The BH index was increased very slowly along with the increase of pre-strain from 2% to 6%, while it increased remarkably when the pre-strain was increased up to 10%. In comparison, the BH index increased more significantly, from 8 MPa to 32 MPa, with the increase of pre-strain from 0% to 10% when baked with 230 °C. Palosaari, *et al*. [3] also found that the BH indexes of three ferritic stainless steels increased with the increase in aging temperature between 150 °C and 250 °C. This is attributed to its high activation energy, higher temperature provides greater thermal energy, which promote the diffusion of solute atoms more and achieve more significant strain aging. However, low temperature could hardly provide sufficient energy for the diffusion of interstitial atoms and Cottrell atmosphere formation.

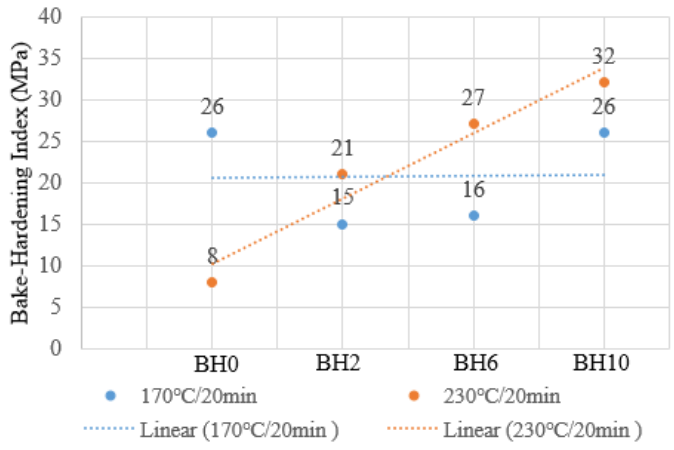

Figure 55. *Bake-hardening indexes for steel C with two bake-hardening heat treatments.*

The comparison between Figures 53-54 and Figure 54 reveals that, the values of BH index of low carbon steels are significantly greater than that of ferritic stainless steel. This indicates that the heat treatment and pre-strain generally produce greater effect on the ΔYS of low carbon steels than ferritic stainless steel. Besides, the index BH_0 of low carbon steels are distinctly greater than that of ferritic stainless steel, the BH_0 values of low carbon steel with two heat treatments are around 72 MPa, while the BH_0 values of EN 1.4003 ferritic stainless steel are 26 MPa with 170 °C/20min heat treatment and 8 MPa with 230 °C/20min heat treatment, respectively. BH index reveals the susceptibility to static strain aging during paint-baking of the material. Thus, it can be revealed that the low carbon steels exhibit stronger bake hardening effect than the stainless steel, at least within 170 °C.

However, it is also noticeable that for the two low carbon steels, with the increase of pre-strain from 0% to 2%, BH index was increased rapidly with both baking temperatures. However, also with the both baking temperatures, the BH index was increased at slower rate along with the further increase of pre-strain. It is possible to predict that if greater level of pre-strain, like 12% and 14%, a very small or almost no increase of BH index would be seen [96-97].

Kuang, *et al*. [97] reported similar result when experimented with dual-phase steel, they pointed out that, the effect of pre-strain on the bake-hardening index contains two stages, when the pre-strain increases within very small range, $\Delta\sigma_{BH}$ increases rapidly, whereas when pre-strain exceeds certain range and continues increasing, the $\Delta\sigma_{BH}$ value is decreased. The same behavior was also found by Tang *et al*, [96] the bake hardening behavior of the Si-Al-Mn TRIP steel showed that, the $\Delta\sigma_{BH}$ value increases with the increasing pre-strain within 0-4%, but the $\Delta\sigma_{BH}$ value decreases when the pre-strain increases over 4%.

The increase of pre-strain increases the amount of mobile dislocations in the matrix. In this case, the high density of dislocations makes atoms migration easier by eliminating the diffusion distance between carbon atoms and free dislocation sites. Therefore, the increase in dislocation density increases the amount of dislocation pinning effect, which leads to the significant increase of BH index.

There is a maximum $\Delta\sigma_{BH}$ value with certain pre-strain, which is attributed to the maximum value of the degree of Cottrell atmosphere formation, above which the further increase of pre-strain does not lead to significant increase of Cottrell atmosphere formation [106]. When the mobile dislocations are saturated or the process is limited due

to the lack of sufficient interstitial C atoms. This is the reason for the decrease of $\Delta\sigma_{BH}$ value with high degree of pre-strain. Ferritic stainless steel exhibited differently that the $\Delta\sigma_{BH}$ value continues increasing with the increasing pre-strain, since the mobile dislocations had not been saturated. A critical degree of Cottrell atmosphere formation had not been reached even with 10% pre-strain. It can be predicted that with greater pre-strain, it will probably show similar decreasing trend as well.

Higher temperature accelerates the diffusion kinetics, which promotes the migration and diffusion of C and N atoms, thus, increasing the Cottrell atmosphere formation, and strengthening effect. That is why the $\Delta\sigma_{BH}$ values were greater when baked at 230 °C than those when baked at 170 °C. The same result and behavior were also found by Kuang, *et al* [97].

4.3 Aging Test Results

Representative stress-strain curves used in aging index determination are presented in Appendix E. In Figure 1 of Appendix E, the engineering stress-strain curve of initial steel A shows around shape, whereas the curve is slightly different after strain aging treatment. However, in Figure 2 of Appendix E, the engineering stress-strain curve of initial steel B shows the same shape as the curve of aged steel A (curve AI-A2), and the aged steel B (curve AI-B1) shows no difference from the curve of initial steel B. This suggest that the steel B had already aged a little bit at room temperature before 100 ˚C/30 min treatment, however, that temperature was not enough to produce more aging effects.

The results of the aging index determination of two low carbon steels are shown in Figure 56 and 57. It can be seen that the aging treatment led to a very slight decrease in strength and increase in elongation of two low carbon steels, but it practically produced no significant influence on the properties.

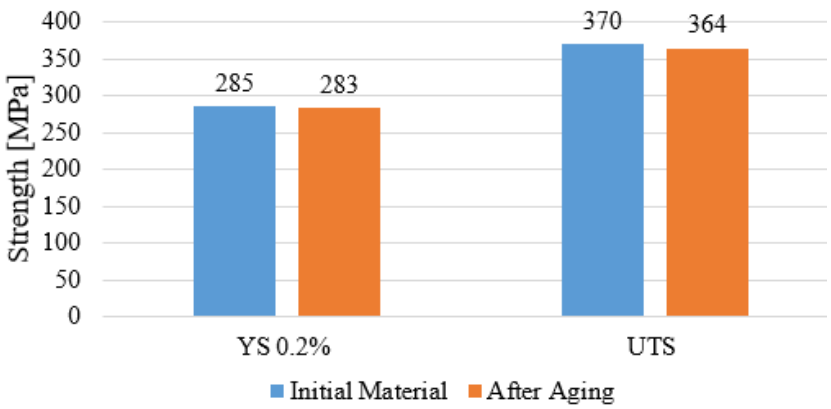

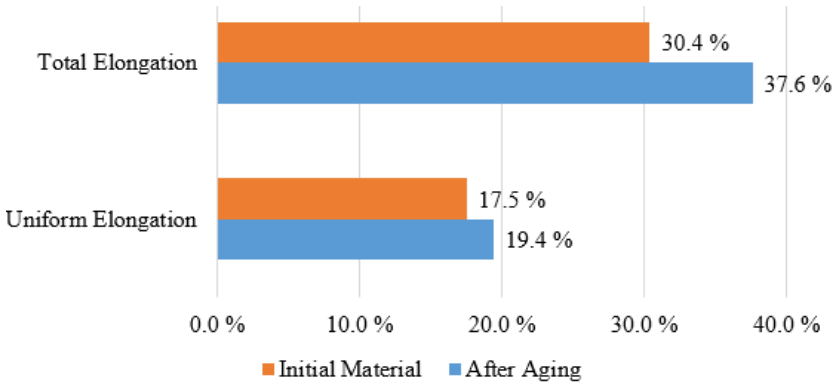

Figure 56. *Mechanical properties of steel A before and after 100 °C/30 min aging treatment.*

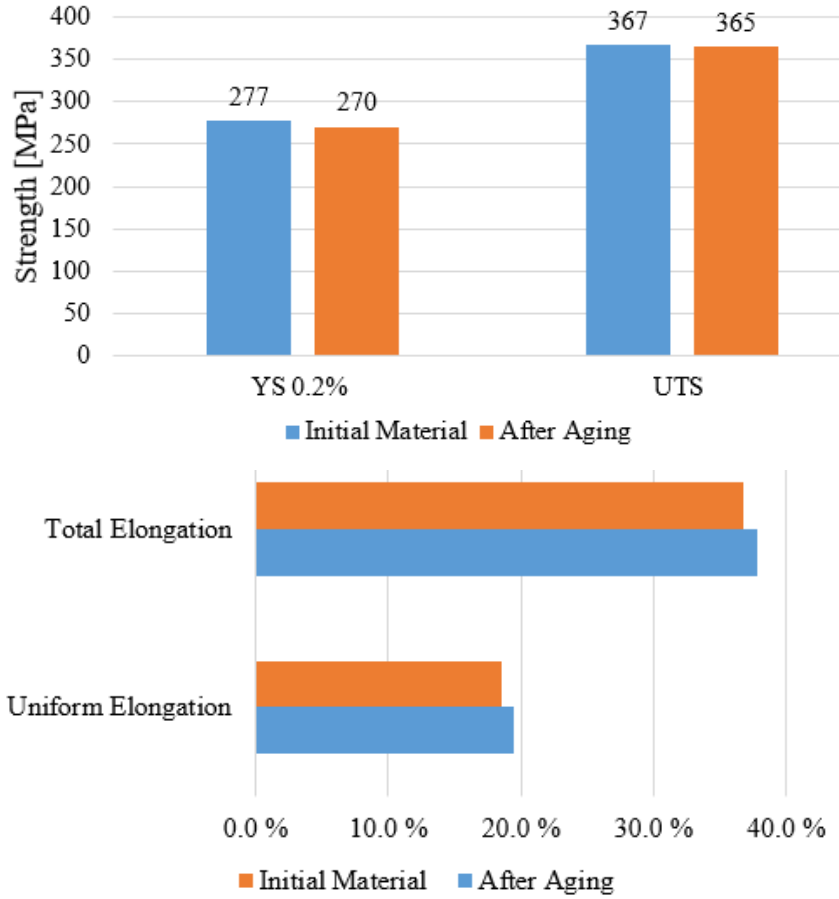

Figure 57. *Mechanical properties of steel B before and after 100 °C/30 min aging treatment.*

The results of the aging index determination of EN 1.4003 ferritic stainless steel are shown in Figure 58. The result is very similar to that of low carbon steels that the 100 °C/30 min aging treatment produced no significant influence on the properties.

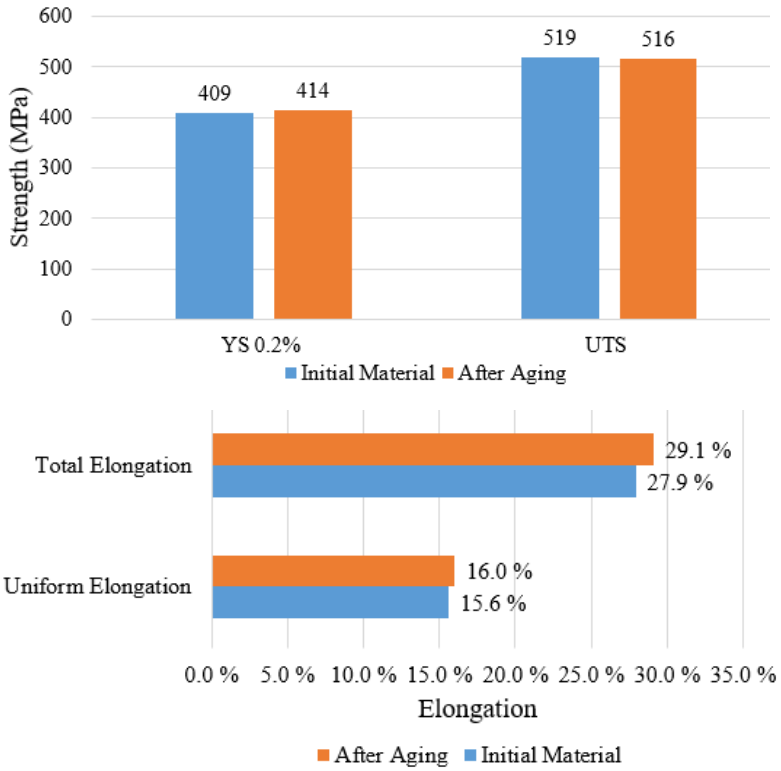

Figure 58. *Mechanical properties of steel C (1.4003 ferritic stainless steel) before and after 100 °C/30 min aging treatment.*

During the heat treatment of 100 °C/30min, the dislocations are recovered to some extent, which in a general level reduces strengths and improves ductility. On the other hand, the dislocations on the grain boundaries are pinned when the carbon migrates towards dislocations, which strengthens the material and decreases the ductility. These processes compete, and the result determines the final effect of aging treatment on the properties. It is most probably that in the ferritic stainless steel, higher temperature and higher activation energy are needed to activate carbon, the 100℃ heat treatment is not sufficient to migrate lots of carbon towards dislocation, M. Palosaari *et al*. [3] also found that activation energies for similar ferritic stainless steels are higher than that for ultra-low carbon bake hardenable steels.

In can be concluded that the aging temperature 100 °C was too low to cause significant aging. The slight increase of the total elongation is most probably aroused by natural scatter in material properties and tensile testing. 100 °C heat treatment is probably not sufficient to provide sufficient energy to activate the free carbon and nitrogen atoms to move. Thus, it suggests that the investigated low carbon steels and ferritic stainless steel are not susceptible to room temperature during storage.

4.4 Discussion of Errors and Future Work

4.4.1 Possible Sources of Errors

First of all, the small differences in the dimensions, compositions, mechanical properties exist among the specimens of the same material. However, the effects on the mechanical properties of the heat treatment and aging treatment are based on different specimens. For example, in Figure 55, the initial properties of C material were determined from two specimens of C material, whereas the properties after aging treatment are from another two C specimens. There can be small difference between these specimens. This error source has also been reported by Gabauer [107], who suggested that the shape and size of specimen and dimensional compliance all produce error in the tensile testing. But in this case, it is not practical to use the same specimen for both experiments. Thus, taking the average value of the results of two specimens has decreased the influence due to scattering.

Secondly, the influence on the data accuracy can also be from the testing data, which can be caused by the extensometer measurement. For example, the vibration of tensile testing machine generated noise to the measured data, which produces scattering curve and reduces the accuracy of the yield strength determination. In addition, the rubber band was used for fixing the extensometer on the specimen surface. However, the stainless steel specimens had very smooth surface and sharp edges. Therefore, to prevent the extensometer slipping in the testing and to prevent the rubber band being broken by the sharp edge, the tape was used between the extensometer and specimen surface. However, this can also reduce the accuracy of the result, especially when the rupture happens to or near the tape.

Some specimens did not exhibit ideal behavior during the tensile tests, as indicated in Figure 36. The backward straining and discontinuous yielding occurred in some tensile tests, which make it difficult to determine the properties. Scattering also happened when some test pieces were subjected to the tensile tests, which influences the accuracy of the data. Some errors also occur in the operation. For example, the sample cutting and grinding can cause stretches on the specimen surface, etching can all influence the surface condition, which consequently influence the microstructure. Errors can also come from the operation of heat treatment and tensile tests, which all influence the material behavior and properties. The errors can be reduced by using repeated experiments, while they cannot be avoided completely.

4.4.2 Further Work

In this study, the static strain aging behavior of selected ferritic steels was investigated by as a function of aging temperature and the amount of pre-strain. Further studies could address, for example, investigating the influence of aging time on the strain aging behavior and properties of the material, Palosaari, *et al*. [3], De, *et al*. [104], Vasilyev, *et al*. [108] have done the research in this field. They found that the strength increases with the increase of aging time within certain limit, while the further increase of aging time does not increase the strength more, or even leads to a decrease of strength. In order to understand the SSA phenomena in general, the influence of aging time on the material behavior can be investigated.

In addition, the effect of individual alloying elements on the bake hardening behavior could be investigated. Pereloma, *et al* [109] reported that the addition of chromium produced significant influence on the aging process. Similar research can be done to gain further understanding on how some specific elements affect the aging process and properties of the materials, and it would also give suggestion on the control of strain aging process.

5 CONCLUSIONS

Bake hardening behavior of two low carbon steels and a ferritic stainless steel (EN 1.4003) were investigated. The most important findings are summarized as below.

(1) It is necessary to reduce the width of the specimens after pre-straining and baking, before final tensile tests, in order to avoid the localization of the necking occurring at the softer areas outside the gauge section, i.e. areas between the grip sections and gauge section of the specimen.

(2) For the two low carbon steels, the strength was increased significantly with the increase of and baking temperature from 170 °C to 230 °C. However, the increase of pre-strain level from 0% to 10% also led to smaller strength increment.

(3) For EN 1.4003 ferritic stainless steel, 170 °C/20min and 230 °C/20min heat treatments led to slight strength increase. However, the increase of pre-strain level from 0% to 10% led to significant strength increase.

(4) Two low carbon steels exhibited very similar BH indexes in all cases. With the increase of pre-strain level from 0% to 10%, the BH indexes of two low carbon steels increased steadily and significantly from around 19 MPa to 54 MPa when baked at 170 °C, while they decreased steadily from around 70 MPa to 58 MPa when baked at 230 °C.

(5) With the increase of pre-strain level from 0% to 10%, the BH index of EN 1.4003 ferritic stainless steel increased not significantly when baked at 170 °C, but it increased steadily from 8 MPa to 32 MPa when baked at 230 °C. The BH index of two low carbon steels were significantly greater than that of EN 1.4003 stainless steel, which is due to the higher activation energy of EN 1.4003 ferritic stainless steel than the low carbon steels.

(6) 100 °C/30min aging treatment did not produce significant influence on the properties of three investigated ferritic steels.

REFERENCES

[1] Y. Y. Yan, F. L. Lian, G. F. Liang, et al., "An Overview of Strain in Low Carbon Steels," *Baosteel Technical Research*, Vol.8, No.2, pp.58-64, June 2014.

[2] A. Banerjee and S. K. Dhal, "Effect of Strain Ageing in Welded and Non-welded Low Carbon Steel," Bachelor's thesis, Dept. Metall. & Mater. Eng., Nat. Inst. of Tech., Rourkela, India, 2010.

[3] M. Palosaari, T. Manninen, R. Toppila, *et al*., "Static Strain Aging of Stabilized Ferritic Stainless Steels," in *Proc. 7th European Stainless Steel Conference, Como, Italy, September 21-23, 2011*, W. Nicodemi, J. O. Nilsoon, A. Tiziani, Eds. Milano, Italy: *La Metallurgia Italiana*, Vol.104, No.9, 2012. pp. 25-28.

[4] V. T. L. Buono, B. M. Gonzalez, and M.S. Andrade, "Strain Aging of AISI 430 Ferritic Stainless Steel," *Scrip Materialia*, Vol.38, No.2, pp. 185-190, Dec. 1997.

[5] B. L. Bramfitt, A. O. Benscoter. "Introduction to Steels and Cast Irons," in *Metallographer's Guide: Practices and Procedures for Irons and Steels*, Materials Park, Ohio: ASM International, 2002, pp. 1-21.

[6] R. Singh, *Applied Welding Engineering (Second Edition): Process, Codes, and Standards*. Oxford: Butterworth-Heinemann, 2016, p.33,

[7] D. T. Liewellyn and R. C. Hudd, "Low Carbon Strip Steels" in *Steels (Third Edition): Metallurgy and Applications*, Oxford: Butterworth-Heinemann, 1998, pp. 1-136.

[8] H. M. Cobb (Ed.), Appendix I: Metals History Timeline, in *Dictionary of Metals*, Materials Park, Ohio: ASM International, 2012, p.304.

[9] B. Boulet, G. Lalli, and M. Ajersch, "Modeling and Control of an Electric Arc Furnace," in *Proceedings of the 2003 American Control Conference, Denver, Colorado, USA, June 4-6, 2003*. Vol.4, July 2003, pp. 3060-3064.

[10] "Understanding the Benefits of Electric Arc Furnace Technology for Ceramics, Refractories, and Other Industries," *Ceramic Industry Magazine*, April 2015, pp. 33-34.

[11] J. Madias, “Electric Furnace Steelmaking,” in *Treatise on Process Metallurgy, Volume 3: Industrial Process*, S. Seetharaman, A. McLean, R. Guthrie, *et al*., Ed. Oxford: Elsevier, 2014, pp. 271-300.

[12] Y. X. Yang, K. Raipala, and L. Holappa, “Ironmaking,” in *Treatise on Process Metallurgy, Volume 3: Industrial Process*, S. Seetharaman, A. McLean, R. Guthrie, et al., Ed. Oxford: Elsevier, 2014, pp. 1-89.

[13] K. I. Satyendra, “Importance of Hearth, Deadman and Tapping in Blast Furnace Operation,” *Ispat GURU,* April 13, 2016. [Online]. Available: http://ispatguru.com/importance-of-hearth-dead-man-and-tapping-in-blast-furnace-operation/. [Accessed April 19, 2017].

[14] Stahl-Zentrum, “Hot Metal and Crude Steel Production,” *Steel Institute VDEh, German Steel Federation*, [Online], Available: http://en.stahl-online.de/index.php/topics/technology/steelmaking/. [Accessed April 19, 2017]

[15] M. M. Wolf, “History of Continuous Casting,” in *75th Steelmaking Conference Proceedings, Toronto, Canada, April 5-8, 1992*, Warrendale, PA: Iron & Steel Society, 1992, pp. 83-137.

[16] B. G. Thomas, “Continuous Casting,” in *Moelding for Casting and Solidification Processing*, New York: Marcel Dekker Inc, 2002, pp. 499-540.

[17] R. Singh, “Classification of Steels,” in *Applied Welding Engineering (2nd Edition): Process, Codes, and Standards,* Amsterdam: Elsevier Inc, 2016, pp. 57-64.

[18] B. J. Hewitt, “High Convention Hydrogen Batch Annealing in British Steel,” in *Review of Annealing Technology, Technical Exchange Session, Brussel, Belgium, May 3-4, 1995*, Brussel, Belgium: Int. Iron and Steel Inst., 1995. p. 51.

[19] M. Imose, Heating and Cooling Technology in the Continuous Cooling. *Trans. ISIJ*, Vol.25, pp. 911-932, 1985.

[20] D. Gandy, *Carbon Steel Handbook (1014670)*. Palo Alto, CA: Electric Power Research Institute, Inc, 2007.

[21] C. C. Anya and T. N. Baker, “The Effect of Silicon on the Grain Size and the Tensile Properties of Low Carbon Steels,” *Mater. Sci. Eng. Sec. A*, Vol.118, pp. 197-206, Oct. 1989.

[22] A. C. Reardon, "Steel Product and Properties," in *Metallurgy for the Non-Metallurgist, 2nd Edition*, Materials Park, Ohio: ASM International, 2011, pp. 175-196.

[23] G. Krauss, "High-Carbon Steels: Fully Pearlitic Microstructures and Applications," in *Steel: Processing, Structure, and Performance*. Materials Park, Ohio: ASM International, 2005, pp. 281-295.

[24] High Carbon Steels, Total Materia. Updated: April 2012. [Online] Available: http://www.totalmateria.com/page.aspx?ID=CheckArticle&site=kts &NM=368. [Accessed: June 13, 2016].

[25] B. Capudean, "Metallurgy Matters: Carbon Content, Steel Classifications, and Alloy Steels," *Practical Welding Today*, August 2003. [Online]. Available: http://www.thefabricator.com/article/metalsmaterials/carbon-content-steel-classifications-and-alloy-steels. [Accessed June 14, 2016].

[26] E. Lugscheider, "Constitution and properties of steels," Edited by F. B. Pickering, in *Vol.7 of Materials Science and Technology—A Comprehensive Treatment*. R. W. Cahn, P. Haasen, E. J. Kramer, Eds. Weinheim: Wiley-VCH, 1991, p.7, 41.

[27] C. Ouchi, "High Strength Low Alloy Steel," in *International Conference on High Strength Low Alloy Steels 1984, Wollongong, Australia, August 20-24, 1984*, Wollongong, Australia: University of Wollongong, 1985. p. 17.

[28] H. K. D. H. Bhadeshia, "Upper & Lower Bainite," in *Bainite in Steels: Transformations, Microstructure and Properties (Second Edition)*. London: IOM Communications, 2001, pp. 189-200.

[29] W. L. Costin and R. Kurji, "Evolution of Weld Metal Microstructure in Shielded Metal Arc Welding of X70 HSLA Steel with Cellulosic Electrodes: A Case Study," *Mater. Charact.*, Vol.107, pp. 317-326, Sept. 2015.

[30] D. Loder, S. K. Michelic, and C. Bernhard, "Acicular Ferrite Formation and Its Influencing Factors – A Review," *J. Mater. Sci. Res.*, Vol.6, No.1, pp. 24-43, Jan. 2017.

[31] I. Madariage, I. Gutierrez, and H. K. D. H. Bhadeshia, "Acicular Ferrite Morphologies in Medium-carbon Microalloyed Steel," *Metall. & Mater. Trans. A*, Vol.32A, No.9, pp. 2187-2197, Sept. 2001.

[32] H. K. D. H. Bhadeshia, "Modelling of Steel Welds," *Mater. Sci. & Tech.*, Vol.8, No.2, pp. 123-133, 1992.

[33] G. I. Rees and H. K. D. H. Bhadeshia, "Thermodynamics of Acicular Ferrite Nucleation," *Mater. Sci. & Tech.*, Vol.10, No.5, pp. 353-358, May 1994.

[34] A. A. B. Sugden and H. K. D. H. Bhadeshia, "Lower Acicular Ferrite," *Metall. Trans. A*, Vol.20, No.9, pp. 1811-1818, Nov. 1989.

[35] B.F. Decker and D. Harker, "Relations Between Initial and Final Orientations in Rolling and Annealing of Silicon Ferrite," *J. of Appl. Phys.*, Vol.22, No.900, 1951.

[36] K. M. Lee, M. Y. Huh, H. J. Lee, *et al*., "Effect of Hot Band Grain Size on Development of Textures and Magnetic Properties in 2.0% Si Non-Oriented Electrical Steel Sheet," *J. Magn. & Magn. Mater.*, Vol.396, pp. 53-64, Dec. 2015.

[37] J. R. Davis, "High-Strength Low-Alloy Steels," in *Alloying: Understanding the Basics*. Materials Park, Ohio: ASM International, 2001, pp. 193-202.

[38] H. D. Hibbard, *Manufacture and Uses of Alloy Steels*. Washington: Government Printing Office, June 1916.

[39] H. M. Cobb, "The Early Discoveries, and Discoveries of Commercial Usefulness of Stainless Steel," in *The History of Stainless Steels*, Materials Park, Ohio: ASM International, 2010, pp. 7-24.

[40] L. Béla, "Stainless – Stainless Steel and Their Properties, 2nd ed." *Weld. J.*, Vol.1, pp. 5-9, 2000/2001.

[41] AZoM, "Stainless Steels – Introduction to the Grades and Families," May 2001. [Online]. Available: http://www.azom.com/article.aspx?ArticleID=470. [Accessed Feb. 27, 2016].

[42] J. R. Davis, *Alloy Digest Sourcebook: Stainless Steels*. Materials Park, Ohio: ASM International, 2000.

[43] C. G. Tiburcio and C. B. Durtewitz, "Electrochemical Corrosion of Ferritic 409 and 439 Stainless Steels 409 and 439 in NaCl and H_2SO_4 Solutions," *Int. J. Electrochem. Sci.*, Vol.11, pp. 1080-1091, Jan. 2016.

[44] S. M. Dubiel and J. Cieslak, "Sigma-phase in Fe-Cr and Fe-V Alloy Systems and Its Physical Properties," *Crit. Rev. Solid State & Mater. Sci.*, Vol.36, No.4, pp. 191 – 208, 2011.

[45] Outokumpu Oy, Handbook of Stainless Steel, Espoo, Finland: Outokumpu Oyj, 2013.

[46] J. Charles, J. D. Mithicux, P. O. Santacreu, *et al*. "The Ferritic Stainless Steel Family: The Appropriate Answer to Nickel Volatility?" in *6th European Stainless Steel Conference: Science and Market, Helsinki, Finland, June 10-13, 2008*, Paris: Revue De Métallurgie, Vol.106, No.3, 2009, pp. 124-139.

[47] M. F. McGuire, "Ferritic Stainless Steels," in *Stainless Steels for Design Engineers*, Materials Park, Ohio: ASM International, 2008, pp. 109-122.

[48] C. C. Hsieh and W. Wu, "Overview of Intermetallic Sigma (σ) Phase Precipitation in Stainless Steels," *ISRN Metallurgy*, Vol.2012, pp. 1-16, Jan. 2012.

[49] R. J. Gray, V. K. Sikka, and R. T. King, "Detecting Transformation of Delta-ferrite to Sigma Phase in Stainless Steels by Advanced Metallographic Techniques," *JOM*, Vol.30, No.11, pp. 18–26, Nov. 1978.

[50] N. Baddoo, K. Cashell, S. Afshan, *et al*., *Structural Applications of Ferritic Stainless Steels*, Luxembourg: Publications Office of the European Union, 2015.

[51] Outokumpu Stainless Oy, Outokumpu Welding Handbook, 10th Edition, Avesta, Sweden, 2010.

[52] EN 10088-1. Stainless Steels – Part 1: List of Stainless Steels, CEN, 2005.

[53] K. A. Cashell and N. R. Baddoo, "Ferritic Stainless Steels in Structural Applications," *Thin-Walled Structures*, Vol.83, pp. 169-181, Oct. 2014

[54] EN 10088-4. Stainless Steels – Part 4: Technical Delivery Condition for Sheet/Plate and Strip of Corrosion Resisting Steels for Construction Purposes. CEN, 2009.

[55] M. Cortie and M. du Toit, "Ferritic Stainless Steels," in *Encyclopedia of Materials: Science and Technology (2nd Edition),"* Amsterdam: Elsevier, 2001, pp. 3037-3039.

[56] Avesta Welding, M. Laren ed, *The Avesta Welding Manual – Practice and Products for Stainless Steel Welding*, Avesta: Avesta Welding AB, 2004. p. 8.

[57] J. Bauschinger, "Variations in the elastic limit of iron and steel," *J. Iron Steel Inst.*, Vol.12, No.1, pp. 442-444, 1887.

[58] R. N. Wright, "Relevant Aspects of Carbon and Low Alloy Steel Metallurgy," in *Wire Technology: Process Engineering and Metallurgy (Second Edition)*, Oxford: Butterworth Heinemann, 2011, pp.199-228.

[59] G.T. Van Rooyen, "The Embrittlement of Hardened, Tempered Low-alloy Steel by Strain Aging," *SAIMM Journal*, Vol.86, No.2, pp. 67-72, 1986.

[60] G. E. Dieter, "Mechanical Behavior Under Tensile and Compressive Loads," in *Mechanical Testing and Evaluation, ASM Handbook*, Vol.8, Materials Park, Ohio: ASM International, 2000, p.100.

[61] M. Ivanchenko, "Dynamic Strain Aging of Austenitic Stainless Steels and Ni-Base Alloys," Ph.D. dissertation, Dept. Eng. Design & Production, Aalto University, Espoo, Finland, 2010.

[62] C. Cornet, K. Wackermann, C. Stöcker, *et al*., "Effects of Temperature and Hold Time on Dynamic Strain Aging in a Nickel Based Superalloy," *Materials at High Temperatures*, Vol.31, No.3, pp. 226-232, 2014.

[63] M. E. Donnelly, "The Flow Stress of Low Carbon Steels under Hot Deformation: A Basic Data Compilation for Process Analysis," Master's thesis, Rensselaer Polytechnic Institute, New York, USA, 1982.

[64] A. H. Cottrell and B. A. Bilby, "Dislocation Theory of Yielding and Strain Aging of Iron," *Proc. Phy, Soc. Sec. A.* Vol.62, No.1, 1949. pp. 49-62.

[65] I. Z. F. Ahmed, M. Ahmed, B. Gemeal, *et al*, "Influence of Skin Pass Design and Aging Phenomena on Steel Sheets Surface Characteristics," *JFAP*, Vol.16, No.1, 2016. pp. 86-94.

[66] A. Pense, "HPS Corrugated Web Girder – Report: Part 4: Literature and Experimental Study of Strain Aging in HPS and Other Bridge Steels," Lehigh University, Bethlehem, PA, April 2004.

[67] T. Rajendra, K. Rachappa, and S. A. Kumar. “Control of Nitrogen Pickup in Steel at Continuous Casting Using Buckinghan PI Theorem,” *IJETAE*, Vol.4, No.8, 2014. pp. 800-806.

[68] F. S. Huo. “The Use of Iron Carbide for the Removal of Nitrogen from Molten Steel,” Master’s thesis, Dept. Mater. Eng., Univ. of Wollongong, Wollongong, Australia, 1997.

[69] W. Craft and D. C. Hilty, “Deoxidation and Inclusion Control for Alloy Steel,” in *Symposium on Production, Properties and Applications of Alloy and Special Steels, Jamshedpur, India, Feb. 1-4, 1956*, B. R. Nijhawan, P. K. Gupte, Eds. New Dehli, India: Council of Scientific and Industrial Research, 1958.

[70] A. Nussbaumer, G. Sedlacek, and B. Kühn, *Use and Application of High Performance Steels for Steel Structures*. Zürich: IABSE-AIPC-IVBH, 2004.

[71] F. Schröter and T. Lehnert, “Trends in the Application of High-Performance Steel in European Bridge Building,” in *The Eight International Conference “Bridges in Danube Basin”*, E. Petzek, R. Bancila, Ed. Wiesbaden, Germany: Springer Fachmedien Wiesbaden GmbH, 2014, pp. 35-50.

[72] H. Kantereit, “Bake Hardening Behavior of Advanced High Strength Steels under Manufacturing Conditions,” SAE International, Pittsburgh, Techn. Paper: 2011-01-1053, Apr. 12, 2011.

[73] S. Das, “Bake Hardening in Low and Medium Carbon Steels,” Ph.D. dissertation, Dept. Metall. & Mater. Eng., Natl. Inst. Tech., Kharagpur, India, Aug. 2012.

[74] P. P. Seth, “Study of Bake-hardening Behavior of Ultra-low Carbon BH 220 Steel at Different Strain Rates,” Master’s thesis, Dept. Metall. & Mater. Eng., Natl. Inst. Tech., Rourkela, India, May 2014.

[75] W. C. Leslie, *The Physical Metallurgy of Steel*. New York: McGraw Hill Book Company, 1981.

[76] L. J. Baker, J. D. Parker, and S. R. Daniel, “Metallurgy and Processing of Ultralow Carbon Bake Hardening Steels,” *Mater. Sci. & Tech.*, Vol.18, No.4, 2002. pp. 541-547.

[77] W. B. Hutchinson, K. L. Nilson, and J. Hirsch, "Annealing Textures in Ultra-Low Carbon Steels," *Metallurgy of Vacuum Degreased Steel Products*, TMS, pp.109-125, 1990.

[78] G. O. Edward, "*Advanced High Strength Steel Application Guidelines, Version 3*," International Iron and Steel Institute, Committee on Automotive Application, Sept. 2006.

[79] A. V. Snick, K. Lips, B. C. De Cooman, *et al*. "Modern LC and ULC Sheet Steels for Cold Forming: Processing and Properties," in *International symposium, RWTH Aachen University of Technology, Germany, Mar.30 – Apr.1, 1998*, W. Bleck, Eds. Aachen: Institute of Ferrous Metallurgy, 1998, pp. 413-424.

[80] P. Elsen and H. P. Hougardy, "On the Mechanism of Bake Hardening," *Steel Res.*, Vol.64, No.8/9, pp. 431-436, 1993.

[81] K. Lindqvist, "Bake Hardening Effect in Advanced High-Strength Steels," Master's thesis, Dept. Appl. Mech., Chalmers Univ. of Tech., Gothenburg, Sweden, 2013.

[82] V. Ballarin, M. Soler, A. Perlade, *et al*, "Mechanisms and Modeling of Bake-Hardening Steels: Part 1. Uniaxial Tension," *Metall. & Mater. Trans. Sec. A*, Vol.40, No.6, pp. 1367-1374, 1999.

[83] A. K. De, K. De Blauwe, S. Vandeputte, *et al*, "Effect of Dislocation Density on the Low Temperature Aging Behavior of an Ultra-low Carbon Bake Hardening Steel," *J. Alloy. & Compd*, Vol.310, pp. 405-410, 2000.

[84] W. Bleck, *Trends in Automotive Steel Development*, Asia Steel International Conference Proceedings, Sept. 23, 2012, Beijing, China. Beijing: Chinese Society of Metals, 2012.

[85] D. V. Wilson, B. Russell, and J. D. Eshelby, "Stress Induced Ordering and Strain-Aging in Low Carbon Steels," *Acta Metallurgica*. Vol.7, No.9, pp. 628-631, 1959.

[86] D. V. Wilson and B. Russell, "The Contribution of Atmosphere Locking to the Strain-Aging of Low Carbon Steels," *Acta Metallurgica*. Vol.8, No.1. pp. 36-45, 1960.

[87] D. V. Wilson and B. Russell, "The Contribution of Precipitations to Strain Aging in Low Carbon Steels," *Acta Metallurgica*. Vol.8, No.7, pp. 468-479, 1960.

[88] J. L. Snoek, "Effect of Small Quantities of Carbon and Nitrogen on the Elastic and Plastic Properties of Iron," *Physica*. Vol.8, No.7, pp. 711-733, 1941.

[89] H. K. D. H. Bhadeshia and R. W. K. Honeycombe, *Steels: Microstructure and Properties, 3rd Edition*. Oxford: Butterworth-Heinemann, 2006.

[90] J. J. M. Exebio. "Metallurgical Phenomena Governing the Bake Hardening Response of Bake Hardenable Steels," Master's thesis, Dept. Mater. Eng., Delft Univ. of Techn., Delft, Netherlands, 2002.

[91] M. Kurosawa, S. Sato, T. Obara, *et al*, "Age-hardening Behavior and Dent Resistance of Bake-hardenable and Extra Deep-drawable High Strength Steel," *Kawasaki Steel Technical Report*. No.18, pp. 61-65, 1988.

[92] A. N. Bhagat, S. J. Baek, and H. C. Lee, "A Simple Method for Prediction of Shelf Life of Bake Hardening Steels," *ISIJ International*, Vol.48, No.12, pp. 1781-1787, 2008.

[93] S. Hainai, N. Takemoto, Y. Tokunaga, *et al*, "Effect of Grain Size and Solid Solution Strengthening Elements on the Bake Hardenability of Low Carbon Aluminum-killed Steel," *Transaction ISIJ*, Vol.24, pp. 17-23, 1984.

[94] J. M. Rubianes and P. Zimmer. *Rev. Metall. Cah. Int. Tech.*, pp. 99-109, 1996.

[95] A. K. De, S. Vandeputte, and B. C. De Cooman, "Static Strain Aging Behavior of Ultra Low Carbon Bake Hardening Steel," *Scripta Materialia*, Vol.41, No.8, pp. 831-837, 1998.

[96] Z. Y. Tang, H. Ding, H. Ding, *et al*, "Effect of Prestrain on Microstructures and Properties of Si-Al-Mn TRIP Steel Sheet with Niobium," *J. Iron & Steel Res. Int.*, Vol.17, No.4, pp. 59-65, 2010.

[97] C. F. Kuang, S. G. Zhang, J. Li, *et al*, "Effect of Prestrain on Microstructures and Bake-hardening Behavior of Dual-phase Steel," *Int. J. Miner., Metall. & Mater.*, Vol.21, No.8, pp. 766-771, 2014.

[98] K. Dehghani and J. J. Jonas, "Dynamic Bake Hardening of Interstitial-free Steels," *Metall. & Mater. Trans. Sec. A*, Vol.31, pp. 1375-1384, 2000.

[99] Instron. Fast Track 8800 – 8801 Series Brochure: 8801 Series Fatigue Testing Systems.

[100] Zwick Roell AG. Booklet: Extensometers for Materials Testing Machines.

[101] J. Pelleg, "Plastic Deformation," in *Mechanical Properties of Materials*, Amsterdam: Springer Netherlands, 2013, pp. 147-194.

[102] S. Hanai, N. Takemoto, Y. Tokunaga, *et al*, "Effect of Grain Size and Solid Solution Strengthening Elements on the Bake Hardenability of Low Carbon Aluminum-killed Steel," *Trans. of ISIJ*, Vol.24, No.1, pp.17-23, 1984.

[103] M. Palosaari and T. Manninen, "Bake-Hardening of Stabilized Ferritic Stainless Steels," in *Proceedings of 14th International Conference on Metal Forming, Metal Forming 2012, AGH University of Science and Technology, Krakow, Poland, Sept. 16-19, 2012*. Weinheim: Wiley-VCH Verlag GmbH & Co. KGaA, 2012. pp. 951-954.

[104] H. A. Ali, "Bake Hardening of Low Carbon Steels," *Sudan Engineering Society Journal*, Vol.54, No.51, 2008, pp. 37-43.

[105] S. Das, S. B. Sigh, O. N. Mohanty, *et al*., "Understanding the Complexity of Bake Hardening," *Mater. Sci. & Tech.*, Vol.24, No.1, pp. 107-111, 2008.

[106] J. Z. Zhao, A. K. De, and B. C. De Cooman, "Formation of the Cottrell Atmosphere During Strain Aging of Bake-hardenable Steels," *Metall. & Mater. Trans. Sec. A*, Vol.32, No.2, pp. 417-432, 2001.

[107] W. Gabauer, "The Determination of Uncertainties in Tensile Testing," *Standards Measurement & Testing Project No. SMT4-CT97-2165*. UNCERT COP 07: 2000.

[108] A. Vasilyev, N. Kuzmin, and A. Lee, "Strain Aging of Bake Hardening Steel for Automotive Application," in *Materials Science & Technology Conference and Exhibition (MS & T 2007), Detorit, Michigan, USA, Sept. 16-20, 2007*. New York: Curran & Associates Inc, 2009. pp. 4029-4043.

[109] E. Pereloma, V. Bata, and A. Gazder, "The Effect of Chromium Addition on the Strain Ageing and Recrystallization Behavior of Low Carbon Steel," in *the 3rd International Symposium on Steel Science, ISSS 2012, Kyoto, Japan, May 27-30, 2012*, T. Furuhara, H. Numakura, and K. Ushioda, Eds. Tokyo: ISIJ, 2012, pp. 41-50.

APPENDICES

Appendix A: Dimensions of the Experimental Specimens

Specimen	Thickness	Width	Specimen	Thickness	Width
A1	0.560	19.293	**B1**	0.533	19.411
A2	0.553	19.279	**B2**	0.552	19.403
A3	0.560	19.316	**B3**	0.549	19.39
A4	0.561	19.364	**B4**	0.551	19.388
A5	0.557	19.361	**B5**	0.545	19.406
A6	0.553	19.339	**B6**	0.554	19.366
A7	0.557	16.007	**B7**	0.546	16.110
A8	0.549	16.055	**B8**	0.547	16.102
A9	0.555	15.995	**B9**	0.547	16.030
A10	0.552	15.996	**B10**	0.554	16.158
A11	0.549	16.010	**B11**	0.551	15.980
A12	0.551	15.988	**B12**	0.553	15.926
A13	0.559	15.995	**B13**	0.55	15.974
A14	0.555	15.916	**B14**	0.552	15.892
A15	0.557	15.868	**B15**	0.549	9.950
A16	0.556	15.832	**B16**	0.547	9.882
A17	0.56	15.895	**B17**	0.551	9.958
A18	0.557	15.921	**B18**	0.556	12.302
Specimen	**Thickness**	**Width[1]**	**Specimen**	**Thickness**	**Width**
C1	1.982	15.9825	**C10**	1.985	15.9825
C2	1.976	15.9825	**C11**	1.976	15.9825
C3	1.971	15.9825	**C12**	1.982	15.9825
C4	1.977	15.9825	**C13**	1.968	15.9825
C5	1.975	15.9825	**C14**	1.971	15.9825
C6	1.968	15.9825	**C15**	1.969	15.9825
C7	1.971	15.9825	**C16**	1.973	15.9825
C8	1.965	15.9825	**C17**	1.969	15.9825
C9	1.970	15.9825	**C18**	1.966	15.9825

N.B: [1] The average value of width was used.

[2] The unit of the values is mm.

[3] Specimens A7-A18, B7-B18, and C1-C18 were re-machined.

[4] The initial dimensions (before re-machining) were used to determine pre-strain curves, the original dimension of the re-machined specimens are presented below.

Original Dimensions of the Re-machined Specimens

Specimen	Thickness	Width	Specimen	Thickness	Width
A7	0.557	19.355	**B7**	0.546	19.404
A8	0.549	19.391	**B8**	0.547	19.423
A9	0.555	19.406	**B9**	0.547	19.392
A10	0.552	19.377	**B10**	0.554	19.224
A11	0.549	19.409	**B11**	0.551	19.323
A12	0.551	19.387	**B12**	0.553	19.296
A13	0.559	19.417	**B13**	0.55	19.364
A14	0.555	19.456	**B14**	0.552	19.402
A15	0.557	19.417	**B15**	0.549	19.405
A16	0.556	19.408	**B16**	0.547	19.397
A17	0.56	19.418	**B17**	0.551	19.306
A18	0.557	19.489	**B18**	0.556	19.28
Specimen	**Thickness**	**Width**	**Specimen**	**Thickness**	**Width**
C1	1.982	20.061	**C10**	1.985	20.142
C2	1.976	20.073	**C11**	1.976	19.95
C3	1.971	20.06	**C12**	1.982	20.085
C4	1.977	19.945	**C13**	1.968	20.129
C5	1.975	19.982	**C14**	1.971	20.11
C6	1.968	20.038	**C15**	1.969	20.056
C7	1.971	20.112	**C16**	1.973	20.083
C8	1.965	20.12	**C17**	1.969	20.044
C9	1.970	20.071	**C18**	1.966	20.121

Appendix B: Representative Engineering Stress-strain Curves for Materials Tested in Initial Condition and After Bake Hardening Heat Treatments, No Pre-strain

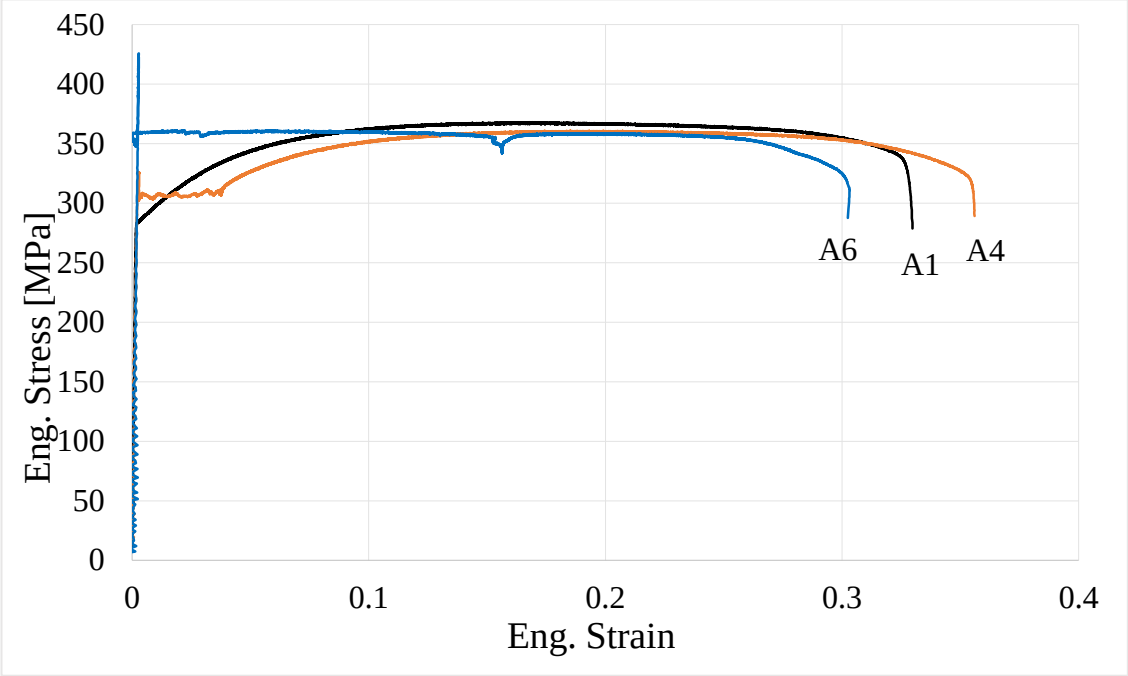

Figure 1. *Engineering stress-strain curves for specimens A1 (initial steel A), A4 (after 170 °C/20min), and A6 (after 230 °C/20min).*

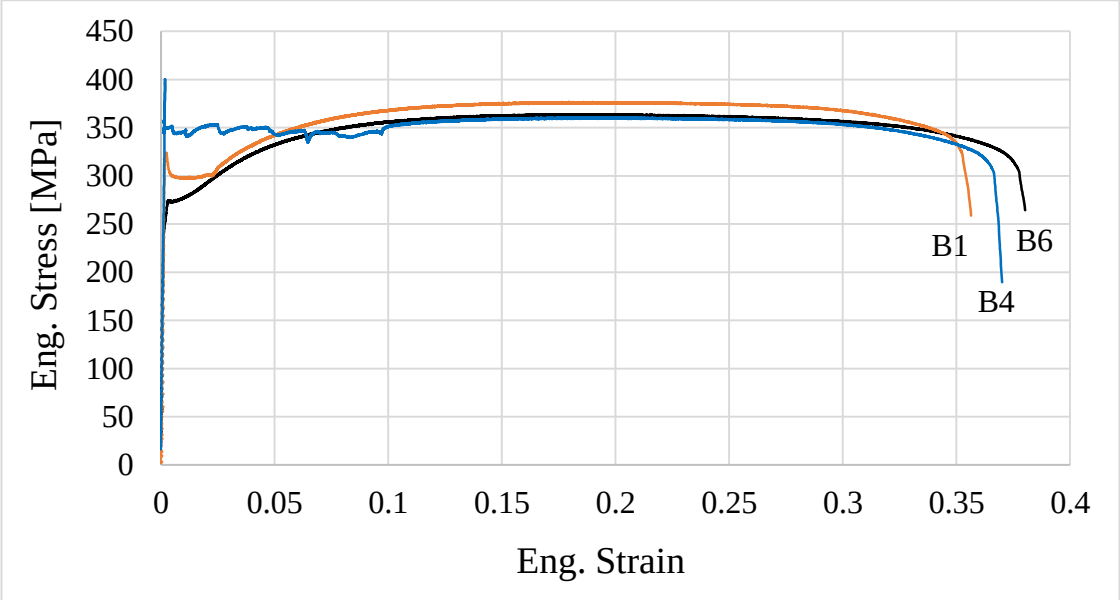

Figure 2. *Engineering stress-strain curves for specimens B6 (initial steel B), B1 (after 170 °C/20min), and B4 (after 230 °C/20min).*

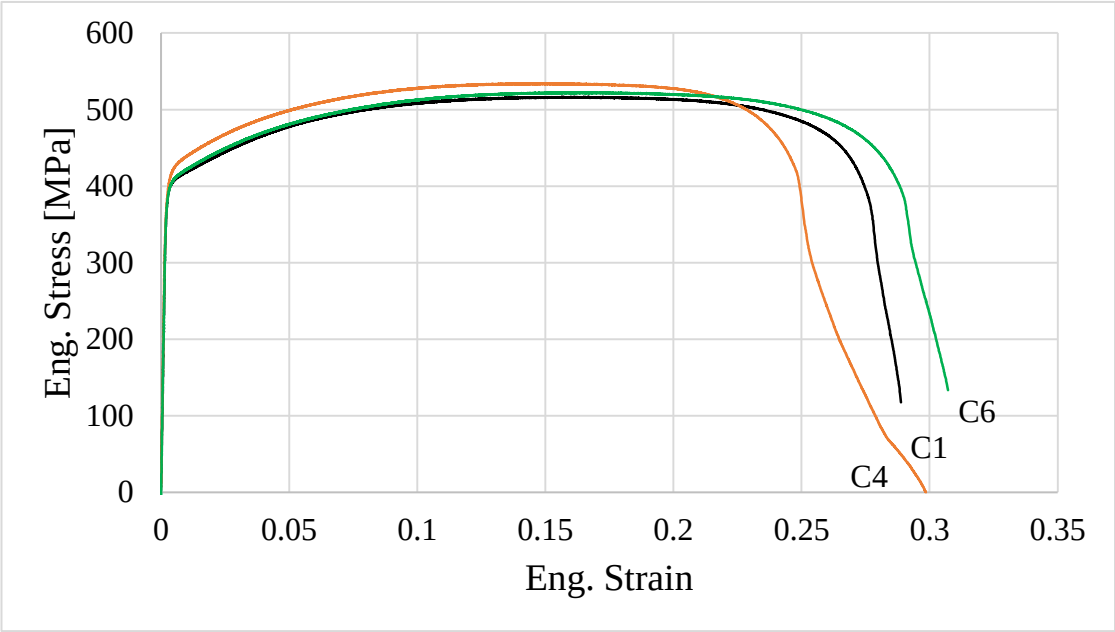

Figure 3. *Engineering stress-strain curves for specimens C1 (initial steel C), C4 (after 170 °C/20min), and C6 (after 230 °C/20min).*

N.B: C1 curve was made by editing the data of the ending part, since the strain measured from extensometer did not follow the variation with the piston, the edition tried to remove the error from vibration.

Appendix C: Representative Engineering Stress-strain Curves Describing the Effects of Pre-straining and Bake Hardening Heat Treatments

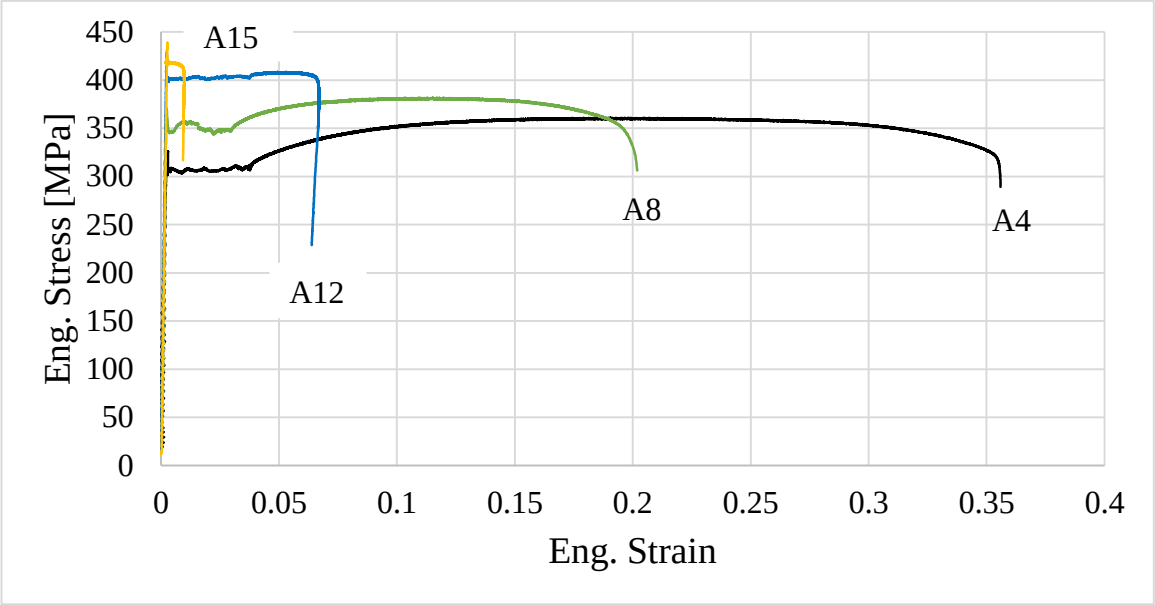

Figure 1. *Engineering stress-strain curves for specimens A4 (170 °C/20min), A8 (2% pre-strain, 170 °C/20min), A12 (6% pre-strain, 170 °C/20min), A15 (10% pre-strain, 170 °C/20min).*

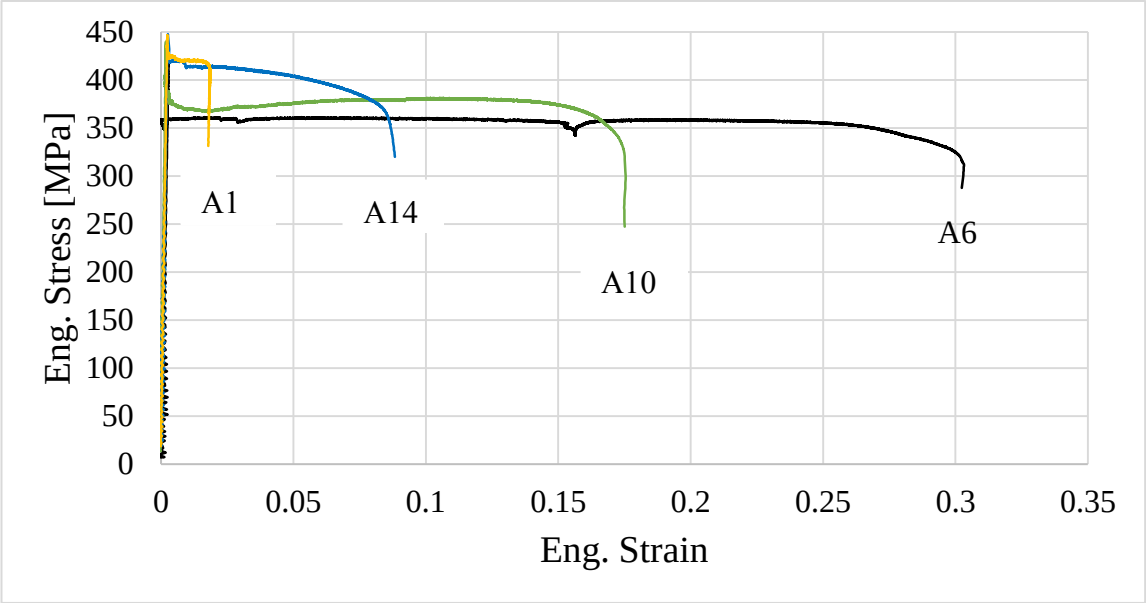

Figure 2. *Engineering stress-strain curves for specimens A6 (230 °C/20min), A10 (2% pre-strain, 230 °C/20min), A14 (6% pre-strain, 230 °C/20min), A18 (10% pre-strain, 230 °C/20min).*

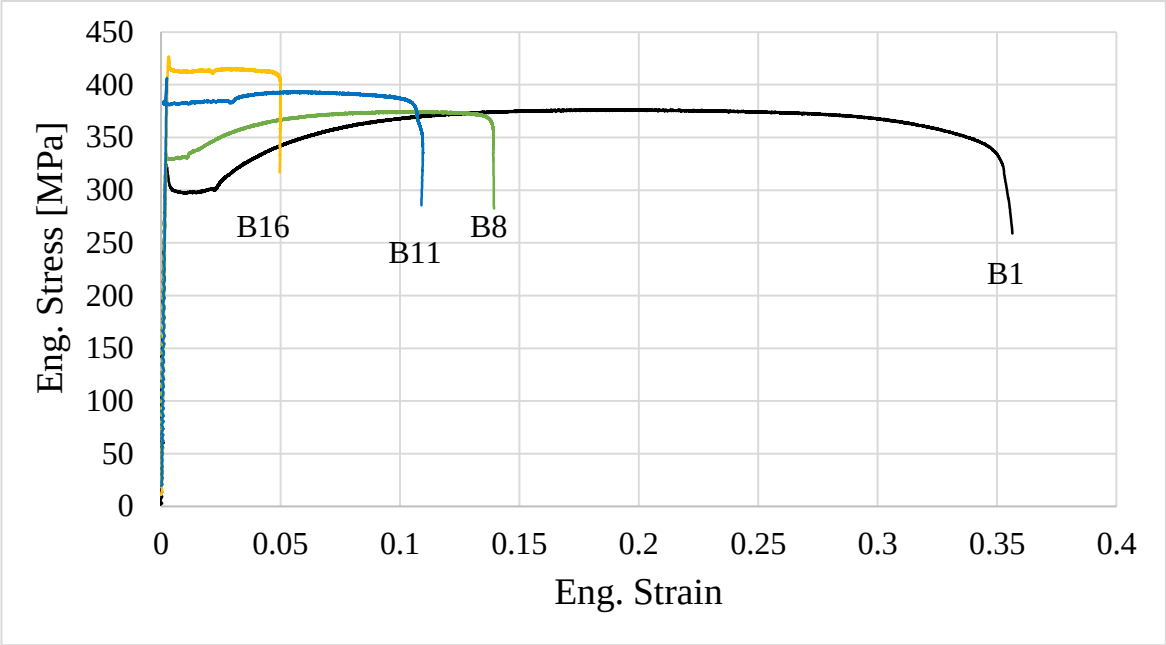

Figure 3. *Engineering stress-strain curves for specimens B1 (170 ℃/20min), B8 (2% pre-strain, 170 °C/20min), B11 (6% pre-strain, 170 °C/20min), B16 (10% pre-strain, 170°C/20min).*

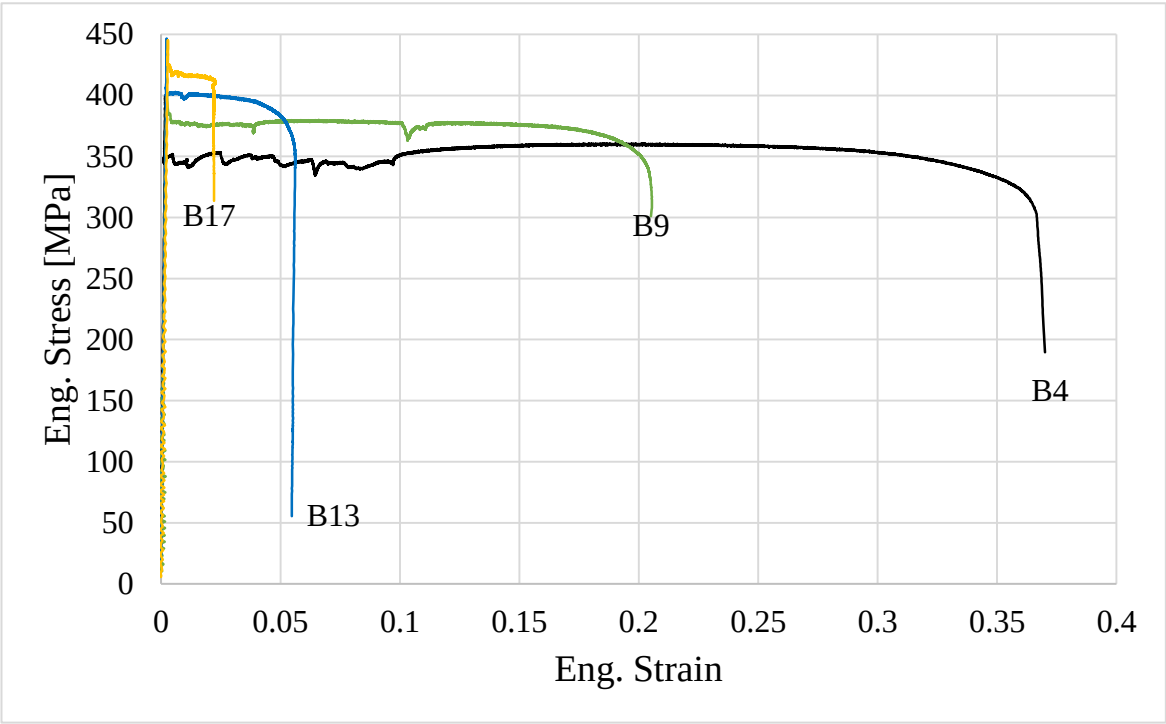

Figure 4. *Engineering stress-strain curves for specimens B4 (230 °C/20min), B9 (2% pre-strain, 230 °C/20min), B13 (6% pre-strain, 230 °C/20min), B17 (10% pre-strain, 230 °C/20min).*

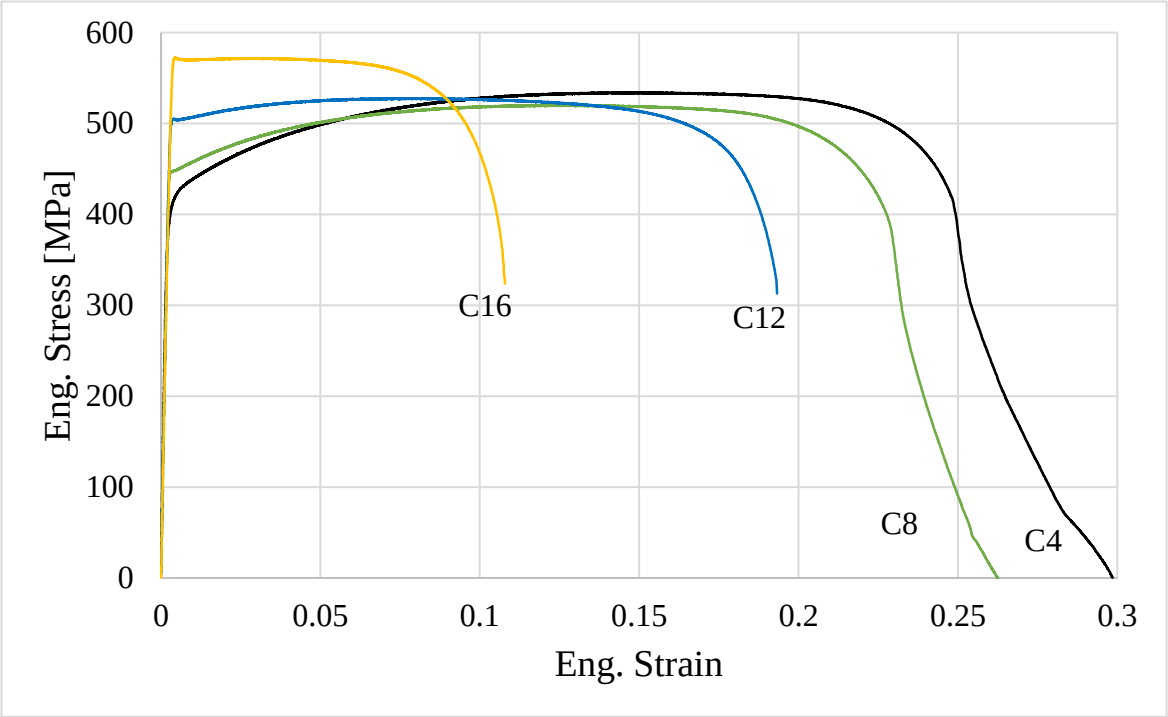

Figure 5. *Engineering stress-strain curves for specimens C4 (170 °C/20min), C8 (2% pre-strain, 170 °C/20min), C12 (6% pre-strain, 170 °C/20min), C16 (10% pre-strain, 170 °C/20min).*

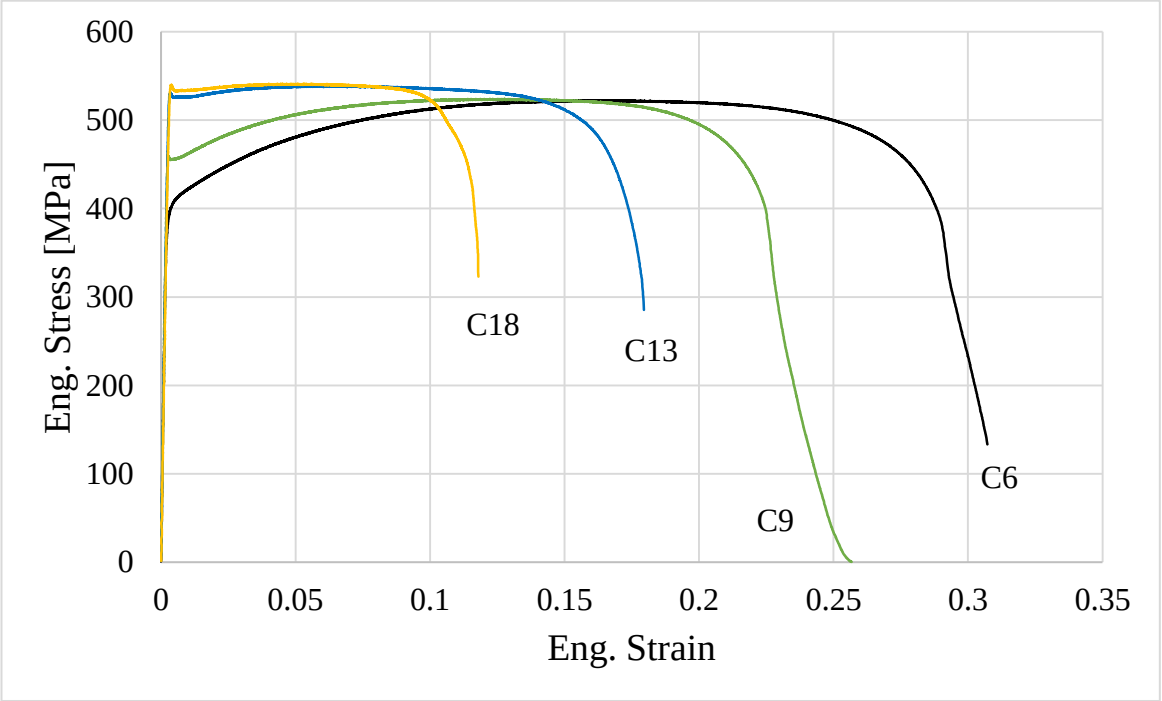

Figure 6. *Engineering stress-strain curves for specimens C6 (230 °C/20min), C9 (2% pre-strain, 230 °C/20min), C13 (6% pre-strain, 230 °C/20min), C18 (10% pre-strain, 230 °C/20min).*

Appendix D: Bake Hardening Indexes of Investigated Steels

BH Indexes of Steel A

Heat Treatment	BH	Specimens	BH Index 1 (MPa)	Specimens	BH Index 2 (MPa)	Average BH Index (MPa)
170℃ /20min	BH0	A1-A3	19.1	A1-A4	21.4	20
	BH2	A7	39.6	A8	44.0	42
	BH6	A11	47.4	A12	48.9	48
	BH10	A15	54.4	A16	55.3	55
230℃ /20min	BH0	A1-A5	73.0	A1-A6	73.8	73
	BH2	A9	69.5	A10	68.7	69
	BH6	A13	65.0	A14	67.9	66
	BH10	A17	50.6	A18	61.5	56

BH Indexes of Steel B

Heat Treatment	BH	Specimens	BH Index 1 (MPa)	Specimens	BH Index 2 (MPa)	Average BH Index (MPa)
170℃ /20min	BH0	B6-B1	23.8	B6-B2	11.3	18
	BH2	B7	38.0	B8	38.7	38
	BH6	B11	42.7	B12	41.7	42
	BH10	B15	52.8	B16	54.2	54
230℃ /20min	BH0	B6-B3	68.0	B6-B4	71.5	70
	BH2	B9	74.5	B10	72.4	73
	BH6	B13	58.6	B14	58.0	58
	BH10	B17	63.5	B18	58.0	61

BH Indexes of Steel C

Heat Treatment	**BH**	**Specimens**	**BH Index 1 (MPa)**	**Specimens**	**BH Index 2 (MPa)**	**Average BH Index (MPa)**
170℃ /20min	BH0	C1-C3	38.8	C1-C4	12.8	26
	BH2	C7	15.2	C8	15.1	15
	BH6	C11	15.5	C12	16.0	16
	BH10	C15	26.0	C16	26.3	26
230℃ /20min	BH0	C1-C5	16.2	C1-C6	0.2	8
	BH2	C9	21.1	C10	20.2	21
	BH6	C13	26.8	C14	26.5	27
	BH10	C17	32.3	C18	32.7	33

N.B: Since there are two repeated tests in each case, BH index 1 and 2 are for two tested results, and their average value is taken as the BH index of the steel.

Appendix E: Representative Engineering Stress-strain Curves of the Specimens Before and After Aging Treatment

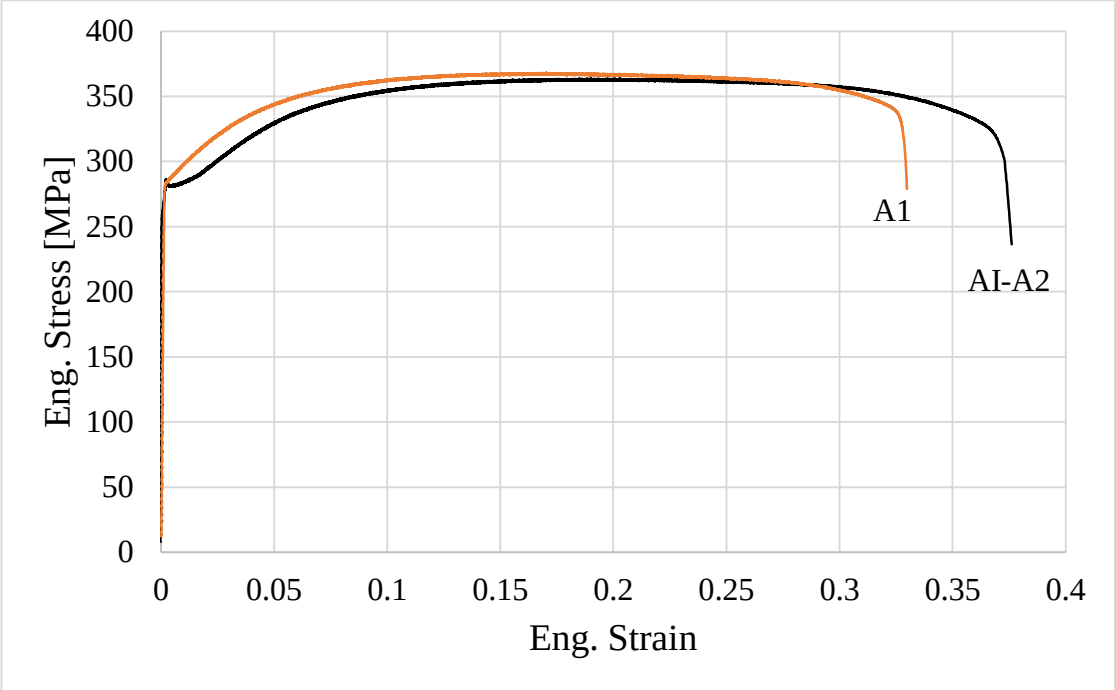

Figure 1. *Comparison of the engineering stress-strain curves for steel A before (A1) and after (AI-A2) 100 °C/30min aging treatment.*

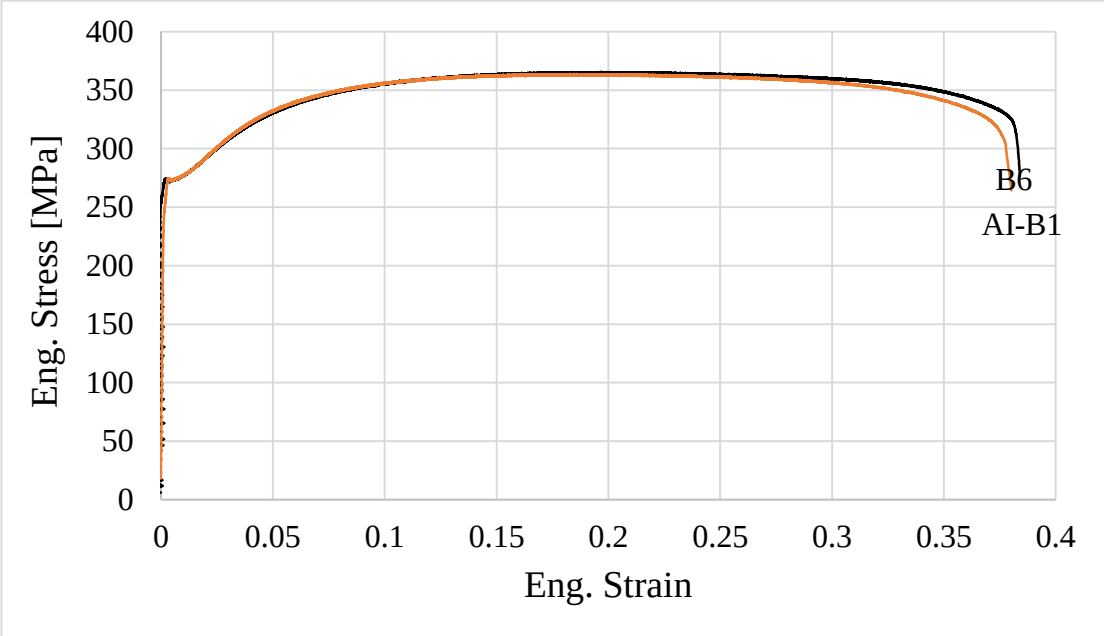

Figure 2. *Comparison of the engineering stress-strain curves for steel B before (B6) and after (AI-B1) 100 °C/30min aging treatment.*

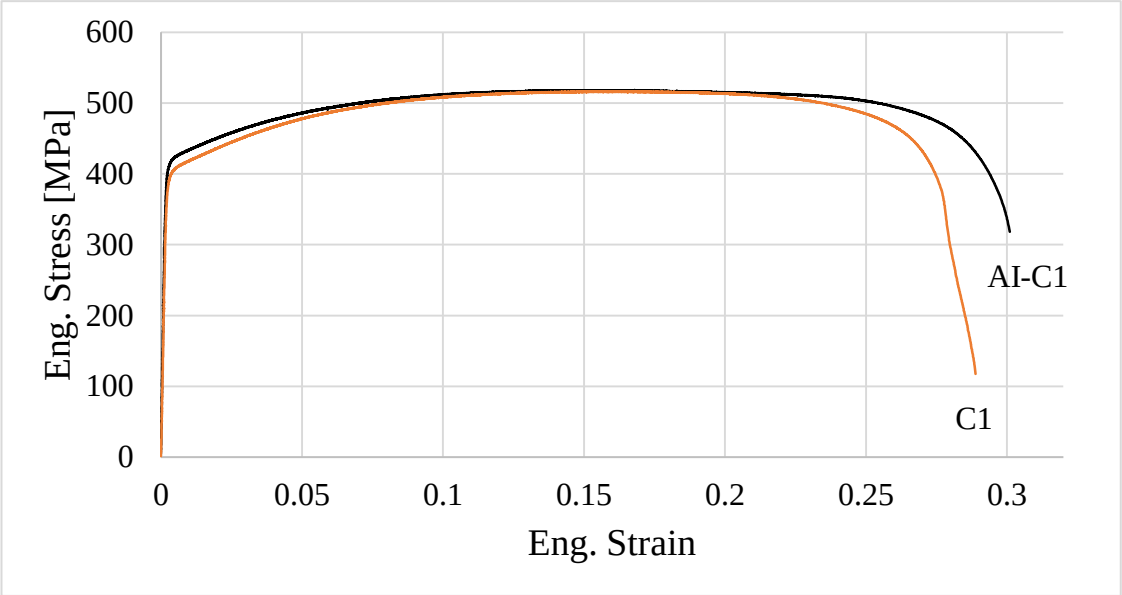

Figure 3. *Comparison of the engineering stress-strain curves for steel C before (C1) and after (AI-C1) 100 °C/30min aging treatment.*